Universidad Nacional Autónoma de México

programa de maestría y doctorado en
ingeniería en energía - sistemas energéticos

Wind power temporal and spatial complementarity and its relation with the regional electricity demand in Mexico

T E S I S

que para optar por el grado de:

Maestra en Ingeniería

presenta:

Ing. Lourdes Guadalupe Zamora García

Tutor principal:

Dr. Osvaldo Rodríguez Hernández

Instituto de Energías Renovables

Temixco, Morelos, Abril 2022

JURADO ASIGNADO:

Presidente:	Dr. Eduardo Ramos Mora
Secretario:	Dr. Miguel Robles Pérez
$1^{er.}$ Vocal:	Dr. Osvaldo Rodríguez Hernández
$2^{do.}$ Vocal:	Dra. Hannah Bloomfield Cheryl
$3^{er.}$ Vocal:	Dr. Óscar Martínez Alvarado

La tesis se realizó en el Instituto de Energías Renovables de la Universidad Nacional Autónoma de México.

Tutor de tesis :
Dr. Osvaldo Rodríguez Hernández

_____

Firma

To all the company on this voyage of discovery (life)...

Acknowledgments

My most esteemed thanks to all the jury for their careful reading of this document, as well as for their detailed observations and valuable suggestions; thereby confirming the need for a scientific approach to objects of study such as the one discussed here; in addition to reaffirming the importance of having explored the knowledge constructed during the development of this project.

I express my deepest gratitude to Dr. Osvaldo Rodríguez Hernández, who edged me to the extraordinary path of wind energy since 2017 and has generously given me his wise academic direction, guiding me in each of the moments, aspects, and themes that intervened in the development of this research. I would also like to thank his willingness to help me sort my mind when I had so many ideas that I didn't know which one to grab first; lastly, thank you, Osvaldo, for allowing me and giving me the confidence to be friends.

My deep and special thanks to Dr. Miguel Robles Pérez for his advice and encouragement in my academic life. A friend that when situations began to be overwhelming, was present to zoom out the case, analyze it, and support me to clarify things to make the best decisions, which were undoubtedly the best because they have led me to this moment.

My very special thanks to Dr. Hannah Bloomfield, for showing sincere interest and disposition in all the virtual meetings and emails, for giving fundamental contributions to the development of this project, and also for her small but powerful comments like "queen of plots" or "good job!" that motivated and prompted me to do my best. Also, thank you, Hannah, for being a role model; I'm your fan.

My sincere thanks to Dr. Oscar Martínez-Alvarado, who received me at the University of Reading in the summer of 2019, where I learned so much under his supervision. He also has supported continuing collaboration in this project, leading to more substantial ideas. Thanks for periodically listening to me on the virtual meetings, analyzing my plots and documents, and giving me valuable recommendations directly and by email, which has been invaluable in achieving the progressive advances.

I acknowledge myself fortunate to have counted with the advice of Dr. Eduardo Ramos Mora, who has shared his valuable knowledge and experience during my academic development and on this project.

I express a special appreciation to the National Autonomous University of Mexico (UNAM) for providing me quality education. My perpetual gratitude and appreciation to all my undergraduate and graduate professors in UNAM's Renewables Energies Institute (IER). Distinctive thanks to the professors who let me be their teaching assistant; the growth I had on this activity was very significant; thanks for your trust and thanks to the students I had for all the mutual learning.

Parráfo especial a mi familia, a mis padres Antonio Zamora y María de Lourdes García, por generar las condiciones especiales y el ambiente familiar siempre afectivo y emocional, brindando un entorno seguro y cómodo para mi desarrollo académico, gracias por todo su apoyo y confianza para que desde pequeña siempre fuese lo que he querido ser, sin dejar de ser una guía junto con nuestros ángeles. Toños y Lulus son totalmente mis idólos y espero algún día ser un poquito como ustedes aunque son insuperables; a mi hermano, Francisco Antonio por su compañía, por escucharme y por los momentos de reláx que le dieron pausa a este mundo que va tan apresurado.

Thanks to all my friends, the ones that had been since my childhood, the BEO's, 5G, my friends from graduate school, from IER, from my exchange to Europe, from work, and from outside of school, thank you for being there and for being part of the balance of life. Also, thanks to Juan Carliux for your support, for listening and being present at all times, in happy moments and moments of frustration where what is most required is a hug; thank you for laughing with me, for all the meals, for enjoying life together and for having nutritious discussions on topics related to wind energy.

Additionally, I am really grateful to the StackOverflow people, and I consider them my friends; they have made enormous contributions to this work with all their tips and solutions for Python; thank you a lot.

When I do not remember something, you probably know that I say I missed eating more almonds for the memory; I apologize to those I did not mention because of this lack of almonds. Still, I likewise extend this feeling of gratitude for all your help, comments, suggestions, and encouragement.

Lastly, thanks to you for your interest in reading my thesis, I hope you enjoy it.

Funding

This project was supported by the National Council of Science and Technology of Mexico (CONACyT), through the National Scholarship (Traditional) 2019-2; the Mexico CONACyT-SENER-Sustentabilidad Energética Project 272063 "Strengthening of the field of Wind Energy in the Doctoral Program in Engineering Field of Knowledge in Energy" based in the Institute of Renewable Energies of the National Autonomous University of Mexico; and the Newton Fund, Grant/Award Number: 432335407, from the British Council, UK Department of Business, Energy and Industrial Strategy.

Abstract

The transition to a low-carbon world requires the implementation of alternative energy sources. Wind energy has enormous potential for its use in Mexico, and there are opportunity areas to increase its percentage of participation in the energy matrix.

Given the nature of the wind, it does not produce a constant generation of electricity. This project aims to study the idea of expanding the generation area and interconnecting wind farms to mitigate the effects of wind variability in the network, taking advantage of the differences in the resource throughout the country by describing and analyzing it.

The project is divided into three objects of study, all interrelated. The first is the accuracy of ERA5 reanalysis data to represent wind resources in Mexico, the second is the wind power temporal and spatial variability, and the third is the demand and wind power correspondence. Therefore, the performance of reanalysis data to represent wind resources in Mexico is studied, which is part of the input data to achieve the objective. The wind power complementarity across the country and the potential of interconnecting regions to increase the generation (magnitude and hours) are analyzed. Lastly, wind power is studied to complement electricity demand and satisfy the clean energy target of Mexico. All approaches are made using reanalysis data that has been evaluated and calibrated with measured data.

Key results are that ERA5 appropriately reproduces the hourly temporal dynamics of the wind; still, its performance reproducing the magnitude depends on the region and post-processing, such as bias correction, translating in Pearson Correlation Coefficient (r) values ranging from 0.35-0.89. It is shown the wind resource diversity in Mexico, and it is highlighted as an advantage to complement wind power generation when regions are interconnected, decreasing the variability of the resource and increasing the generation hours; potential regions to interconnect are detected with negative or low correlations, like the northeastern and eastern region (r=-0.20). Also, there are presented consumption and generation patterns helpful to plan its development and management, common points of peaks during the evening when wind energy could significantly contribute, and the number of wind turbines needed to achieve the clean energy target.

This project shows solutions to the variability problem and encourages the use of wind power, contributing to moving towards a sustainable energy system.

Contents

List of Figures

List of Tables

Chapter 1

Introduction

Climate change caused by anthropogenic reasons has been a topic of serious research for decades, driven by studies and an increasingly intense focus on extreme events worldwide (forest fires, heat waves, melting ice, among others) [1]. The *Energy Transition*, which we are facing as a means of coping with anthropogenic climate change, is a challenge at the current time; it involves economic, technical, and political aspects to move towards a low carbon world. A detailed analysis of the different aspects has to be made in order to plan the best path. This document lay in the technical category; it studies the energy source: wind power, an essential component of the energy transition since it is renewable energy.

Wind power is a variable resource, which supposes a problem to the electric grid. The present project studies and analyzes a methodology that proposes expanding the wind power generation area to reduce the variability problem and encourage the increment of this renewable source in the electricity matrix, moving towards a sustainable electrical system.

This introductory chapter presents the drivers, background, aims, and outline of the current project. In Section **1.1**, it is displayed the thesis motivation, which is based on the advantages that wind energy provides to move towards an electrical system with low emissions, and the research work required to achieve its integration into the grid in a dynamic way. In Section **1.2** the background of the study problem is described; first are introduced the concepts referring to the wind resource assessment and the complementarity of the wind between regions; then, it is presented how the research topic has been worked on in other countries and Mexico. The scope of the project is discussed in Section 1.3. The general aim and specific objectives are listed in Section 1.4. Lastly, in Section 1.5 it is presented the thesis outline.

1.1 Thesis motivation. Wind power as a source of electricity, present contribution, and future integration.

Today living without electricity is inconceivable. From home lighting with small light bulbs to large industrial motors, everyday electrical energy is used for diverse activities in the different consumer sectors: residential, commercial, and public; transport; agricultural; and industrial. In 2018, electricity was the most used energy source in the residential, commercial, public, and industrial sectors, representing 36.10% of the total energy consumed in each of them [2].

The sources where the electricity comes from differ according to the country. In Mexico, in 2020, the distribution of the electricity matrix was: 74.75% fossil fuels, 22.78% renewables [1], and 2.47% other clean energies [2] [3]. On an international level, a considerable effort is being made to reduce the percentage of fossil fuels used in electricity generation since they emit many greenhouse gases (GHG) that cause global warming; this movement from fossil fuels to renewable energies is part of the energy transition. The goal of Mexico is to have a minimum share of clean energy in the electricity generation of 30.00% by 2021 and 35.00% by 2024 [4].

Within the renewable energies developed in Mexico with high growth potential is on-shore wind energy. The wind is the displacement of air masses caused by pressure gradients and by the Coriolis force [5, 6] due to the Earth-Sun interaction. Wind power harnesses the wind's kinetic energy to generate electricity through wind turbines.

The contribution of wind energy to electricity generation in Mexico is important. In 2019, this energy source reported an installed capacity of 6,591.00 MW, representing 25.70% of the total renewable energy installed capacity [7]. It is the second renewable with the highest installed capacity; the first is hydroelectric with 49.40% [7]. In 2020, wind energy generated 19,613.86 GWh, which is equivalent to 6.20% of the total electrical energy generation in Mexico [3]. In 2017, the Mexican Wind Energy Association (AMDEE, by its initials in Spanish) estimated a wind potential of more than 50,000 MW in the country [8]. By 2024, it is expected that the installed capacity of wind energy in Mexico will increase to 14,558 MW [9].

There are still certain technical factors to consider to increase wind energy in the Mexican electricity matrix. Due to the nature of the wind, wind power does not have a constant generation, but the electricity demand must be satisfied when required. The spatial and temporal variability of the wind could suppose a problem when meeting the

[1] Geothermal energy, solar photovoltaic (PV) energy, wind energy, and hydro power
[2] Nuclear energy and biomass

requested demand. However, various mechanisms can be applied to increase the flexibility of the grid and thus reduce the problem of variability.

The flexibility of the grid refers to the ability of an electrical system to respond to changes in electricity demand and generation [10]. The methods to increase it are grouped into system operation, demand management, flexible generators, transmission networks, and storage [10]; Table 1.1 summarizes the characteristics of each mechanism.

System operation	**Demand response**	**Flexible generation**
Improve system operation. For example: - Implementing solar and wind power forecasting. - Expanding the balancing area footprint (interconnection of neighboring networks).	Modify the magnitude and timing of the electricity demand, in order to better adapt it to the generation sources. For example: reduce demand peaks, through their distribution over a period of time.	Modernize and incentivize generation plants, so that they can quickly modify their electricity production depending on what is required. For example: replace old equipment with new, more efficient and flexible.

Transmission	**Storage**
Enhance the physical transmission system and implement technologies and management practices that improve its usage and enable a broader geographic distribution of generation sources.	Employ storage technologies that allow excess power generation to be saved for use when demand is high

Table 1.1: Mechanisms to increase grid flexibility. Information obtained from [10].

Electricity will continue to be a daily necessity for most people in Mexico. The resources used to generate it can affect our future. This work describes and analyzes the regional complementarity of the country's wind generation and its relationship with electricity demand. The motivation to carry out this research work is to contribute to promoting a more sustainable electrical matrix. It is expected that the incorporation of wind energy into the electrical system will be greater by illustrating that the variability of the wind can be mitigated by combining wind farms from different regions (System Operation mechanism to increase flexibility), as well as by presenting the relationship wind generation-demand, which shows the potential of the country's wind resource to satisfy electricity needs.

1.2 Background. Wind resource assessment and wind complementarity

Wind resource assessment

Wind resource assessment is the process of estimating the energy potential of a site [11]. It is a fundamental step when selecting a place to develop a wind project [12] since it allows determining the expected energy production and profitability of the project [13]. To evaluate the wind resource is necessary to know the wind conditions of the study site.

The wind speeds of the site of interest are possible to know through different methods. Measurements can be made on-site, using a measuring tower with one or more anemometers at different heights, which can be cup or ultrasonic. There are also remote measurement equipment, such as the Light Detection and Ranging (LiDAR) and the Sound Detection and Ranging (SoDAR). Table 1.2 provides a brief description of the cup and ultrasonic anemometers and the LiDAR and SoDAR equipment.

Cup anemometer	**Ultrasonic anemometer**
The airflow passes through the cups, turning the shaft. The rotation of the shaft is proportional to the wind speed; the revolutions of the shaft are counted over a certain time [14].	It uses ultrasonic sound waves to measure wind speed. It measures the wind speed as a function of the time required for the sonic pulses to move between pairs of transducers [14].
LiDAR and SoDAR	
The basic principle of these instruments is the interaction between them and the environment. LiDARs and SoDARs emit a wave of light and sound, respectively. The instrument's transducers measure the returning signal, which is different from the emitted signal. Through the Doppler effect equation, it is possible to know the characteristics of the return signal and the wind speed at different heights in the atmosphere. The target that interacts with the emitted signal can be liquid, such as raindrops, solid, for example ice crystals, or smaller particles, such as aerosols. [15]	

Table 1.2: On-site and remote measurement equipment description.

Obtaining wind speeds through the devices mentioned in Table 1.2 is a complex activity. Its installation, operation, and maintenance have a high cost; besides, the measured wind speeds are from a specific site; this makes it challenging to characterize large regions. Alternative methods for obtaining wind speed data cheaper and faster for larger regions are numerical weather prediction models or reanalysis data.

Numerical weather prediction models solve what happens in the atmosphere using a set of equations and parametrizations. These models describe the temporal and spatial change of the wind, pressure, density, and temperature of air parcels in the atmosphere, through the Navier-Stokes Equation, the Mass and Energy Conservation Equation, the Ideal Gas Law, and include the effects of the Earth's rotation [16]. The parametrizations fit the abovementioned equations, representing the radiative, convective, and diffusive phenomena on a small scale [16]. The main disadvantages of these models are that they require a high computational time, and the parametrizations must be chosen appropriately according to the site. One of the most widely used numerical weather prediction models is the *Weather Research and Forecasting* (WRF) model [17].

The reanalysis data integrates numerical modeling and observations. Observations are obtained from a wide variety of sources, including ground weather stations, buoys, radiosonde balloons, satellites, and airplanes [18]. *Data assimilation* is the process that matches the results of a model with the observations. A summary description of its operation is: 1) The model runs and gives a forecast of the result, 2) The result is compared with the observations, 3) Using the observations, the model is adjusted to run again but now resulting in a prediction closer to reality [19]. The products are time series of a large set of meteorological variables, at different heights in the atmosphere, for the whole world, and for an extended time. The variables can be freely downloaded from various sources of reanalysis information. Some of these sources are presented in Table 1.3. The reanalysis data is an inexpensive, quick and practical option to obtain time series of variables of interest.

Dataset	**Spatial resolution**	**Period of time**	**Vertical levels**	**Temporal resolution**	**Institution**
NCEP-R2	2.50°x2.50°	1979-Present	28	6 hours	NCEP
NARR	0.30°x0.30°	1979 - Present	29	3 hours	NCEP
CFSR	0.50°x0.50°	1979-Present	64	1 hour	NCEP
MERRA	0.50°x0.66°	1979-Present	72	1 hour	NASA
MERRA2	0.62°x0.50°	1979-2020	72	1 hour	NASA
CFDDA	0.40°x0.40°	1985-2005	28	6 hours	NCAR RDA
ERA - Interim	0.75°x0.75°	1979-Present	60	6 hours	ECMWF
ERA5	0.28°x0.28°	1950-Present	137	1 hour	ECMWF
JRA-55	0.56°x0.56°	1957-Present	60	6 hours	JMA

Table 1.3: Renalysis datasets sources. Information obtained from [20]

Wind complementarity

The study of wind complementarity focuses on having a constant energy generation through the combination of wind generation sources. It is usually measured using correlation coefficients, especially Pearson's Correlation Coefficient, which is explained in Chapter 2 and represents the degree of relationship between two variables [21]. This coefficient takes values between -1 and 1 [21]; the lower its value, the less correlated variables, which means their behavior is not similar. The two variables compared are time series of wind speeds of at least one year, obtained in the wind resource assessment stage.

Wind complementarity around the world

The regional description of the wind and its complementarity has been studied in different places worldwide. Some cases found in the literature review are mentioned below:

- Asia: China.

  Yu *et al.* [22] described the diurnal variation of the surface wind in the country's central-eastern region, using wind speed data from 452 meteorological stations during 1991-2007. The results show high wind speeds during the afternoon in spring and summer and low after sunrise. Also, it was concluded that the topography of the place modifies the behavior of wind speeds.

  Ren *et al.* [23], apart from studying the seasonal variation of the wind in China, studied its complementarity. They used time series of wind speed obtained from MERRA-2 of twelve sites (seven on land and five on sea) for 1998 to 2017. The correlations with which they measured complementarity had coefficients between - 0.4 and 1. The correlation values decreased as the distance increased. There were no remarkable changes between the seasons of the year. It was concluded that interconnecting wind farms could significantly mitigate the hourly variation of the wind with each other.

- Africa

  Fant *et al.* [24] characterized the wind resource in Africa and measured the potential of interconnection. They used MERRA data from 1979 to 2009 and found high wind speeds in the southwest and low in the northwest. Areas of good wind resources were identified in Tanzania, South Africa, Kenya, Botswana, Zimbabwe, Mozambique, and Zambia; South Africa has higher wind resources than the other countries. They mapped the value of interconnection using two methods; on the

first one, for each grid box, they counted the number of hours with unusable power and correlated with the neighbor grid box; the second method was a principal component analysis. Thus, through maps, potential sites to interconnect were observed; for example, the resource on the Atlantic ocean could interconnect wind the inland resource.

- Europe

  Malvaldi *et al.* [25] studied wind generation's spatial and temporal correlation in 10 European Union countries: Austria, Belgium, Denmark, Germany, Great Britain, Ireland, Italy, Romania, Spain, and Sweden. They analyzed 3-year data (2012-2014) obtained from national institutions. Correlations between countries vary from 0.03 (Denmark-Romania) to 0.65 (Denmark-Germany). The analysis showed that the correlations decrease as the distance increases, and the wind generation of some countries has a probability distribution loaded towards low values. It was concluded that interconnecting the countries reduces the variability of the wind and contributes to a more symmetrical wind power generation.

- Oceania: Australia

  McVicar *et al.* [26] developed a high-resolution (0.01°) daily wind speeds grids using an expanded anemometer database for 1975 to 2006. This new data was compared with reanalysis data (NCEP/NCAR, NCEP/DOE, and ERA-40), the reanalysis data values are larger than the data proposed, but it is because of the height difference (2m/10m). They found that wind speed decreases at mid-latitudes and increases at high-latitudes, wind speed is high in arid regions and low in coastal regions, and the average wind speed is higher in summer than in winter.

Other countries have studied the complementarity of various sources of renewable energy generation, not only wind energy, which is the case of Portugal [27] (solar PV, wind and small hydro), Sweden [28] (solar PV, wind, wave and tidal), China [29] (solar PV and wind), Brazil [30] (solar PV, wind and small hydro), Colombia [31] (solar PV and wind), Vietnam [32] (solar PV and wind), as well as Mexico [33] (solar PV, wind and biomass), among others.

To the best of the author's knowledge, at an international level, three studies have linked the production of renewable energy with electricity demand:

- Drew *et al.* [34] temporarily studied the proportion of demand met by the United Kingdom wind and solar generation. They used 36-year MERRA reanalysis data for wind speeds, and demand data was modeled. One remarkable result was that

the days with the highest penetration of renewables are usually sunny and windy days on weekends when a significant contribution from wind and solar generation and demand is suppressed due to human behavior.

- Bell *et al.* [35] calculated the correlation between energy demand and wind generation in Eastern Australia for the years 2010-2012. They used wind speed data obtained from WRF and demand data obtained from a national institution. Three of the five states studied showed positive correlations to actively meeting demand; the other two presented negative correlations, meaning it would be necessary to implement storage mechanisms or interconnection methods between regions.
- McVicar *et al.* [26] analyzed the hourly profiles of the wind generation and the electricity demand of South Africa. They found that the demand has a peak in winter, while for that season, the wind generation is low; however, on a daily scale, generation and demand peaks correspond in the morning (3:30 to 12:30).

Mexico

In respect of Mexico, several projects have estimated the country's wind potential. For example, Yañez *et al.* [36] estimated the capacity credit of three Mexican states: Oaxaca, Tamaulipas, and Nuevo León, considering the available wind resource, terrain slope, access to transmission lines, road access, and construction restrictions; with data from the North American Regional Reanalysis (NARR-NCEP). Another example is Hernández-Escobedo *et al.* [37] which determines the wind power potential of Mexico, producing maps to show the areas of the greatest potential in terms of mean annual wind speed, the mean annual number of useful hours of wind, and the electrical power that could be generated; the data were collected from 133 automatic weather stations from 2008-2008. The results shows that Mexico has great wind power potential.

Regarding the temporal and spatial variability, it has been studied for specific regions. Some cases are:

- Gulf of Mexico

  Perea-Moreno *et al.* [38] describe 141 locations in the Gulf of Mexico using the Weibull distribution; moreover, locations with similar characteristics have been clustered using the k-means algorithm; the study was made using MERRA-2 reanalysis data. The featured results show different wind seasons along the states of the Gulf of Mexico; also, three wind speed clusters were found: 2:4, 4:8, and >8 m/s.

- Veracruz

  Cancino-Solórzano *et al.* [39] give a statistical analysis of the wind characteristics in the region of Veracruz. The daily, monthly and annual wind speed values have been studied; the data correspond to five meteorological stations and two anemometric stations. The variation throughout the day in the sites analyzed shows similar behavior; the highest velocities happen after 8:00 and start to decline from 18:00.

To the best of the author's knowledge, one study has linked wind power generation with electricity demand. Hernandez-Escobedo *et al.* [40], studied the wind speed daily profile of 4 sites located along the Gulf of Mexico near thermal plants and compared them to the electricity demand trajectory to detect shared peaks which can support the electricity demand; the sites analyzed present generation peaks at the same time as the demand, all of them in the evening/night.

1.3 Study scope

The energy transition is a reality. The technical aspects interfering with the movement towards a sustainable world must be addressed. Mexico has an enormous wind power resource, but the variability might be a risk for the electrical grid. Understanding wind behavior carrying out complementarity studies across a country could decrease wind power variability by indicating the interdependence between regions to plan interconnections.

Wind speed data is required to study wind behavior. The data could be obtained by measurement towers, simulations, or reanalysis data, all of them with cons and pros previously discussed in Section 1.2. This project uses ERA5 reanalysis data bias-corrected with observations. ERA5 has one of the best resolutions regarding reanalyses (shown in Table 1.3), it is evaluated its performance to represent the wind resource across Mexico, and it is also evaluated how it is improved, for most of the sites, by applying the bias correction.

Diverse approaches could be made to understand the variability of this resource. The temporal variability between thirty sites of Mexico that covers the nine regions of the National Electrical System (SEN, by its initials in Spanish) for forty-one years was analyzed, exploring the different hourly profiles and generation magnitudes and occurrences. Furthermore, it is studied the spatial variability in terms of complementarity by estimating the correlation and number of generation hours; it is reflected how the temporal variability could be decreased taking advantage of the spatial variability.

Electricity must be available when it is demanded. This project links the SEN's electricity demand with the wind power generation to study its behavior and correspondence. It is highlighted the common peaks/events between generation and demand of the same region and the generation and demand of different regions, showing that interconnections expand the generation area, and a constant generation could be achieved to satisfy demand at any time.

In summary, the result is a critical and integral analysis of the wind resource of Mexico, the potential of reanalysis data to represent it, the spatial and temporal variability on a local and regional scale, and the collective behavior of the wind generation and electricity demand.

1.4 Objectives

The general objective of the project is:

To describe the wind generation of thirty sites in Mexico on a regional, seasonal, and monthly scale, using reanalysis data and to analyze their complementarity to satisfy electricity demand.

1.4.1 Specific objectives

The general objective is achieved by fulfilling a series of specific objectives, which are:

- To build a database with the observed wind speeds extrapolated to different heights.
- To evaluate the performance of ERA5 reanalysis data to represent Mexico's wind resource through wind speeds and capacity factors.
- To bias correct ERA5 reanalysis data using wind speed observations.
- To estimate the regional capacity factors.
- To measure the complementarity of the wind between sites and between regions.
- To temporarily describe electricity demand and wind generation, using daily and hourly profiles.
- To measure the complementarity of wind generation with demand.
- To calculate the number of wind turbines needed to satisfy a percentage of the regional demand.

1.5 Thesis outline

This thesis is structured in seven chapters. The first three chapters give information about the project: introduction, framework, data, and methods; the following three chapters present the results; lastly, the thesis is ended with a conclusions chapter.

Chapter 1 presents the motivation, given in the context of wind power potential to contribute towards a sustainable energy transition; the background concerning wind resource assessment and wind complementarity; it is also presented in this chapter the study scope and the objectives of the project.

Chapter 2 gives a theoretical framework for the analysis performed in this thesis. It includes the concepts related to wind energy and reanalysis data and explains the statistical methods employed and the electricity demand forecasting.

Chapter 3 describes the data and methodology used in this thesis. It presents specifications of the observations wind speed and reanalysis data, such as location, measurement height, data availability, and other aspects. The methodology is given generally, covering what was done in the three results chapters [3].

Chapter 4 assess the suitability of ERA5 for wind power estimation in Mexico. There are compared the wind speeds and capacity factors obtained from the observations and the reanalysis dataset. Also, ERA5 performance is improved, in most of the sites, by applying a bias correction.

Chapter 5 focuses on characterizing wind resource variability and understanding its temporal and spatial features. The time series of the forty-one years are analyzed on a national, regional, and local scale to describe the behavior monthly and hourly, using different graphical methods, such as maps, radar charts, and hourly profiles. The wind complementarity is presented by the Pearson correlation coefficient and the increment of generation hours.

Chapter 6 investigates the potential of wind power to meet electricity demand in Mexico. It describes the wind generation and electricity demand compatibility in terms of behavior, using the Pearson correlation coefficient and categorizing events. Also, the installed capacity needed to accomplish two-thirds of Mexico's clean electricity generation target for 2024 is estimated, under certain circumstances and considering the temporal variability of the wind resource.

In Chapter 7, the thesis is concluded, and suggestions for future work are given.

[3] A detailed methodology is displayed in each of the results chapters.

1.6 Chapter summary

In this chapter, the thesis theme has been presented and contextualized its importance. The wind is a variable source of energy; however, it should not be considered an impediment to increasing its proportion in the energy matrix since there are mechanisms that can be implemented to reduce this challenge, such as expanding the generation area, which is explored on this work by studying the wind complementarity in Mexico and its behavior with the demand.

General concepts set in the thesis: wind resource assessment and wind complementarity, and their background have been addressed, as well as the study scope where the contribution of this work is expressed. As mentioned before in Section 1.3, this thesis provides a never seen before critical and integral analysis of the wind resource of Mexico, the potential of reanalysis data to represent it, the spatial and temporal variability on a local and regional scale, and the collective behavior of the wind generation and electricity demand.

Also, the structure and the objectives to be achieved have been presented. In essence, this chapter gives a base from which to start so as the chapters are developed, concepts, information, results, and conclusions are added to the primary idea explained on these first pages enabling all together to assemble the project "Wind power temporal and spatial complementarity and its relation with the regional electricity demand in Mexico."

Chapter 2

Conceptual Framework

This chapter introduces the concepts and explains the methods relevant to this thesis. The first part of this chapter, Section 2.1, centers on wind power-related concepts (Section 2.1). In Section 2.2, the statistical and graphical methods used for calibrating and evaluating wind speed time series from reanalysis data and for studying the wind variability and complementarity are described. Then, in Section 2.3 it is explained the growth-rate base method used on electricity demand forecasting. Lastly, this chapter ends with Section 2.4, in which the meteorological seasons used on the seasonal analysis are presented, and Section 2.5 with the main Mexican orographic systems, which will be mentioned in the description of the wind resource characteristics.

2.1 Wind Energy

Wind energy has become a significant factor for promoting sustainable development by supplying clean electricity to the increasing electricity demand [41]. Wind energy is considered clean because it comes from renewable zero-emission sources; also, there is no combustion in the process, which leads to cheaper electricity as there are no fuel costs, and to the reduction of CO_2 emissions [42].

Wind turbines convert the power in the wind into electricity [13]. They are classified depending on the rotor orientation, which could be horizontal or vertical. The most common design of wind turbines is the horizontal axis wind turbine (HAWT); its principal components are shown in Figure 2.1, which include:

- Rotor. It consists of the blades and the hub.
- Drive train. It includes the rotating parts of the wind turbine, such as the shafts (low and high speed), support bearings, gearbox, couplings, mechanical brake, and generator.
- Nacelle. It is the casing of the wind turbine, inside it contains the drive train,

generator, and machine controls.

- Yaw system. It keeps the rotor properly aligned with the wind.
- Tower and the foundations. They support the nacelle, the yaw system, and the rotor.
- Machine controls. It includes sensors, controllers, power amplifiers, and actuators.
- Balance of electrical system. Including cables, switchgear, transformers, power electronic converters, and motors.

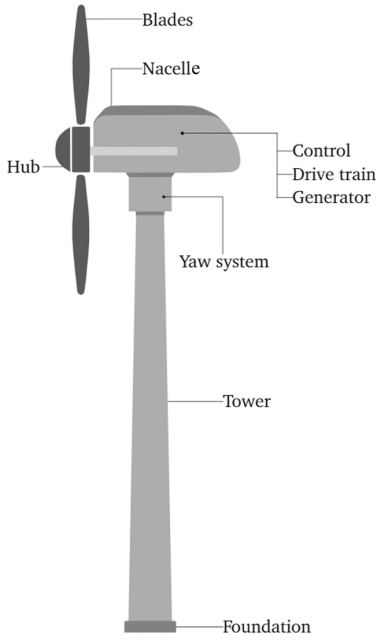

Figure 2.1: Principal components of a horizontal axis wind turbine. Modified from [43]

The principle of operation of a wind turbine to generate electricity from the wind is presented in Figure 2.2. Although not all the principal components are mentioned, synergy exists between them, making them all together get energy from the wind. For example, the yaw system keeps the rotor facing the wind as the wind direction changes, increasing the power output of the wind turbine; the gearbox speed up the rate of rotation of the rotor from a low value to a rate suitable for driving a standard generator; the pitch control, which is in the machine controls category, adjust the angle of the wind turbine to capture the optimal amount of wind energy, resulting in the best power output, it also rotates the blades from power to feathered position when the wind speeds are too high that could damage the wind turbine; the transformers on the electrical system steps up or down the voltage to transport electricity with the appropriate characteristics in the electrical grid [13].

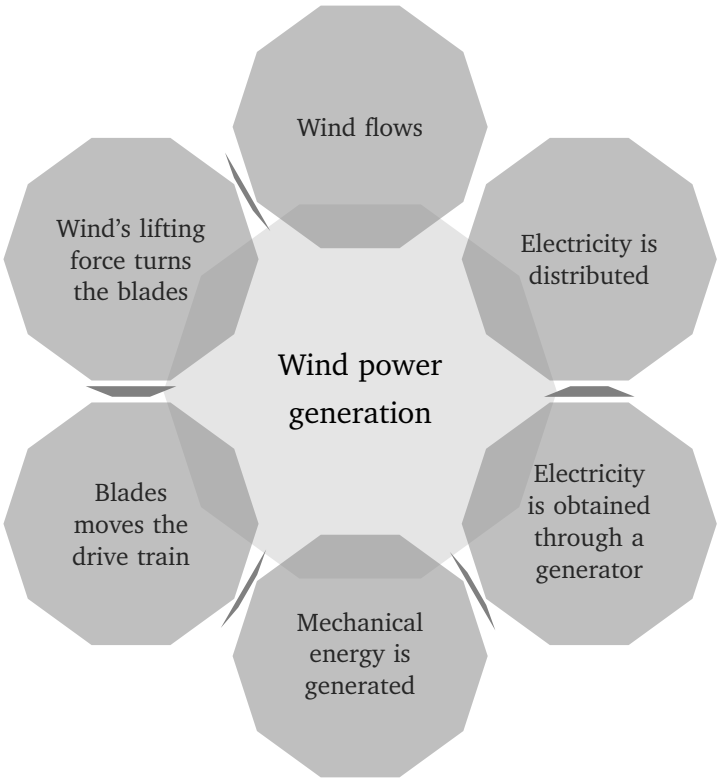

Figure 2.2: Wind power generation

2.1.1 Wind Patterns

The wind characteristics and resource availability depend on the global circulation of the winds and meteorological conditions and are influenced by the site's orography.

Global Circulation Patterns

Atmospheric winds have global circulation patterns caused by pressure differences across the Earth's surface due to the uneven heating of the Earth by solar radiation and are also influenced by the Coriolis effect.

The spatial variation in heat transfer to the Earth's atmosphere leads to a convective heat transfer phenomenon, known as Rayleigh-Bénard convection, and creates variations in the atmospheric pressure field. When the Sun heats the Earth's surface, the air near it raises its temperature, expands, and becomes less dense, so it rises (low-pressure zone); then the air above it with a lower temperature sinks to take its place (high-pressure zone); the same hot air that rises, loses energy as it expands, so its temperature drops. The Rayleigh-Bénard convection is a continuous process that generates convection cells in the atmosphere [5].

On Earth, there are three groups of convection cells: Hadley, Ferrel, and Polar (Figure 2.3a) [6]. These cells are created by the difference in temperature between the Equator and the Poles; its amplitudes are: Hadley cells, from the Equator to approximately 30°N and S; Ferrel cells, around 30° to 60° N and S, and Polar cells from approximately 60°N and S to the poles. Each of the cells goes from a low-pressure region to a high-pressure region. Neighboring cells vertically have opposite directions of rotation.

The Coriolis effect influences the circulation of the wind in the atmosphere. This force results from the different speeds of rotation of the Earth's surface at different heights. It deflects the wind to the right in the Northern Hemisphere and to the left in the Southern Hemisphere [6].

The combination of the Coriolis effect and the global convection cells creates prevailing winds throughout the Earth (Figure 2.3b):

- **Hadley cells**. In the Northern Hemisphere, the returning surface winds are moving towards the Equator; the Coriolis effect deviates them to the west generating an airflow from the northeast to the southwest known as the *trade winds*. In the Southern Hemisphere, the surface winds go from the south to the Equator and are deviated to the west, generating airflow with direction southeast-northwest.
- **Ferrel cells**. In the Northern Hemisphere, surface winds run from 30° to 60 ° N and get swept to the east by the Coriolis effect, creating a prevailing wind called the *westerlies*, also called *jet streams* or *storm tracks*, which flows from southwest to northeast. The Ferrel cell of the Southern Hemisphere has the same patterns as the north one; wind flows from 30° to 60 ° S and gets swept by the Coriolis effect to the left, also creating westerlies from the northwest to the southeast.
- **Polar cells**. Recalling that neighboring cells have an opposite sense of rotation, the Polar cells circulate opposite the Ferrel cells but identical to the Hadley cells. Surface winds move towards the Equator and are deviated to the west, creating prevailing winds called *easterlies* that flow from the northeast to the southwest in the Northern Hemisphere and from the southeast to the northwest in the Southern Hemisphere.

Small-scale Circulations Patterns

Global circulation patterns describe the planetary winds. On a smaller scale, whether regional or local, wind circulation is affected by the Earth's surface, which varies considerably, with extensive ocean and land masses and inland with diverse continental reliefs.

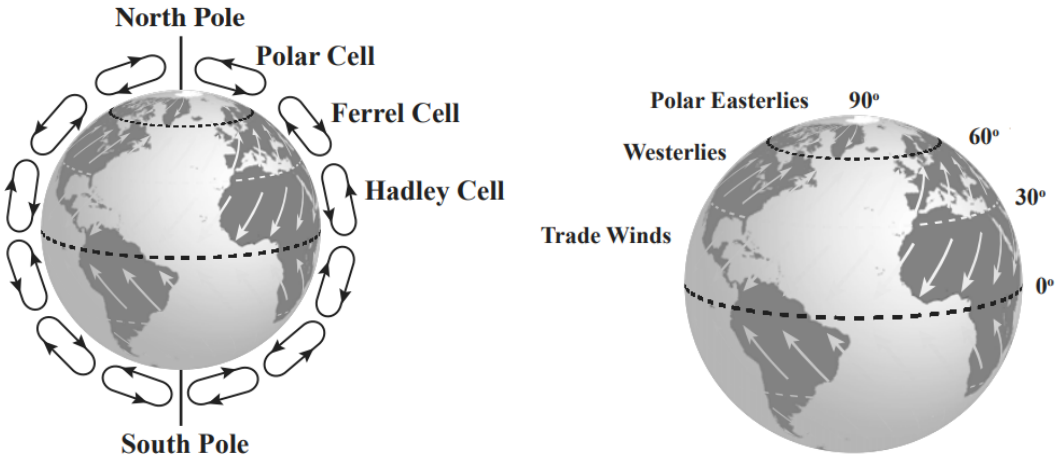

(a) Convection cells

(b) Prevailing winds

Figure 2.3: Global wind patterns. a) Convection cells: Hadley, Ferrel, and Polar, with the opposite vertical direction. The wind flows towards the Equator in the Hadley and Polar cells; the wind flows towards the North and South Poles in the Ferrel cells. b) Prevailing winds: Trade winds from 0° to 30° N and S, direction NE-SW and SE-NW, respectively; Westerlies from 30° to 60° N and S, direction SW-NE and NW-SE; Polar Easterlies from 60° to 90° N and S, direction NE-SW and SE-NW. Obtained from [6]

The different surfaces can affect the flow of air due to variation in pressure fields, the absorption of solar radiation, and the amount of moisture available [13]. The small-scale circulation patterns are divided into secondary and tertiary. Secondary circulation occurs if the centers of high and low pressure are caused by heating or cooling of the lower atmosphere; examples of this are hurricanes, monsoon circulation, and extra-tropical cyclones. Tertiary circulations are characterized by local winds, such as land and sea breezes, valley and mountain wind, thunderstorms, and tornadoes.

Examples of tertiary circulation, valley and mountain winds, and land and sea breezes are explained hereunder:

- Land and sea breezes (Figure 2.4). The parameter that explains the land and sea breezes is the heat capacity of water. It takes longer to heat the water, and it can hold more heat than air. Land heats faster than the ocean during the day and loses heat faster during the night. At night, the land cools down rapidly, air over the ocean is hotter and rise, its departure dragged air from land, the air over the ocean enter the land, become colder and sink; the air will blow from land to the sea, generating a *land breeze*. During the day, the trend is reversed, the hot air from land raises, and the cold air from the ocean takes its place; once over colder water, the warm air cools and sinks toward the ocean; the result is airflow from the water to land, a *sea breeze*.

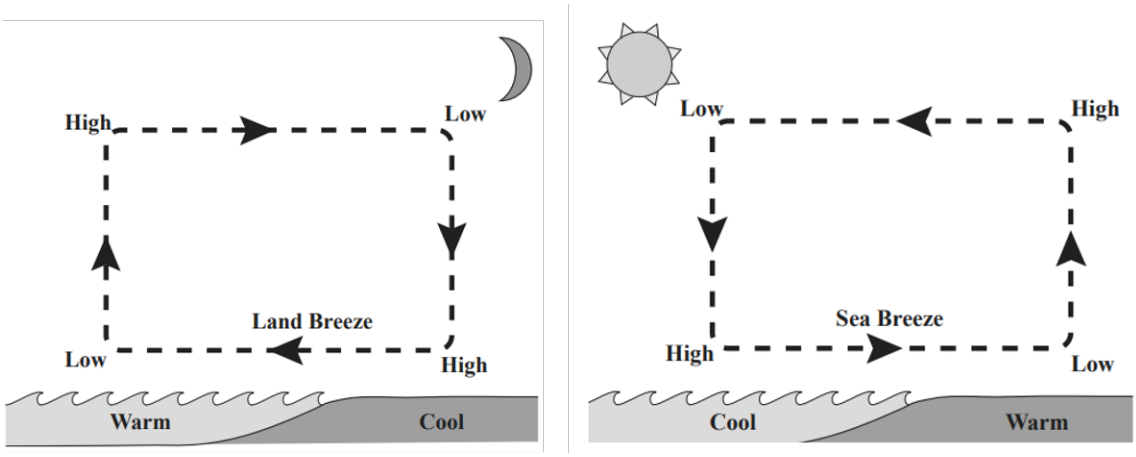

Figure 2.4: Land and sea breezes. During the day, the ocean is warmer than the land; this generates a land breeze. During the night, the land is warmer than the ocean, which generates a sea breeze. Obtained from [6]

- Valley and mountain winds. During the day, the Sun heats mountain air rapidly, convection causes it to rise, and the cooler air of the valley takes its place, generating a *valley wind*. At night, the process reverses the air of the mountain slope is no longer heated, the warmer air is located at the valley which rises, and the cool air of the mountain descends generating a *mountain wind*.

An understanding of global and small-scale circulation patterns, is important for the evaluation of potential wind energy sites [13].

2.1.2 Wind Speed Extrapolation: Power Law Profile

The assessment of wind resources might require having the data at a specific elevation (usually at the hub height). When the measurement equipment does not report data at the desired height, a model of the wind speed variation with height is used. A model commonly used in these cases for wind energy applications is the Power Law Profile.

The Power Law Profile (Eq. 2.1) represents a simple model of the vertical wind profile. The vertical profile of the wind describes the variation of the wind speed concerning height. The wind varies with height due to friction with the Earth's surface or with some obstacle, up to a limit distance where the speed is not affected; therefore, at a higher altitude, a greater wind resource is expected [44].

$$U(z) = U(z_r)\left(\frac{z}{z_r}\right)^{\alpha} \tag{2.1}$$

Where:

$U(z)$ - Wind speed at height z

$U(z_r)$ - Reference wind speed

z - Extrapolation height

z_r - Reference height

α - Power law exponent

The Power Law exponent (α) is a representation of the thickness of the wind speed boundary layer between two points [44]. If its value is small, it represents that the wind speed between two points at different heights does not vary too much; as the difference between the wind speeds increases, the value of α also increases. Empirical results indicate that the value of $\alpha = 1/7$ works well for several places, but not for all, because α is a highly variable value, it depends on the elevation of the terrain, the hour, the season, the type of terrain, the wind speed, the temperature, among other parameters [13].

2.1.3 Power Curve

The power output of a wind turbine varies with the wind speed, and every wind turbine has a characteristic power performance curve, which is typically obtained from the manufacturer [13]. The power curve gives the power output as a function of the wind speed at the hub height; it is an fundamental factor to model the power output of a wind turbine. Figure 2.5 presents the power curve of a General Electric 2.5 MW wind turbine.

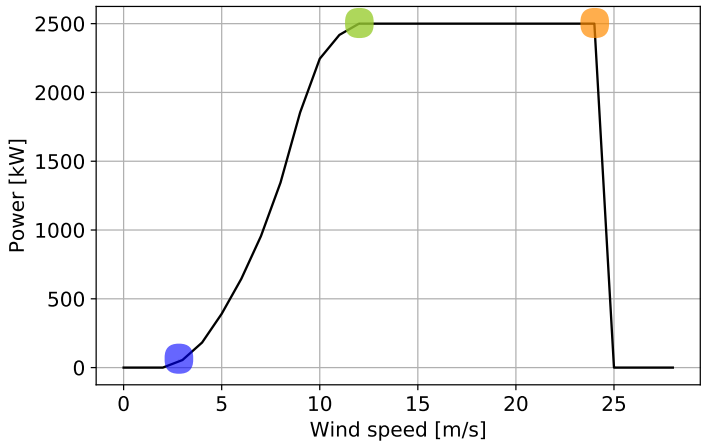

Figure 2.5: General Electric 2.5 MW wind turbine power curve. Blue point represent the cut-in speed, green point represent the rated wind speed, and the orange point represent the cut-out speed.

The performance of a wind turbine can be related to three particular wind speeds:

- **Cut-in speed.** Minimum wind speed at which the wind turbine starts to generate power.
- **Rated speed**. Wind speed at which the wind turbine reaches the rated power.

- **Cut-out speed**. Maximum wind speed at which the wind turbine is allowed to deliver power, to keep loads and generator power from reaching reaching damaging levels.

2.1.4 Annual Energy Production

The Annual Energy Production (AEP) is the amount of electrical energy generated by a wind turbine over a year. It could be estimated by the direct use of data as follows:

1. The power curve of a wind turbine is modeled with a mathematical function.
2. The wind speeds are evaluated in the function, which gives the power output.
3. The power output is summed up for the period.
4. The result of the sum is multiplied by the measurement range; for example, 1/6 if data is reported every ten minutes or one if it is reported every hour.

The steps to estimate the energy obtained from a wind turbine using the direct use of the data method are summarized in Equation 2.2.

$$E = \sum_{i=1}^{N} P(U_i) \triangle t \tag{2.2}$$

Where:

E - Energy Production
U_i - Wind speed
P - Power curve function
$\triangle t$ - Wind speed measurement range

This method does not consider losses in the electrical transmission system, wake effects, or maintenance seasons.

2.1.5 Capacity Factor

The Capacity Factor (CF) is the estimation of the maximum possible energy that a specific wind turbine can generate at a given location in reference to the maximum energy that the wind turbine can produce theoretically if it operates at 100% of its capacity throughout the year [13]. It represents the suitability of a wind turbine to the wind profile or selected site [45], and it is calculated using Equation 2.3.

$$CF = \frac{AEP}{Rated\ power * 8760} \tag{2.3}$$

2.2 Statistical and Graphical Methods

The statistical and graphical methods applied to use, calibrate and evaluate the wind speed time series from reanalysis data and to study the wind variability and complementary are described in this section.

2.2.1 Bilinear Interpolation

The bilinear interpolation interpolates in two-dimensions x and y. This method is used to obtain the data from reanalysis for a specific point as the data downloaded is on a rectangular grid form, encompassing the Mexican domain: 33°N, -123°W, 11.5°N, -84.5°W.

The basic geometry of interpolation on a grid is shown in Figure 2.6. The initial data is given at discrete points in (x, y). To find an interpolated value at an arbitrary point requires first locating the four grid points surrounding the point (x, y) [46].

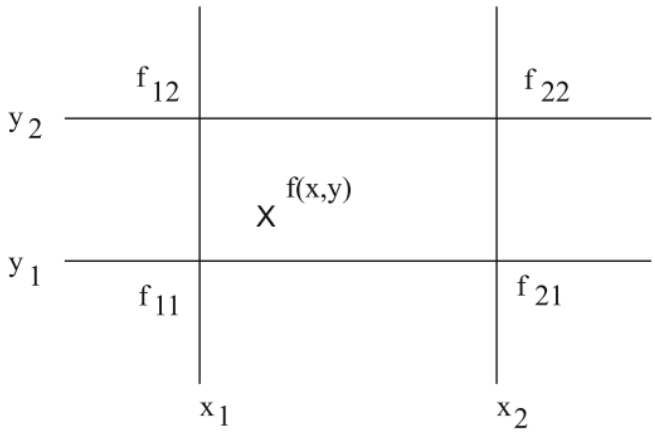

Figure 2.6: Interpolation in a two-dimensional rectangular grid. The function $f(x, y)$ can be found at an arbitrary point (x, y) given only the values sampled at discrete values of $x = x_1, x_2$ and $y = y_1, y_2$ surrounding point (x, y). Obtained from [46]

In Figure 2.6 the new point is located between x_1 and x_2 in x, and between y_1 and y_2 in y. The values of the four grid points surrounding (x, y) are f_{11}, f_{12}, f_{22}, and f_{21}. The bilinear interpolation is performed using linear interpolation first in one direction, x-direction, through Equations 2.4 and 2.5.

$$f(x, y_1) = \frac{x_2 - x}{x_2 - x_1} f_{11} + \frac{x - x_1}{x_2 - x_1} f_{21} \tag{2.4}$$

$$f(x, y_2) = \frac{x_2 - x}{x_2 - x_1} f_{12} + \frac{x - x_1}{x_2 - x_1} f_{22} \tag{2.5}$$

Then, the interpolation is performed in the y-direction to obtain the desired estimate, $f(x, y)$, using Equation 2.6.

$$f(x,y) = \frac{y_2 - y}{y_2 - y_1} f(x, y_1) + \frac{y - y_1}{y_2 - y_1} f(x, y_2) \tag{2.6}$$

2.2.2 Bias Correction

Global Climate Models have systematic errors in their output caused by a range of factors, for example, limited spatial resolution or simplified thermodynamic processes. Bias correction is the process of scaling outputs to account for their systematic errors, to improve their fitting to observations [47]. The Quantile Mapping approach is often used for the correction of climate data [48, 49]; the following steps describe it:

1. Determine the percentile values of observations and models' outputs.
2. Find the difference between measurements and models for each percentile; this will be the correction value.
3. Identify the proportional percentile for each value of models' time series.
4. Apply the correction to the models' time series by subtracting the correction value from each model's time series value.

Two graphical methods could be applied to visualize the bias:

- **Scatter plots.** A scatter plot uses dots to represent two different numeric variables; each variable is assigned to an axis. It provides an idea of the type of relationship between the variables: identical relationship (same values), no relationship (a disperse cloud of points), positive linear relationship (ascending points), negative linear relationship (descending points), and non-linear relationship (the points make a form but is not a line); and it also show the bias when an identical relationship is expected.
- **Kernel Density Estimate (KDE) bivariate plots.** A KDE plot allows visualizing the distribution of observations in a dataset, using a continuous probability density curve [1]. Each point is plotted, and its color means the density. Its distribution representation is similar to the scatter plot value; if the points are concentrated along the $x = y$ line, the values are identical; if the points draw a circle, there is no linear relationship.

Figure 2.7 presents an example of a scatter plot (Figure 2.7a) and a KDE plot (Figure 2.7b), the data on each of them is discussed in more detailed on Chapter 4.

[1] The default probability density curve in Python Seaborn is a Gaussian.

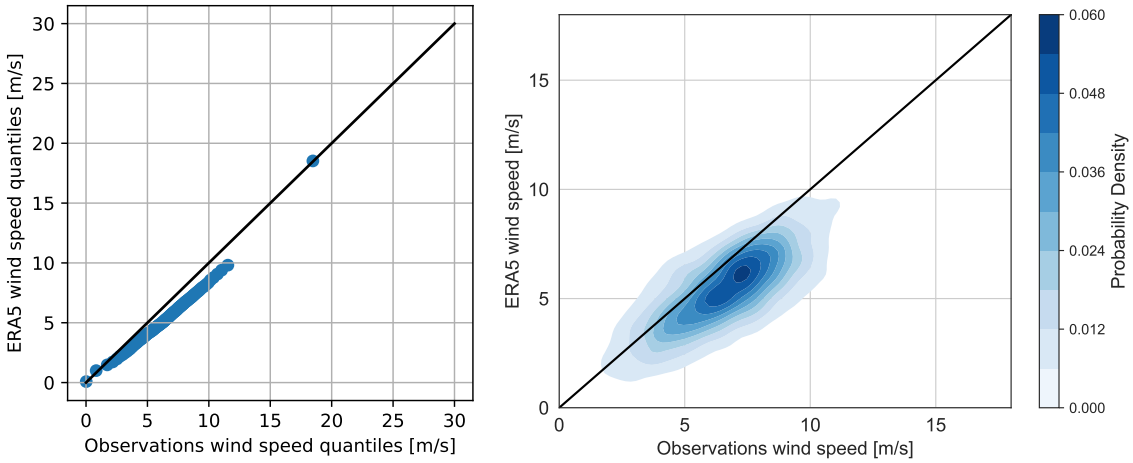

(a) Scatter Plot

(b) Kernel Density Estimate Plot

Figure 2.7: Scatter Plot and KDE Plot. The scatter plot (a) represents with dots the value of the quantiles for the reanalysis and observations wind speed; the bias is observed as the dots are not aligned with the identity line. The KDE plot (b) represents the distribution of the values with contours and a scale of color; the time series is concentrated around 6 and 9 m/s, where the blue color is dark.

2.2.3 Ordinary Least Squares Adjustment

The Ordinary Least Squares Adjustment estimates the relationship between one independent variable and a dependent variable by minimizing the sum of the square differences between two variables and fitting a straight line to the data series [50]. The Ordinary Least Squares Adjustment is described by Equation 2.7.

$$y = a + bx \tag{2.7}$$

The slope value, b, is given by Equation 2.8, and the intercept, a, is given by Equation 2.9.

$$b = \frac{\sum_{i=1}^{n}[(x_i - \bar{x})(y_i - \bar{y})]}{\sum_{i=1}^{n}(x_i - \bar{x})^2} \tag{2.8}$$

$$a = \bar{y} - b\bar{x} \tag{2.9}$$

For this project, the variables to which the estimation was done are the observations and reanalysis values. This method is applied to evaluate the performance of reanalysis data before bias correction and after bias correction by measuring the improvement of the calibration regarding the slope value.

2.2.4 Pearson Correlation Coefficient

The Pearson Correlation Coefficient, also known as r value, measures the degree of relationship between two variables. The Pearson Correlation Coefficient is estimated through Equation 2.10.

$$r = \frac{\delta_{xy}}{\delta_x \delta_y} \tag{2.10}$$

Where, δ_{xy} is the covariance (Equation 2.11), it gives the direction of relationship, either positive (x and y increase) or negative (x increase and y decrease).

$$\delta_{xy} = \frac{1}{n-1} \sum_{i=1}^{n} (x_i - \bar{x})(y_i - \bar{y}) \tag{2.11}$$

δ_x (Equation 2.12) and δ_y (Equation 2.13) are the standard deviation of x and y, respectively, they represent the strength of the relationship.

$$\delta_x = \sqrt{\frac{\sum_{i=1}^{n} (x_i - \bar{x})^2}{n-1}} \tag{2.12}$$

$$\delta_y = \sqrt{\frac{\sum_{i=1}^{n} (y_i - \bar{y})^2}{n-1}} \tag{2.13}$$

The Pearson Correlation Coefficient range between -1 and 1. Table 2.1 presents the degree of the correlation strength, depending on the sign it would be positive or negative.

Value (±)	Meaning
0.90 to 1.00	Strong correlation
0.70 to 0.89	Significative correlation
0.50 to 0.69	Moderate correlation
0.30 to 0.49	Weak correlation
0.00 to 0.29	Little or any correlation

Table 2.1: Pearson Correlation Coefficient Value Scale. Obtained from [51]

The interpretation of the values is the following:

- $r = 1$ (Figure 2.8a), x increase and y increase proportionally, it exists a perfect positive correlation, the relationship is direct.
- $r = -1$ (Figure 2.8c), x increase and y decrease proportionally, it exists a perfect negative correlation, the relationship is inverse.
- $r = 0$, there is no relationship, all the points are dispersed.
- $0 < r < 1$ (Figure 2.8b) or $-1 < r < 0$, although the points do not represent a straight line, it exists a correlation, positive or a negative, respectively.

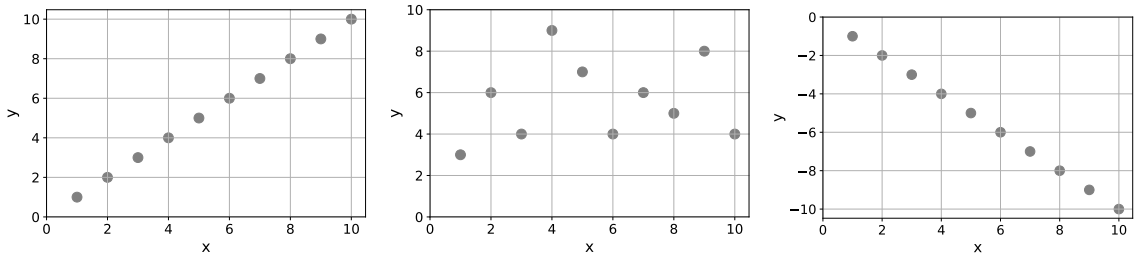

(a) r = 1.00 (b) r = 0.15 (c) r = -1.00

Figure 2.8: Pearson Correlation Coefficient Example Scenarios

The Pearson Correlation Coefficient has been used to evaluate reanalysis data performance and study wind variability and complementarity. In some cases, it is just given the value, but in others, it has been used the graphical method *heatmap* to visualize the results. A heatmap plots rectangular data as a color-encoded matrix. It shows the correlation insights of two variables; the variables are on the axis, and the cells, with a particular color depending on the value, have the Pearson coefficient annotated. This graphical tool also allows identifying clusters. Figure 2.9 presents a heatmap example; its data will be discussed in more detail on Chapter 5.

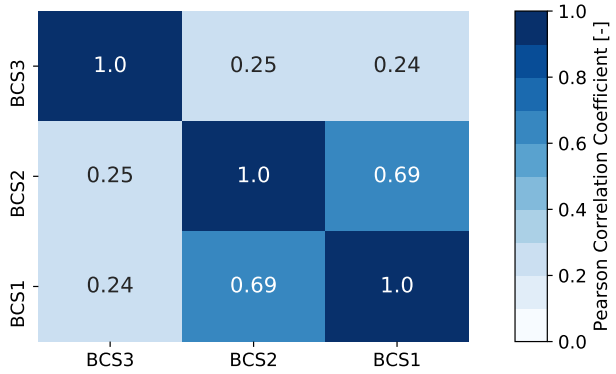

Figure 2.9: Heatmap. The correlation is estimated between the axis variables axis, the r values are on the cells and the color represent its magnitude; darker blue means high values.

2.3 Electricity demand forecasting

The electricity demand forecasting could be done using simple approaches that provide a quick understanding of the situation. The simple indicators commonly used for these forecasting approaches are: growth rate, elasticities, specific or unit consumption, and energy intensity [42]. In this work, electricity demand forecasting is done using the growth-rate-based method.

Growth-rate based method

The growth-rate is an easily understood indicator useful to capture the speed of change in demand [42]. It can be estimated year-on-year (Eq. 2.14):

$$a = \frac{E_{T+1} - E_t}{E_t} \tag{2.14}$$

Or the annual average over a period of time (Eq. 2.15):

$$a_g = \left(\frac{ET1}{ET0}\right)^{1/(T1-T0)} - 1 \tag{2.15}$$

Year-on-year growth rates are calculated using the energy consumption of the year t + 1 (Et + 1) and year t (Et). Annual average growth rates over a period of time are calculated using the energy consumption in period T1 (ET1) and the energy consumption in period T0 (ET0).

The electricity demand forecasting employing growth rates is calculated through Equation 2.16.

$$D_t = D_o(1+g)^t \tag{2.16}$$

Where:

g = Growth rate

D_t = Demand of year t

D_0 = Demand of year 0

t = Time in years (year t - year 0)

2.4 Meteorological seasons

The seasons mentioned in this work are based on the meteorological seasons based on the annual temperature cycle. Instead of using the periods between solstices and equinoxes (or vice versa), they go by calendar month.

Table 2.2 shows the months corresponding to each meteorological season.

Spring	Sumer	Fall	Winter
March	June	September	December
April	July	October	January
May	August	November	February

Table 2.2: Meteorological seasons. Obtained from [52]

2.5 Mexican orography

The main orographic systems in Mexico are: Sierra Madre Occidental (I), Sierra Madre Oriental (II), Mexican Plateau (III), Transmexican Volcanic Belt (IV), Sierra Madre del Sur (V) and Sierra Madre de Chiapas (VI). The systems are presented in Figure 2.10 labeled with the number between branches.

Figure 2.10: Mexican Orography. Obtained from [53]

I. The **Sierra Madre Oriental** has a length of approximately 1,300 kilometers and an average width of 50 kilometers; it goes from northwest to southeast starting in the Rio Grande, and it finishes when it joins the Transvolcanic Belt, it crosses the states of Sonora, Sinaloa, Chihuahua, Durango, Nayarit, Jalisco, Zacatecas, and Aguascalientes.

II. The **Sierra Madre Occidental** has approximately 1,250 kilometers in length; it covers all the western Mexican territory which include the states of Coahuila, Nuevo León, Tamaulipas, San Luis Potosí, Hidalgo, Puebla, Querétaro, Texas, Tlaxcala, Veracruz.

III. The **Mexican Plateu** extends from the United States border in the north to the Trans-volcanic Belt in the south and is bounded by the Sierra Madre Occidental and the Sierra Madre Oriental to the west and east, respectively.

IV. The **Transvolcanic Belt** is an active volcanic belt that covers central-southern Mexico fro approximatly 880 kilometers; it crosses the states of Veracruz, Puebla, Tlaxcala, Hidalgo, Mexico, Morelos, Querétaro, Guanajuato, Michoacán, Guerrero, Jalisco, Colima, Nayarit, and Mexico City.

V. The **Sierra Madre del Sur** is located in southern Mexico and extends for 1200 kilometers with an average width of 100 kilometers between western Jalisco and the Isthmus of Tehuantepec, east of Oaxaca; it runs parallel to the coast of the Pacific Ocean and the Transvolcanic Belt.

VI. The **Sierra Madre de Chiapas** crosses southeastern Mexico, Guatemala, El Salvador, and part of Honduras. In Mexico, the sierra begins at the Ostuta River and continues to the border with Guatemala; it has a length of approximately 250 kilometers and a width of 50-65 kilometers.

2.6 Chapter summary

In this chapter, the concepts and statistical and graphical methods behind the development of this thesis have been addressed. In the first section, wind power-related notions were presented, which enable understanding wind principles, obtaining hub height values, and calculating wind energy production and capacity factors.

The second and third sections defined the metrics and graphical tools used to investigate the wind power complementarity and its relation with the demand. Therefore, the methods presented represent how to calibrate and evaluate the wind speed time series from reanalysis data and study the wind variability. Some methods are used to handle the data, such as bilinear interpolation, and others to guide the performance of reanalysis data and the potential of interconnecting regions results, like the Pearson Correlation Coefficient.

The fourth and fifth sections explained concepts mentioned throughout the work, so those unfamiliar with them find it easier to follow the ideas by having this background information, as is the case of the Mexican orography, by introducing how it is made up, and its characteristics.

Chapter 3

Data and Methods

In this chapter, the data used and the methodology followed are described. The sets of data and steps, together with the tools commented on Chapter 2, enable the achievement of the objectives. The data used are wind speed time series from observations and reanalysis, the technology power curve, the electricity demand time series, and the average annual growth rate values of electricity consumption. The methodology focuses on the steps to evaluate reanalysis data performance, study wind variability and complementarity, and analyze the relation between wind generation and electricity demand.

The chapter begins with Section 3.1, in which a general description of the study sites and regions is presented. Then, Section 3.2 deploys the data sources and file's characteristics for the wind speed and electricity demand time series, also it is commented a dataset which was not directly used but outputs from it are compared in Chapter 4. Section 3.3 presents the values of the average annual growth rate of electricity consumption per region used on the demand forecast. Section 3.4 shows the power curve of the technology selected, which allows the estimation of the electricity generation and capacity factors. The chapter concludes with Section 3.5 by presenting the general thesis methodology.

3.1 Study sites and regions

On a first step, on a local scale, the thesis focus on the study of thirty sites (Figure 3.1) from which observations wind speeds are available. These sites are located across the Mexican territory in various places, generating a diversity of wind resource characteristics.

On a second step, the approach is on a regional scale. The time series of the same region sites are combined, looking to have the maximum generation, but also to set the time series to be comparable with the demand data reported regionally. Therefore, the regions are selected according to the National Electric System division.

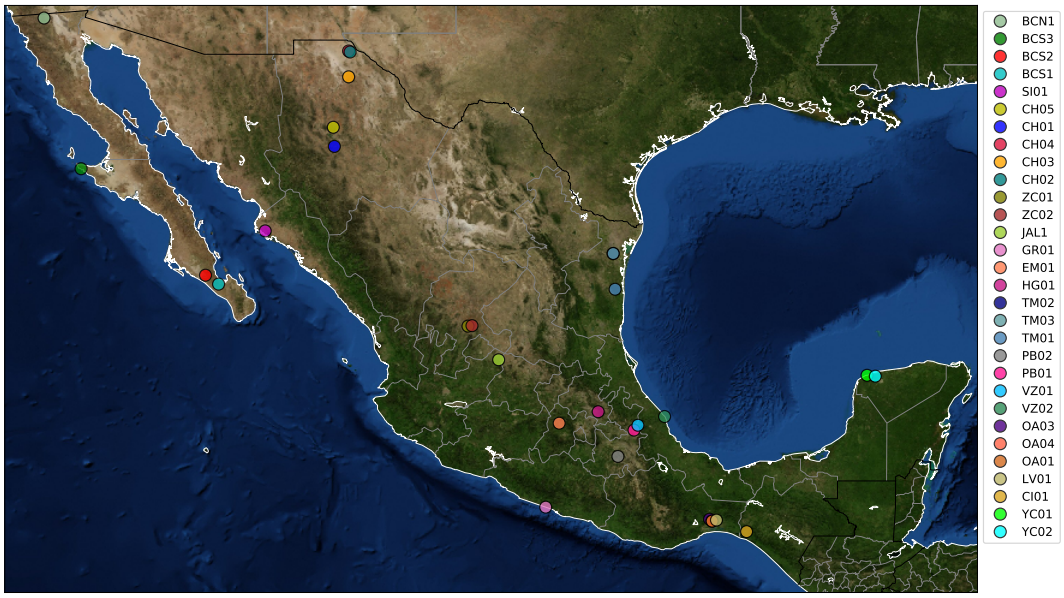

Figure 3.1: Study Sites Location

The National Electric System (SEN, by its initials in Spanish) is organized into nine control regions and a small electrical system. The control regions are mapped in Figure 3.2, the acronyms correspond to: BCA, Baja California; BCS, Baja California Sur; NOR, north-west; NTE, north; NES, north-east; CEN, central; OCC, western; ORI [1], eastern; and PEN, Peninsular. There is a small electrical system named Mulége in Baja California Sur, but it is not considered as there is no data for it.

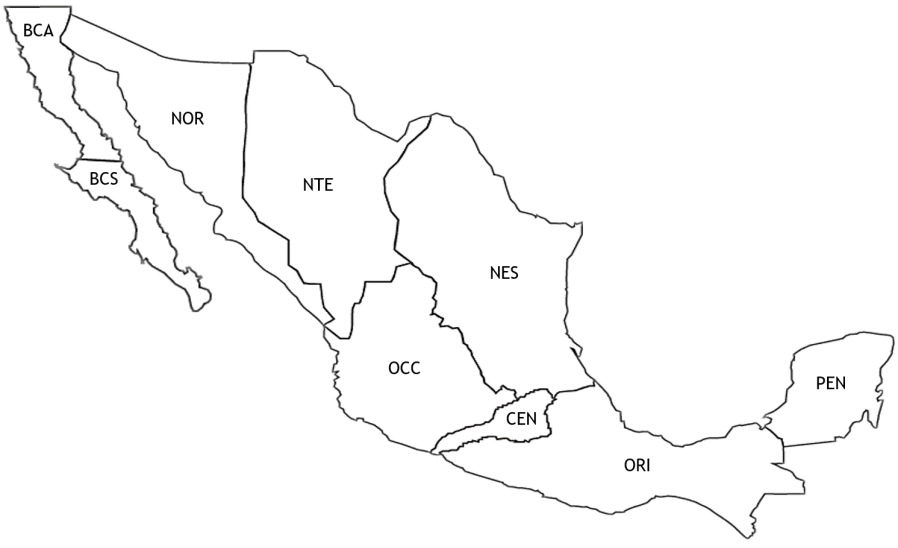

Figure 3.2: National Electric System Regions. Modified from [54]

[1] Later the ORI2 region is introduced, it corresponds to ORI but only with the sites of Oaxaca and Chiapas

The BCA and BCS region and the Mulegé electrical systems are electrically isolated from each other and from the rest of the national electricity grid. The other seven regions are interconnected and form the National Interconnected System (SIN, by its initials in Spanish); they share the resources and capacity reserves. The interconnection studied in this project does not consider the Mexican electrical infrastructure.

As mentioned before, the sites are located all over Mexico, at least one site per region. Table 3.1 presents the complete name of the study sites, along with its acronym, height at which wind speed is reported on it, and region where it is located.

Name	Acronym	Height	Region
La rumorosa	BCN1	20, 40, 60, 80	BCA
El Paso	BCS1	15	BCS
San Hilario	BCS2	15	BCS
Bahía Tortugas	BCS3	20, 40	BCS
Los Mochis	SI01	20, 40	NOR
Cuauhtémoc	CH01	20	NTE
Samalayuca	CH02	16	NTE
Villa Ahumada	CH03	15, 30	NTE
Samalayuca II	CH04	15, 30	NTE
Cd. Cuauhtémoc	CH05	20, 40, 60, 80	NTE
Cieneguillas	ZC01	20, 40	OCC
La Virgen	ZC02	20, 40	OCC
Ojuelo	JAL1	20, 40, 60, 80	OCC
Los Naranjos	TM01	20, 40	NES
Fco. Villa	TM02	20, 40	NES
San Fernanado	TM03	20, 40, 60, 80	NES
Barra de Coyuca	GR01	10	ORI
Pastejé	EM01	10	ORI
Cerro Pelón	HG01	20, 30	ORI
Alchichica	PB01	20, 40	ORI
Tepexi	PB02	20, 40, 60, 80	ORI
Perote	VZ01	20, 40	ORI
Punta Delgada	VZ02	20, 40	ORI
La Ventosa	OA01	20, 40	ORI2
Cd. Ixtepec	OA03	20, 40	ORI2
CERTE	OA04	20, 40, 60, 80	ORI2
La Venta	LV01	15, 32	ORI2
El Progreso	CI01	20, 40	ORI2
Sisal	YC01	20, 40	PEN
Mérida	YC02	20, 40, 60, 80	PEN

Table 3.1: Study sites, name, acronym, height and region.

The wind resource on each site depends on its location; global and local patterns might influence it. Some relevant aspects of the study sites are the complex orography and the rapid transition between land and sea. The first aspect involves the sites located in the Occidental, Central, and Oriental regions (not in Oaxaca and Chiapas). They are located along the Eje Transversal Neovolcanico, the Sierra Madre Oriental, and the Siera Madre Occidental zones characterized by many mountain chains. The second aspect involves the sites located in the BCS region because the continent land that conforms Baja California Sur state is too narrow; therefore, the grid might have ocean and land on the same grid box affecting the result.

3.2 Data description

This Section presents the general features of the observations and ERA5 sources, the data files characteristics of both, and the data available from the measurement towers. Additionally, it is described the electricity demand data.

3.2.1 ERA5 reanalysis data

Reanalyses produce spatially and temporally complete data sets that capture the state of the atmosphere over several decades by assimilating observations [55]. ERA5 provides a broad set of atmospheric, oceanographic, and land surface variables. It integrates numerical modeling and observations through the data assimilation process. ERA5 is based on the European Centre for Medium-Range Weather Forecasts (ECMWF) Integrated Forecast System and the 4-dimensional variational analysis (4D-var).

The Integrated Forecast System describes the existent flow of energy, humidity, and momentum between the atmosphere, land, and ocean, using seven models: atmospheric including ozone, ocean wave, ocean, sea ice, land surface, lake, and radiative [19]. The climate model equation set includes equations of motion, state, thermodynamics, mass balance, and water balance. The forecast model divides the atmosphere into grid boxes, there are considered uniform properties in each box, and then the equations are integrated numerically forward in time.

The 4D-var objective is to find the best estimate of the state of the atmosphere within an assimilation time window, given a background forecast x_b valid at the start of the window and observations y_o falling within that window [19], such that the forecast best fits the observations. The analysis window is of 12 hours, and the process is the following:

1) The model is started with reasonable conditions; 2) The outputs (x_b) are compared with observations (y_o), and the deviation is measured; 3) The model is adjusted to reduce the deviation, and it is rerun with different initial conditions. In summary, 4D-var seeks an initial condition to reconstruct the global weather model from the local time series given.

The assimilation is made over a wide range of surface, and upper-air observational data from both in-situ instruments and satellites, among which are ground weather stations, buoys, radiosonde balloons, satellites, and airplanes [18]. One example, for America, is the satellites GOES-8 to -16 from NASA from which infrared radiance's are obtained [19].

Characteristics of ERA5 reanalysis data are:

- **Spatial resolution:** 30km horizontal and 137 levels from the surface up to a height of 80km.
- **Output frequency:** Hourly.
- **Data availability:** From 1950 to the present five days of real-time [2]

Recently ERA5 had an update, on the end of 2020/early 2021 where the period was expanded, before this date ERA5 used to cover from 1979 to the present five days of real-time [3] [19]. The data could be downloaded from the Copernicus Climate Data Store [56].

As mentioned before, ERA5 provides a broad set of data of atmospheric, oceanographic, and land surface variables. For this project, the fields used were 100 meters u and v component of wind, which are useful for wind energy because hub heights are reported around this height.

3.2.2 Observations wind speeds

The observed data are time series from measurement towers. These data were obtained from two projects: "Mexican Wind Atlas" [57] and "Action plan to eliminate barriers to the development of wind power generation in Mexico" ("Wind project") [58]. The measurement equipment used in both projects was cup anemometers.

The **Mexican Wind Atlas** focuses on wind energy planning and identifying in more significant detail potential places where small, medium, and large-scale wind-electric generation projects can be developed [59]. It is a joint project between the Renewable Energy Department of the Electricity Research Institute (IIE, by its initials in Spanish), now

[2] Five days is the preliminary product, the final product is two to three months of real-time.

[3] The results from this thesis were obtained before that date that is why it is only considered 41 years from 1979 to 2019

the National Institute of Electricity and Clean Energy (INEEL, by its initials in Spanish), the Civil Engineering Studies Department of the Federal Electricity Commission (CFE, by its initials in Spanish), the Institute of Geography of the National Autonomous University of Mexico (UNAM, by its initials in Spanish), and the Technical University of Denmark (DTU). The project was created in 2014. It consists of 8 stages; the data available are from stage 3, corresponding to the measurement campaigns.

The **Wind Project** was carried out by IIE, now INEEL, with support from the United Nations Development Program (UNDP). The project was endorsed to the Global Environment Facility (GEF) in October 2003 [60] and began operations in January 2004 [61]. This project aims to eliminate the barriers that limit wind-electric development in Mexico and develop elements that contribute to making wind-electric development in Mexico meaningful and sustainable [61]. The project proposes four goals; the wind speed measurements are within the first goal: "Capacity Development" [61].

Each project measures the wind speed of different sites and of a different number of sites. From the Mexican Wind Atlas were obtained the wind speed time series of seven sites, which are BCN1, CH05, TM03, JAL1, PB02, OA04, YC02; and from the Wind project, the wind speed time series of the remaining 23 sites.

File's properties

The data files characteristics are described in Table 3.2. The data is reported differently for each project, with different formats, different file extensions, different years, and different heights.

Mexican Wind Atlas	Wind Project
- Text files (.txt). - Days reported on the range (1,31). - Data reported every 10 minutes. - For all sites, wind speeds are reported at 4 heights: 20, 40, 60, and 80 meters, for the years: 2018, 2019, and the first 7 months of 2020.	- Comma-separated values files (.csv). - Days reported on the range (1,360). - Data reported every 10 minutes. - Wind speeds are reported at 1 height or 2 heights, among which there are values at 15, 20, 32, and 40 meters. The years for which data is reported varies from 2005 to 2007.

Table 3.2: Files characteristics of the Mexican Wind Atlas and Wind Project.

In the files of the Mexican Wind Atlas, other variables are included. There is wind direction data, the maximum and minimum wind speed, pressure, temperature, relative humidity at different heights, and air density. However, these variables were not considered, but they are mentioned because they can extend the analysis.

Data availability

The time series of the study sites have homogeneity problems. Anemometers record data automatically, but instrumental problems could occur, resulting in unreliable or unreported values. The unreported values are presented in Figure 3.3, as well as the percentage of data available for each site.

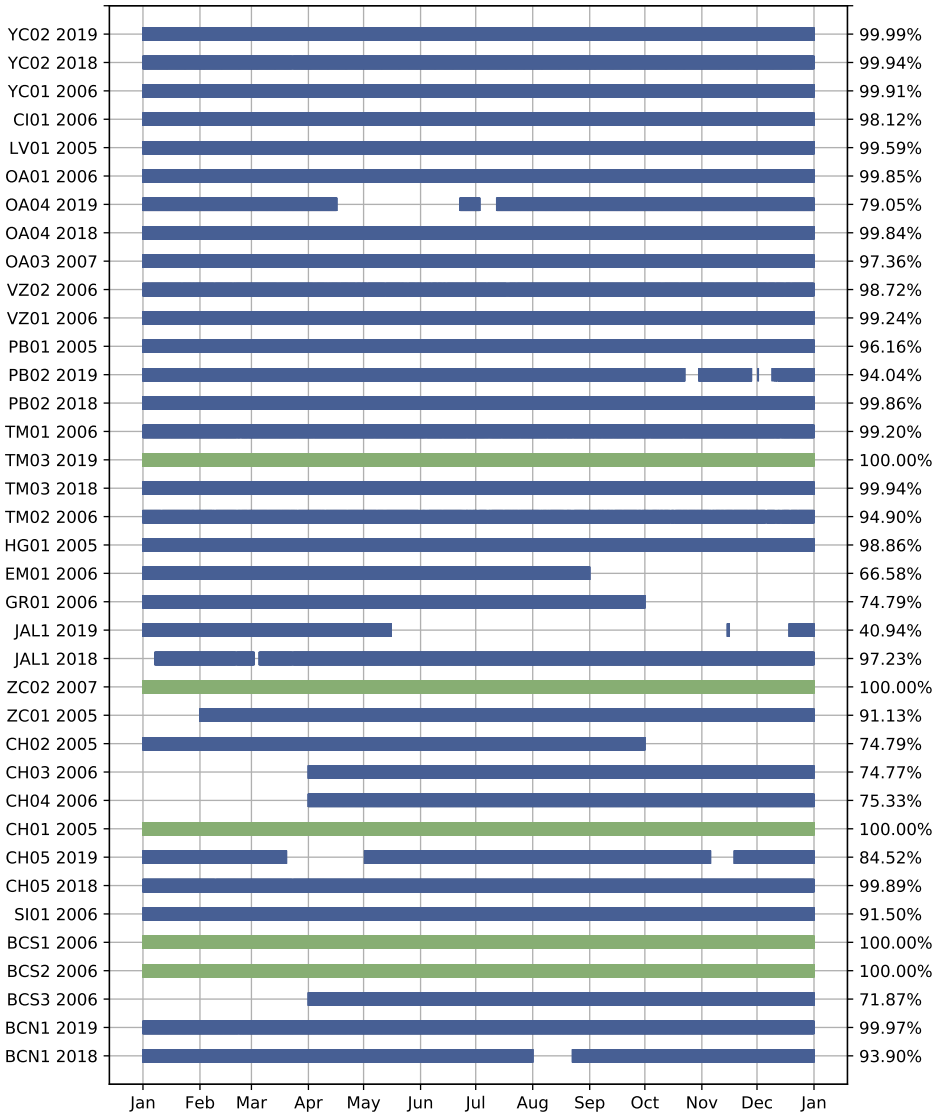

Figure 3.3: Observations data availability. Green bars represent complete time series and blue bars incomplete time series. The measurements are averaged hourly, so 100% means 8760 hours.

More than half of the sites have time series with a high amount of data. Five sites have complete time series, which are TM03 2019, ZC02 2007, CH01 2005, BCS2 2006, and BCS1 2006. Seventeen sites have a time series with 95% of the data, and four sites

have a time series with less than 75% of the data. JAL1 is the site with the least amount of data reported, with 40.94% in 2019; this is not a problem because, for 2018, its time series has 97.23%. Regarding this, for the sites with time series of two years, the year used for the bias correction was the most complete.

As the time series will be compared with ERA5 data, which has an hourly temporal resolution, the time stamp was homologated by averaging the observations wind speed from 10 minutes to an hour.

3.2.3 Electricity demand data

The electricity demand data are hourly time series grouped for each of SEN's control region. The data is obtained from the National Centre of Energy Control (CENACE, by its initials in Spanish), which estimates the actual demand using a balanced method by considering the net electricity generation injected into the system, minus the exported energy, including technical and non-technical losses [62].

The time series correspond to the years 2017, 2018, and 2019 and are reported on UTC-6 for the SIN, UTC-7 for BCS, and UTC-8 for BCA [63]. The data availability is 99.90%; in total, there are missing 27 hours per region: the entire day of July 16, 2019, and each year one hour in March for BCA, and one in April for the rest of the regions [4].

3.2.4 MERRA2 reanalysis data

The Modern-Era Retrospective analysis for Research and Applications version (MERRA2) is a reanalysis data produced by the NASA Global Modeling and Assimilation Office (GMAO) [64].

On Chapter 4 results obtained using MERRA2, from a paper who also evaluates the performance of reanalysis across Mexico [65] are discussed. Therefore, the most important characteristics of MERRA2 are presented below:

- **Spatial resolution:** 50 km horizontal and 72 levels.
- **Output frequency:** Hourly.
- **Data availability:** From 1979 to the present (up to three months ago).
- **Maxium height of wind field:** 50 meters.

[4] In March the days are 11,12 and 13, in April 08,02 and 03, for 2019, 2018 and 2017, respectively

3.3 Electricity demand growth rate

The values of the annual average electricity demand growth rate per region (Table 3.3) are obtained from the Electricity Sector Prospective 2018-2032 [66]. These values are estimated considering the energy consumption, losses, and exchange between countries.

Region	BCA	BCS	NOR	NTE	NES	OCC	CEN	ORI	PEN
Electricity demand growth rate [%]	3.2	3.6	3.3	3.1	3.4	3.3	2.6	2.8	3.9

Table 3.3: Electricity demand annual average growth rate by control region, 2018-2032.

The control regions with the highest rates of growth in its consumption will be Peninsular, 3.9%, and Baja California Sur, 3.6%; the ones with the lowest rates will be Central, 2.6%, and Oriental, 2.8%.

3.4 Wind turbine selected

The wind turbine used is the Vestas V90-2MW. This technology has a rated power of 2 MW, the hub height is considered at 100m, the rotor diameter is 90m, its cut-in speed is 4m/s, the cut-out speed is 25 m/s, and the rated speed is 12 m/s [67]. In Figure 3.4 it is presented the Vestas V90 power curve, which is used for all sites considering the standard air density value 1.225 kg/m^3.

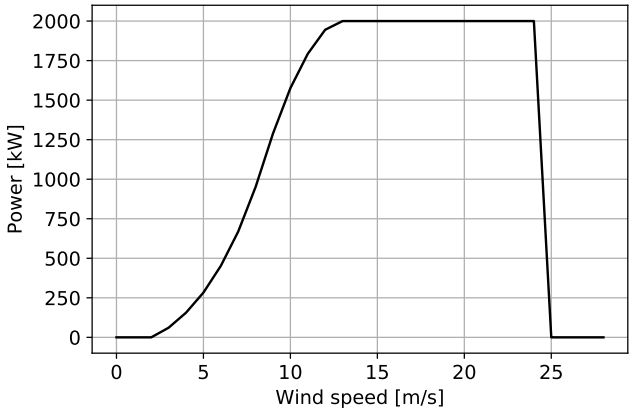

Figure 3.4: Vestas V90-2MW power curve

3.5 Methodology

The project's aim is achieved with three main steps, which are presented as the results chapters (Figure 3.5). There is synergy and interrelation between them; indeed, they have this order because the first produces inputs for the second and the second for the third. In this Section, the general methodology is commented on; later, it is presented in each chapter a detailed methodology of the processes followed on them.

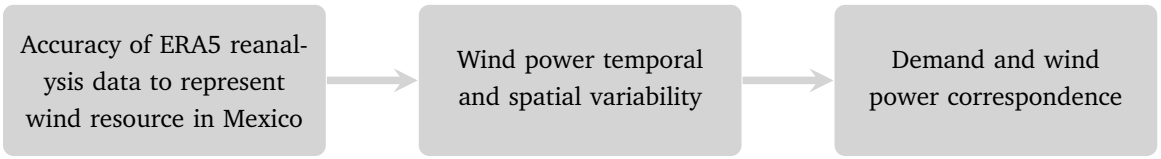

Figure 3.5: Thesis' results chapters

The first part allows having time series of the same year and the same characteristics for all the study sites. Besides reporting the data differently, the observations time series are for different years; therefore, they cannot be correlated. This step assesses the suitability of ERA5 reanalysis data for wind power estimation in Mexico. The observations time series of wind speed and capacity factor are compared with the ERA5 time series, using statistical and graphical methods. Corrections are made to improve its performance, and the results obtained provide comparable time series for the next step.

The second step, characterize the wind resource variability and measure the interconnection potential. The sites' wind resource is analyzed on different temporal scales, allowing one to understand the wind's temporal and spatial variability and see how it could be decreased, taking advantage of the resource diversity. Apart from the analysis, this step output is the regional time series obtained since the analysis is also made on a regional scale. The regional time series are needed because the demand data is reported by region.

The last results chapter investigates the potential of wind power to meet electricity demand in Mexico. It describes the wind generation and electricity demand compatibility, and the installed capacity needed to accomplish two-thirds of Mexico's clean electricity generation target for 2024 is estimated, under certain circumstances and considering the temporal variability of the wind resource.

3.6 Chapter summary

In this chapter, it has been described the data and the methodology used in this work. The study sites have been located on the map of Mexico, and the demand regions have been presented for the wind-demand analysis and to group the sites by region. The data used are wind speed time series from observations and reanalysis, the technology power curve, the electricity demand time series, and the average annual growth rate values of electricity consumption. The detailed characteristics of each data set have been mentioned, including their availability, where they were obtained, resolution, and features of the files and reanalysis.

The methodology focuses on three steps which are the general actions of each chapter: 1) Obtain reliable data of wind speed for the study sites for the same year, 2) Calculate the temporal and spatial complementarity on a local and regional scale, 3) Estimate the correspondence of the wind generation and demand, and with the knowledge of 2 calculate the number of wind turbines needed to meet two-thirds of Mexico's clean energy goal with wind energy.

Chapter 4

Accuracy of ERA5 reanalysis data to represent wind resource in Mexico

A close look at the site's characteristics is needed on a wind farm project to ensure suitability. One of the features studied is wind speed, through this variable different aspects could be selected, estimated, and modeled, such as the wind turbine, the energy production, and the electrical grid [13].

Wind speed observations are high-resolution data, but the time and cost to measure for a specific place are downsides. Reanalyses are an important information source for wind energy applications [68]. They are gaining popularity because the data are accessible, describe long periods, and have a global coverage [69]. However, reanalyses data sets come with their uncertainties stemming from biases in the observations and model parameterizations, the assimilation data processes, and the output of atmospheric variables into discreet points [55], so before using them, the data should be validated. They should only be relied upon once thoroughly proven [69].

The content of this chapter is part of the approach to achieve the thesis's general aim. Given that the observations wind speeds are from different years, ERA5 provides data of the same year for all sites; from it, the sites can be correlated and their complementarity studied; nevertheless, these data should be validated. This chapter aims to assess the suitability of ERA5 for wind power estimation in Mexico by comparing the wind speeds and capacity factors obtained from the observations and the reanalysis dataset.

The chapter begins by describing the methodology followed to measure ERA5 precision and the statistical technique (bias correction) applied to improve the output data (Section 4.1). In Section 4.2, the overall performance of ERA5 is presented, describing it by wind speed (Subsection 4.2.1) and by capacity factor (Subsection 4.2.2). In these last sections, the ERA5 data without bias-correction and with bias-correction are compared and analyzed using graphical and statistical methods.

4.1 Chapter methodology

This section explains the methodology followed (Figure 4.1) to compare and analyze wind speed data of measurement towers against reanalysis data from ERA5 at different spatiotemporal scales. Also, the method applied to improve ERA5 performance by using the time series of the observations wind speeds is explained.

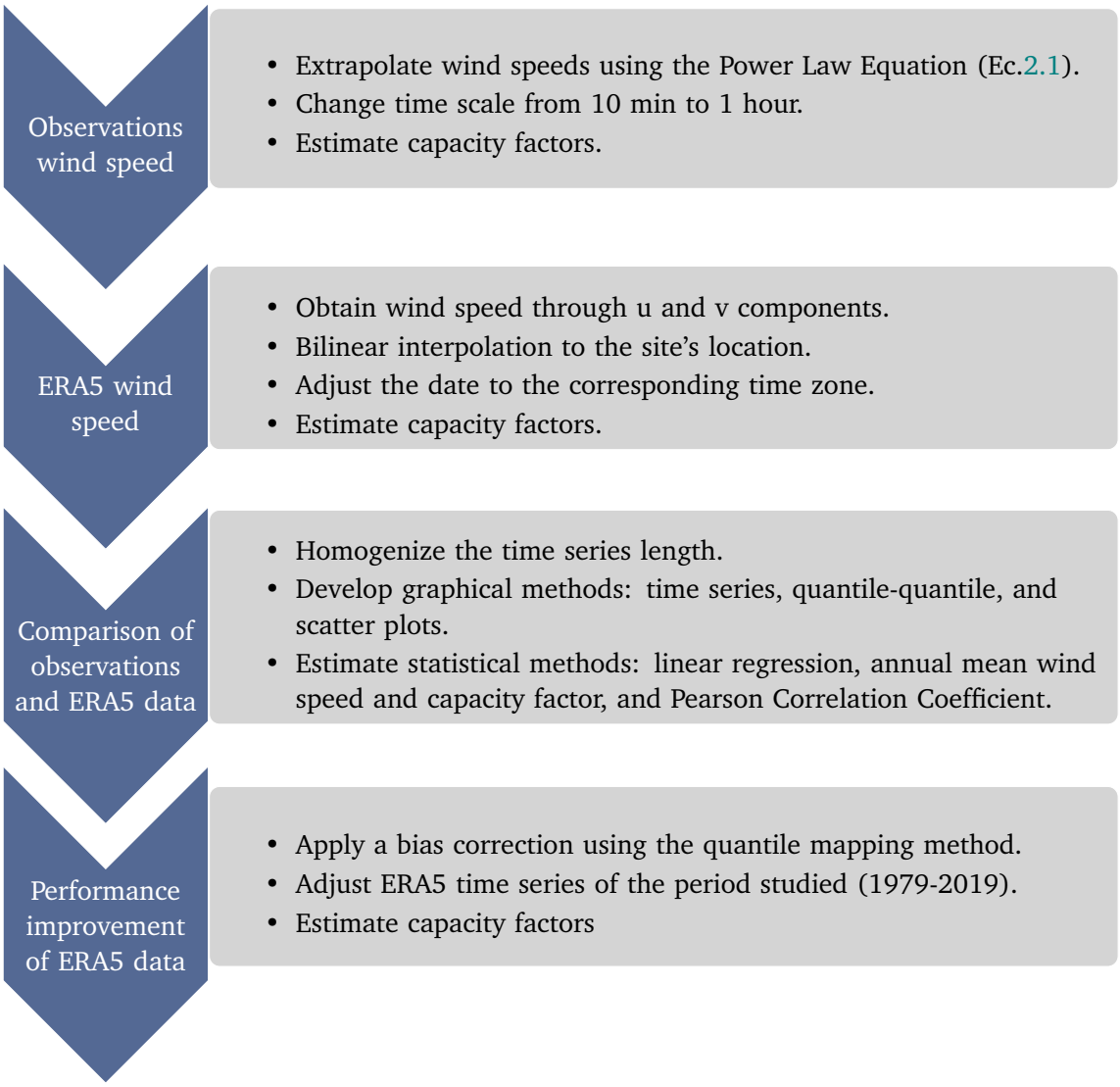

Figure 4.1: Methodology to assess the accuracy of ERA5 reanalysis data to represent the wind resource in Mexico

The methodology displayed follows a similar technique to what is presented in [65], where wind speed and capacity factors in Mexico are also estimated using reanalysis data to measure how well it represents the wind resource. Differences are that in the present

work, the observations wind speed time series were extrapolated using the Power Law Equation to the reanalysis data height, 30 sites of Mexico were analyzed, and ERA5 reanalysis data was used. While in [65], the reanalysis data were interpolated assuming a logarithmic vertical wind profile to the specific height of the measurements, 24 sites were analyzed, and it was used MERRA-2 reanalysis data.

4.1.1 Observations wind speed adjustment

The observed data were adjusted to be comparable with the ERA5 data. Therefore, hourly wind speed time series at 100 m were desirable. It was created and saved as a NetCDF file, a database with wind speeds at eight heights: 20, 30, 40, 50, 60, 70, 80, and 100 meters, for the thirty study sites. Although only the wind speeds at 100 m were used, this database can be helpful for future projects, for example, to study the vertical wind profile of the covered sites.

As presented in Table 3.2 the wind speeds time series are reported at different heights. The time series sites whose reported wind speeds were not at the heights defined for the database were extrapolated using the Power Law (Ec. 2.1). The value of α was chosen depending on the number of known heights, either constant or dynamic. Figure 4.2 presents the process followed to determine the α to be used depending on the reported height of the different sites.

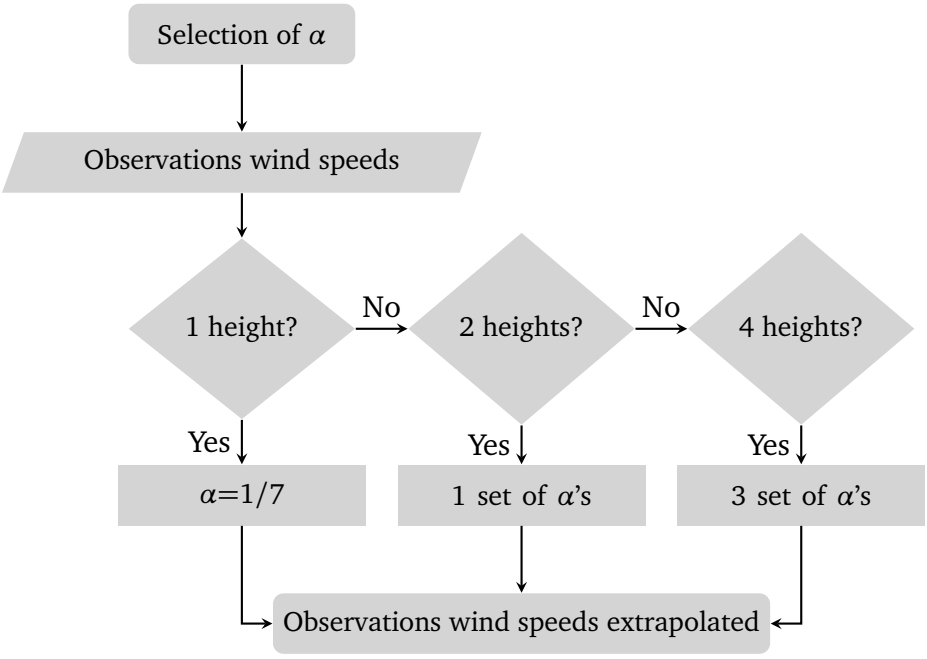

Figure 4.2: Process to determine the value of the Power Law exponent (α).

For sites with one and two heights, the α selected and estimated was used to extrapolate to all heights. The original measurements of these sites were not above 20 m, so there were no interpolations. For the sites with four heights, which are the ones obtained from the Mexican Wind Atlas, the sets of dynamic α's were calculated as follows:

1. From 20 to 40 m to extrapolate from 20 to 30 m.
2. From 40 to 60 m to extrapolate from 40 to 50 m.
3. From 60 to 80 m to extrapolate from 60 to 70 m and from 80 to 100 m.

Figure 4.3 presents an error-bar plot showing the mean and standard deviation of the sites with two heights. The color represents the range in which a more significant number of values are reported. The values and the standard deviation obtained show the dynamism of the atmosphere. For 17 of the 24 sites with more than one height, the higher frequencies were around the typical value of 1/7.

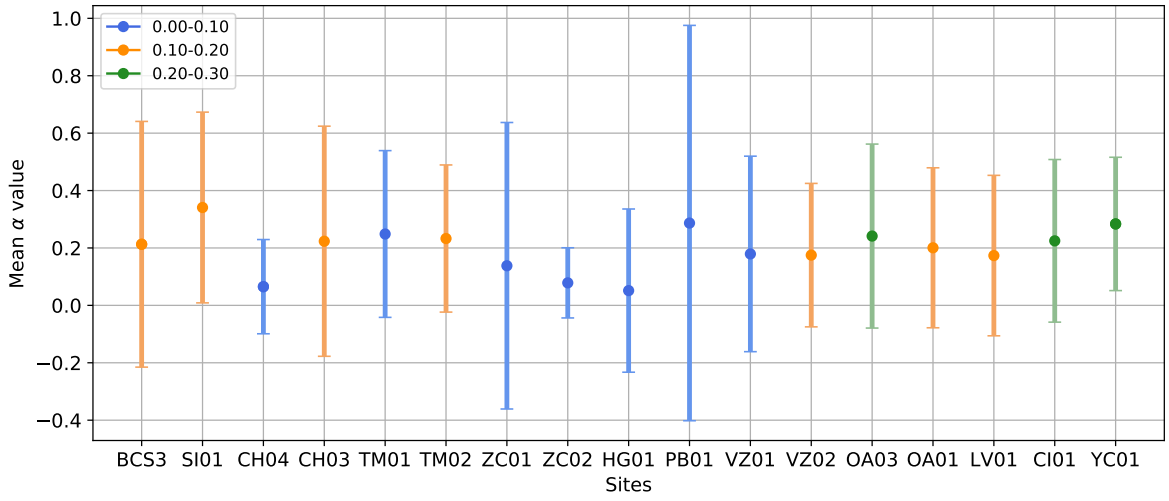

Figure 4.3: Error bar plot representing the mean and standard deviation of the dynamic α's of the sites with two heights. The color represents the most common range. The dynamism of the atmosphere is observed with no small error bars.

The α's that produce wind speed peaks were filtered. These errors are due to inaccuracies in the measurement equipment, which reports low values, and therefore a peak is generated.

Once the wind speeds were extrapolated, they were averaged to an hour to have the same timestamp as ERA5.

4.1.2 ERA5 wind speeds obtainment

The wind speed components of the respective year at the location of the measurement stations were obtained from a bi-linear interpolation (Subsection 2.2.1). Wind speed was

calculated at each timestep through the expression: $\sqrt{u^2 + v^2}$. Then, it was adjusted to the corresponding time zone (UTC-6, UTC-7, or UTC-8).

4.1.3 Comparison between ERA5 and observations

The first steps rearranged the temporal and spatial scales to compare the measured and reanalysis data. The observations wind speed does not have complete measurements (Figure 3.3), so the length of the time series was homogenized to compute the metrics used; accordingly, if a time step of the observations was missing, it was removed from the ERA5 data set.

The observed and ERA5 wind speeds and capacity factors inter-comparison was made using graphic and statistical methods. The graphic techniques used were:

- Times series plots.
- Quantile-Quantile plots (Q-Q plots).
- Scatter plots.

The statistical techniques used were:

- Linear trends (Subsection 2.2.3).
- Annual mean wind speed and capacity factor.
- Pearson Correlation Coefficient (Subsection 2.2.4).

4.1.4 ERA5 calibration

A bias correction (Subsection 2.2.1) was made to improve the performance of the reanalysis data. The same methods (graphic and statistical) were used to compare the observations and ERA bias-corrected wind speeds.

The correction found was assumed valid for the rest of the studied period (1979-2019). It was applied to the wind speeds of the 41 (complete) years for their use in the following chapters.

4.1.5 Capacity Factor estimation

The Capacity Factors (CF) were estimated following Eq. 2.3. The Annual Energy Produced (AEP), which is used to estimate the CF, was calculated using Eq. 2.2, the power was obtained by evaluating the time series wind speed on a polynomial that fits the power curve of the selected technology (Vestas V90-2MW).

4.2 Overall Performance of ERA5

In this section, it is discussed the comparison between observations and ERA5 wind speeds and capacity factors. Site-specific plots depicting group patterns are presented.

4.2.1 Wind speed

ERA5 data non bias-corrected

The wind speeds obtained from ERA5 appropriately reproduce the dynamics of the observations wind speeds apart from the magnitude (Figure 4.4). When the wind speed goes up in the measured data, it also goes up in the ERA5 data; the same happens when it goes down. ERA5 considers the prevailing winds [70]. During a few hours, the wind speeds data sets do not link together; a reason could be that ERA5 does not detect local winds.

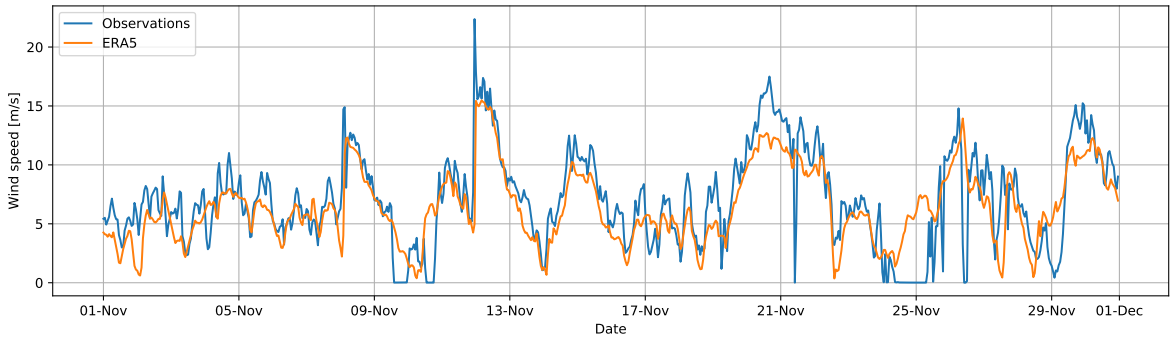

Figure 4.4: Observations wind speed (blue) and ERA5 wind speed (orange) of San Fernando, Tamaulipas (TM03), November 2019. The dynamics of the winds speed are accurately reproduced apart from the magnitude; the observations line tends to be above the ERA5 line.

ERA5 tends to underestimate or overestimate the wind speeds; however, there are some sites in which for a range of wind speeds ERA5 represents them well. Figure 4.5 presents the Quantile-Quantile plots of the observations and ERA5 wind speeds. What is desired is that the points fall on the identity line (black line), meaning that the reanalysis data perfectly coincide with what was observed.

In all the sites, ERA5 underestimates the wind speed. Except for five sites, the underestimation range differs according to the site, but in JAL1 (Figure 4.5b), ZC02, CH02, TM02, and YC01, it occurs for all the wind speeds. In two sites: BCS3 (4.5a) and BCS2, the underestimation happens for values above 10 m/s. In three sites: TM03 (Figure 4.5c), CH03, and CH01, it happens for values above 5 m/s, and in the other sites, the underestimation occurs from values between 3 and 1 m/s.

There is an overestimation of the wind speeds in five sites. In three sites: ZC01, GR01, TM03 (Figure 4.5c), the overestimation happens for values below 2 or 1 m/s; and in two sites: BCS3 (Figure 4.5a) and BCS2, it happens below 7 m/s.

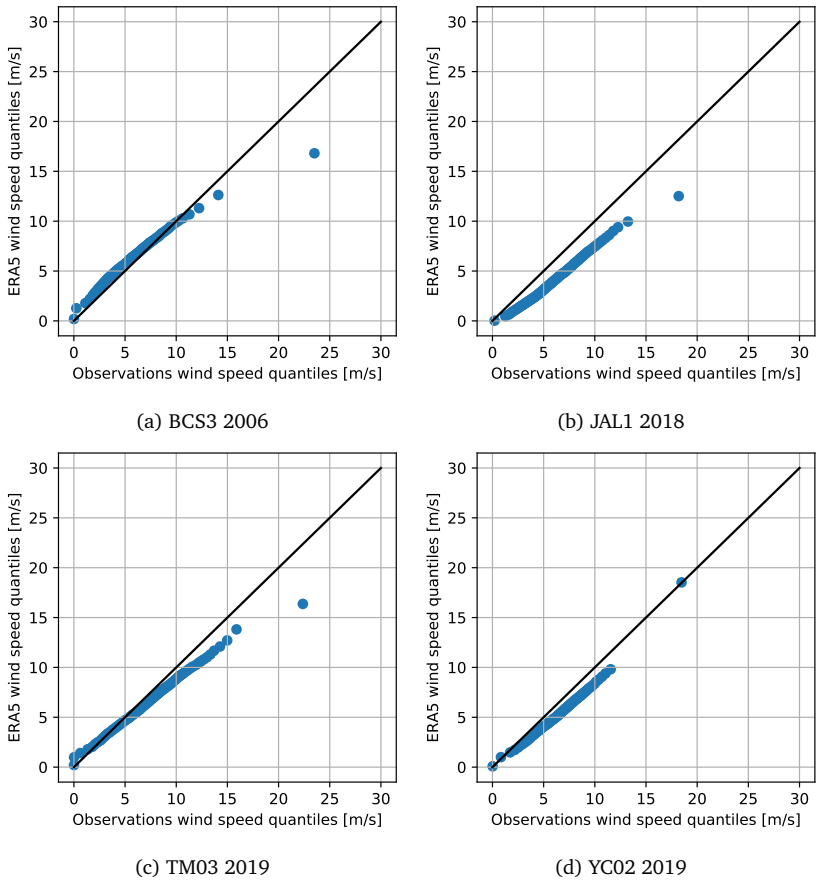

(a) BCS3 2006

(b) JAL1 2018

(c) TM03 2019

(d) YC02 2019

Figure 4.5: Q-Q plots of observations and ERA5 wind speeds representing the overestimation and underestimation of ERA5 data. In BCS3 (a), the wind speeds below 10 m/s are overestimated, and above 10 m/s are underestimated. In JAL1 (b), all the wind speeds are underestimated. In TM03 (c), the low wind speeds are overestimated, and the high wind speeds are underestimated. In YC02 (d), the low wind and high wind speeds are well represented.

Aside from the sites where all values are overestimated, the others are well represented around a particular range. The range in which ERA5 and observations wind speeds correspond is between the underestimation and overestimation values mentioned before, except in YC02. For example, in BCS3 (Figure 4.5a), the wind speeds between 7 and 10 m/s are well represented, in TM03 (Figure 4.5c), the wind speeds between 1 and 5 m/s, and in YC02 (Figure 4.5d) the wind speeds between 0-2 and around 18 m/s.

In all the sites, the difference between observations and ERA5 wind speeds increase on the high values but in YC02 (Figure 4.5d) not. In this site, the last quantile is well represented.

ERA5 data bias-corrected

The ERA5 wind speed bias-corrected continues following the observations wind speed dynamics. After the correction, the overestimated values decreased, and the underestimated values increased (Figure 4.6).

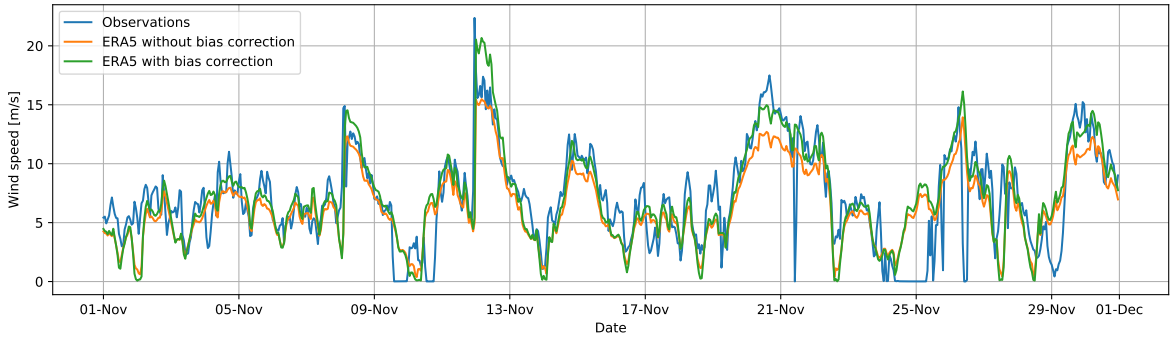

Figure 4.6: Observations wind speed (blue), ERA5 wind speed bias-corrected (green) and non-bias-corrected (orange) of San Fernando, Tamaulipas (TM03), November 2019. The decrease of the underestimation is noticeable on the green line, which is above the orange line.

The statistical methods were used to have an indicator of the comparison between ERA5 data with real values. In this sense, Figure 4.7 presents scatter plots of observations wind speeds and ERA5 data bias-corrected and non-bias-corrected with the regression line that adjust the data sets for three sites: OA04, ZC01 and BCS3, and its Pearson Correlation Coefficient (r).

The bias correction improves the linear least-squares fit; hence the slope value increases. After the correction, in sixteen sites, the slope is between 0.70 and 0.90, these sites are all the sites of BCA (1), NES (3), ORI2 (5), four of the five sites of NTE, two of the three sites of NES, and one of the two sites of PEN region; from these, the slope is closer to 1 on the ORI2 sites, for example in OA04 (Figure 4.7a) the slope is 0.89 for 2019. In twelve sites, the slope is between 0.5 and 0.7, which is the case of ZC01, with a value of 0.64 (Figure 4.7b). The two remaining sites, BCS3 (Figure 4.7c) and PB01 have a slope of 0.35 and 0.44, respectively.

The sites presented in Figure 4.7 exemplify the categories of the slopes. Something else that can be commented on these sites is their distributions. OA04 has bi-modal distribution; one cluster is around 5 m/s and the other around 13 m/s; for ZC01 and BCS3, there is a big cluster around 5 m/s. Also, the BCS3 distribution is circular, representing more dispersed data and thus a weak Pearson value. In OA04, many points align with the identity line; consequently, the Pearson value is strong.

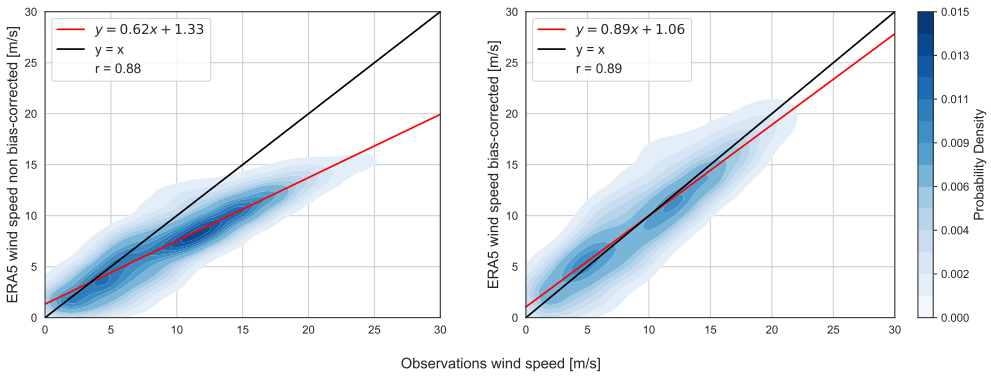

(a) OA04 2019

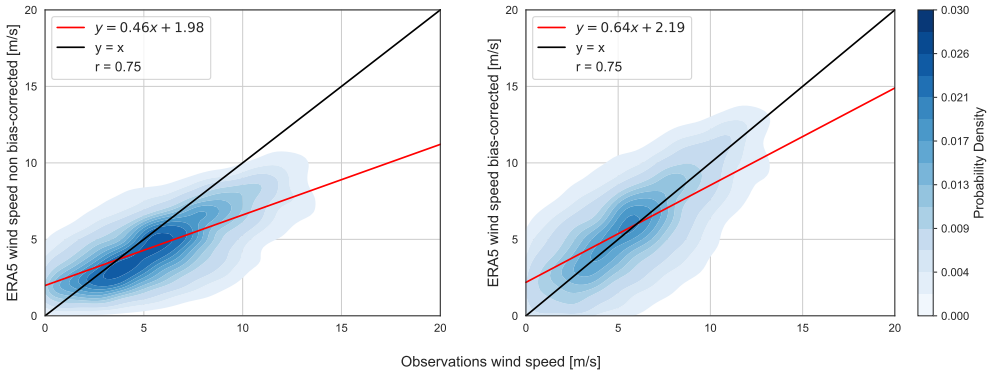

(b) ZC01 2005

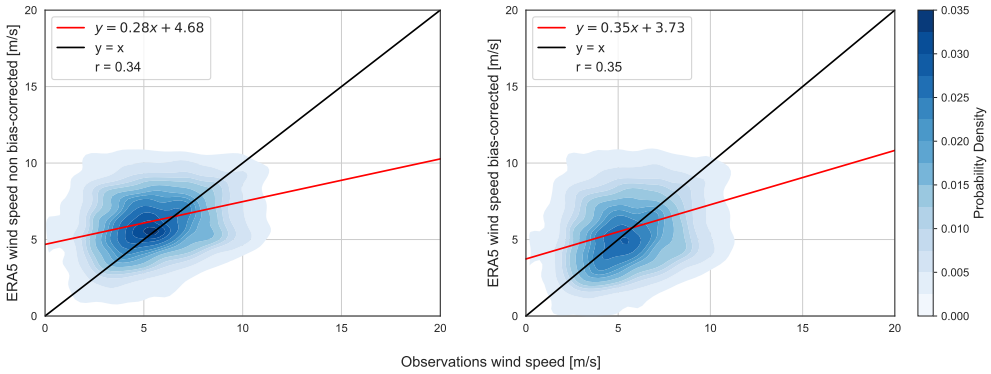

(c) BCS3 2006

Figure 4.7: Scatter plots of wind speed observations against non-bias-corrected (left) and bias-corrected (right) wind speeds from ERA5. The black line represents an identity relationship. The red line represents the regression line. The shading indicates the probability density of points. The Pearson value (r) is located on the legend on the top left.

Figure 4.8 shows the annual mean wind speed of observations, ERA5 non-bias-corrected, and bias-corrected wind speed data. The correction improvement is seen on the values of this variable, where the annual mean wind speed estimated with the ERA5 data bias-corrected is practically the same as the observations. The commented question regarding underestimation and overestimation is appreciated. The two sites, BCS3 and BCS2,

where the wind speed was overestimated, have ERA5 corrected markers below the initial ERA5 values. The wind speed was principally underestimated on the rest of the sites, so the fixed marker is above the initial one.

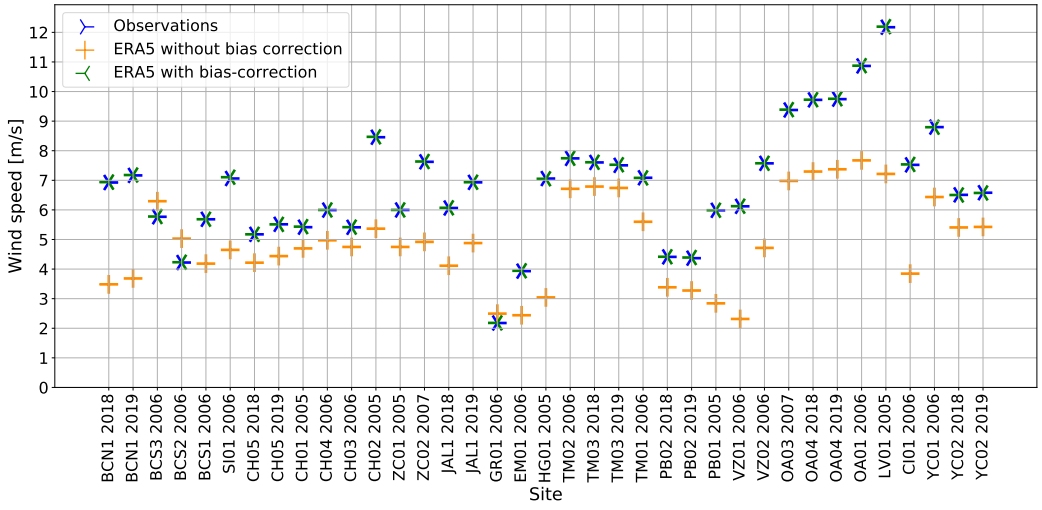

Figure 4.8: Annual mean wind speed of of observations (blue), ERA5 non-bias-corrected (orange), and bias corrected wind speed data (green).

Correlative analysis

In Figure 4.9, the results of the Pearson Correlation Coefficient (r value) before (a) and after (b) the bias correction are presented. The color of the points represents the strength of the correlation: red, weak; yellow, moderate; blue, significant; and green, strong. The range of the r values goes between 0.35-0.89, indicating that the performance of the reanalysis data is not uniform across the country; it depends on the site.

The yellow and red points are primarily located in the Baja California Peninsula and the Trans-volcanic Belt (central region). In these regions, ERA5 struggles to represent the resource probably because of the complexity of the terrain. In Baja California, the rapid transition between land and sea on both sides of the Peninsula impacts the result; it is also a narrow piece of land where few model grids fit, between five and nine. In the central region, the orography is complex due to many mountains; moreover, the PB01 site, red point, is near a big lagoon, whose surface area is 1.81 km^2, so this body of water could be affecting.

The blue and green points are primarily located in Tamaulipas, Oaxaca, and Chiapas, where the flow is determined by large-scale circulation and its interaction with the large-scale orography. For example, in Oaxaca and Chiapas, there is a gap between the mountain ranges, so it generates a canal effect.

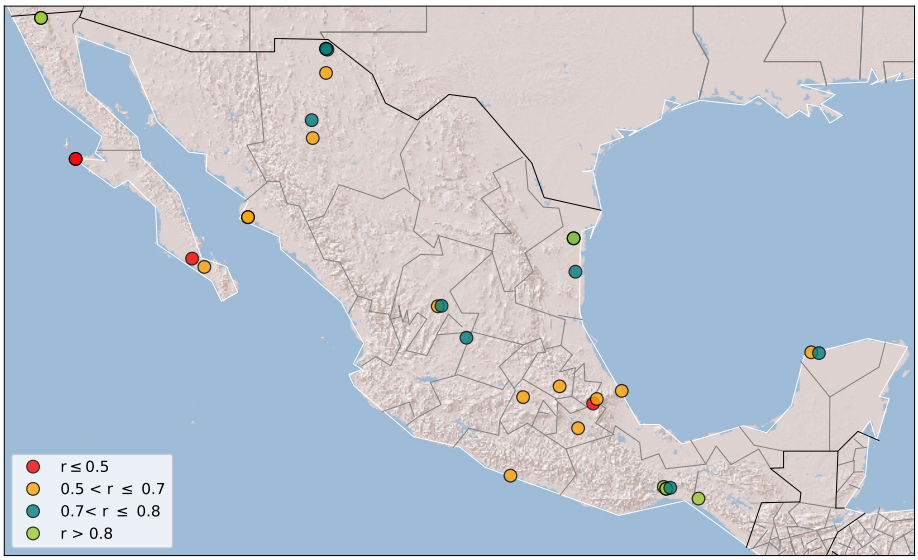

(a) Before bias correction

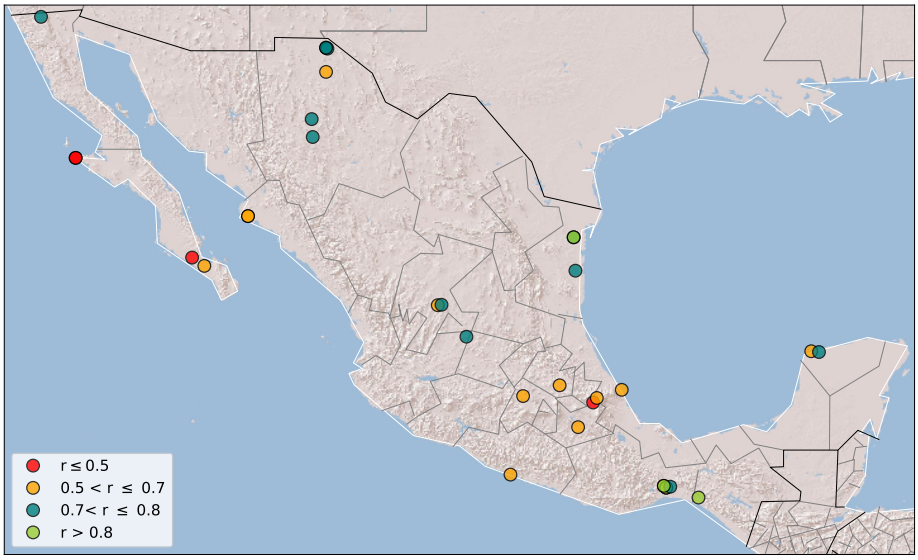

(b) After bias correction

Figure 4.9: Sites location and Pearson Correlation Coefficient using ERA5 non-bias-corrected (a) and bias-corrected (b) data. The marker color represent the strength of the correlation: red, weak; yellow, moderate; blue, significant; and green, strong.

The bias correction does not significantly change the r value. Two sites' points change color after the bias correction, but the rest remain the same. In CH01 the value increase, which is expected, changing from yellow to blue; and in BCN1, the value decreases. What happens in BCN1 is that large values exist from the beginning, when the correction is applied, these values that are within the underestimated last quantile increase more; they are not a lot but still impact increasing the dispersion. What happens in the other sites

is related to what happens in BCN1; the covariance will increase because the variation between the two values decreases after applying the bias correction; however, the values will define the change on the standard deviation.

Even though the r value does not change, there is an improvement in the data representation. For example, in OA04 2019 (Figure 4.7a), the data after the bias correction is duly aligned and distributed along the identity line.

The reanalyses resolution influence the results. The Pearson Correlation Coefficient estimated using ERA5 and MERRA-2 [65] hourly time series bias-corrected are compared on Figure 4.10.

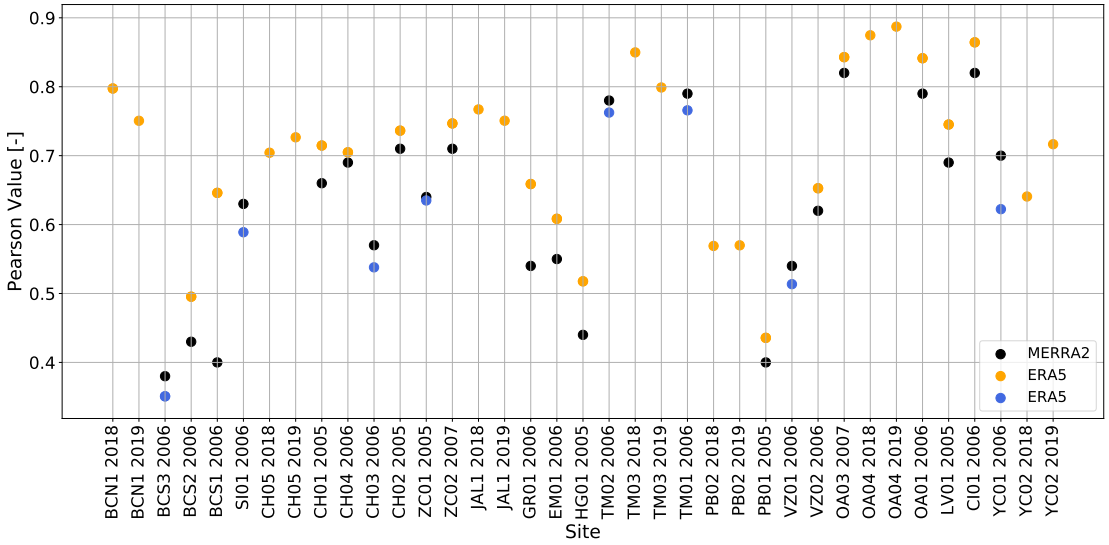

Figure 4.10: Pearson Correlation Coefficient estimated with the bias-corrected data of ERA5 and MERRA-2. The MERRA-2 values are represented with black points, and the ERA5 values with yellow points if the value is higher than in MERRA-2, for example, BCS2 2006; and with blue points, if it is lower, like in BCS2 2006.

The sites compared are those that do not report wind speeds in 2018 and 2019 because the Mexican Wind Atlas sites were not considered in [65]. The black points represent the MERRA-2 values, and the yellow and blue points the ERA5 values. The blue and yellow color means a higher value than MERRA-2 and a lower value, respectively.

For twenty-two sites, the Pearson coefficient is better using ERA5, and the improvement is significant. ERA5 has a better horizontal resolution, 30km grid compared with MERRA-2 50 km grid [71, 72], so this may explain the improvement of the values, as other physical conditions are considered. Likewise, the reanalyses are performed by different institutions, ERA5 by the European Centre for Medium-Range Weather Forecast and MERRA-2 by the National Aeronautics and Space Administration; thus, the numerical models used for the prediction might change.

Taking up the ERA5 performance topic, it was mentioned that it was influenced by the complex orography and the rapid transition between land and sea/water; however, the hypothesis exists that other variables could affect the magnitude of the wind speeds. The extra variables analyzed are the percentage of data and the number of heights at which wind speed is reported. In Figure 4.10, the specific Pearson values are presented, and they were related to these two variables.

The number of heights is not affecting significantly. Sites that report wind speeds at four heights (measured in 2018 and 2019) have a performance similar to the surrounding places, despite the year; for example, the sites starting with CH, OA or, YC (one year), and also JAL, which is in the same region as ZC02. The values are a little higher but not more than one decimal (except CH03), like YC01 reports 0.62 and YC02 0.72 (Table 4.1). Furthermore, it cannot be assumed that the number of heights causes it because different years are being compared.

The percentage of data is not affecting the strength of the correlation. Seven sites have a data percentage below 80%; four out of seven (CH02, CH03, CH04, and JAL1) have a Pearson between 0.70-0.80. It is concluded that it does not affect because all Chihuahua (CH) sites have a similar Pearson coefficient despite the percentage of the data, except CH03. Also, an interesting thing related happens in JAL1: the portion of data reported for 2018 and 2019 are entirely different, 97.23% and 40.94%, respectively (Figure 3.3); even so, the values are similar 0.77 and 0.75. In this case, the missing data is during summer and fall, where the wind speeds are not high, which could explain that the higher wind speeds possibly dominate the correlation.

Mentioning another case related to the performances is GR01. The low Pearson value could be because of measurement equipment errors in this site since a significant percentage of the data, 51%, is between 0-1 m/s.

The impact of the time scale was studied by comparing the Pearson coefficients obtained after the bias correction at different time averages. Table 4.1 presents the values using hourly, 6-hourly, 12-hourly, daily, and weekly bias-corrected wind speed time series. For the sites that report for two years, both results were presented. The cell color represents the strength of the correlation as in Figure 4.9.

As the average time increases, the correlations improve. Using the hourly time series, eight elements have a Pearson value above 0.80, and using the weekly time series, the number increase to twenty-seven. This happens because the influence of local weather conditions decreases as averaging occurs, and the effects of driving large-scale circulation increase.

Sites	Hourly	6-Hourly	12-Hourly	Daily	Weekly
BCN1 2018	0.80	0.86	0.90	0.93	0.93
BCN1 2019	0.79	0.85	0.88	0.90	0.87
BCS3 2006	0.35	0.41	0.47	0.48	0.59
BCS2 2006	0.50	0.56	0.64	0.79	0.83
BCS1 2006	0.65	0.69	0.74	0.75	0.80
SI01 2006	0.59	0.69	0.73	0.82	0.88
CH05 2018	0.70	0.79	0.83	0.86	0.87
CH05 2019	0.73	0.80	0.84	0.89	0.92
CH01 2005	0.71	0.79	0.82	0.88	0.90
CH04 2006	0.70	0.80	0.83	0.86	0.91
CH03 2006	0.54	0.66	0.67	0.71	0.64
CH02 2005	0.74	0.81	0.85	0.88	0.91
ZC01 2005	0.63	0.74	0.78	0.81	0.89
ZC02 2007	0.75	0.81	0.84	0.92	0.94
JAL1 2018	0.77	0.85	0.88	0.92	0.94
JAL1 2019	0.75	0.80	0.81	0.81	0.64
GR01 2006	0.66	0.74	0.78	0.77	0.71
EM01 2006	0.61	0.69	0.73	0.78	0.78
HG01 2005	0.52	0.57	0.63	0.53	0.54
TM02 2006	0.76	0.83	0.88	0.91	0.91
TM03 2018	0.85	0.91	0.93	0.96	0.96
TM03 2019	0.80	0.85	0.87	0.89	0.89
TM01 2006	0.77	0.85	0.89	0.91	0.92
PB02 2018	0.57	0.66	0.72	0.75	0.84
PB02 2019	0.57	0.69	0.74	0.76	0.86
PB01 2005	0.44	0.51	0.55	0.59	0.53
VZ01 2006	0.51	0.6	0.64	0.64	0.59
VZ02 2006	0.65	0.71	0.73	0.72	0.65
OA03 2007	0.84	0.88	0.91	0.93	0.96
OA04 2018	0.87	0.90	0.92	0.93	0.95
OA04 2019	0.89	0.92	0.93	0.94	0.96
OA01 2006	0.84	0.88	0.90	0.93	0.96
LV01 2005	0.75	0.78	0.79	0.82	0.92
CI01 2006	0.86	0.90	0.92	0.93	0.96
YC01 2006	0.62	0.69	0.81	0.81	0.79
YC02 2018	0.64	0.73	0.87	0.90	0.95
YC02 2019	0.72	0.79	0.89	0.92	0.95

Table 4.1: Pearson Correlation Coefficient using ERA5 bias-corrected data at different time scales. The cell color represents the strength of the correlation. As the average time increases, the correlations improve.

A site-specific example of the previously mentioned correlation behavior regarding the time average is ZC01, which has hourly correlations of 0.63 and weekly of 0.89. The correlations are always high in some stations, like the Oaxaca and Chiapas sites. At the same time, there are others where it does not improve, such as BCS3, HG01, PB01, and VZ01, because the orographic conditions are very complicated.

4.2.2 Capacity factor

The annual CF's are well represented with the ERA5 data bias-corrected (Figure 4.11). Before the bias correction, CF's are sub-estimated for twenty-eight sites and overestimated for two sites: BCS2 and BCS3, which is consistent with the commented before.

The annual mean wind speed value corresponds to the annual capacity factor. Sites with high wind speed and, consequently, high energy generation potential were found to have a high capacity factor, which likewise occurs the same with the low wind speed sites.

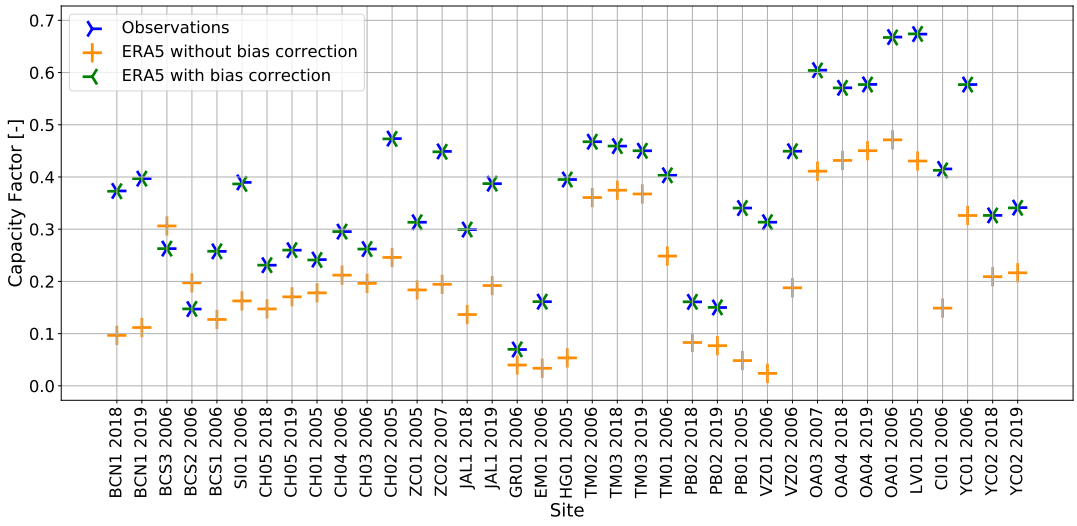

Figure 4.11: Annual capacity factors for observations (blue), ERA5 non bias-corrected (orange) and ERA 5 bias-corrected (green)

4.3 Chapter summary

This chapter studied the accuracy of ERA5 to assess the wind resource across Mexico by comparing time series from observations and reanalysis (non-bias-corrected and bias-corrected) for 30 sites. The time series were adjusted temporally and spatially to have uniformity on the data, and the evaluation was made using graphic and statistical techniques.

It is highlighted the Mexican wind resource diversity and the importance of validating ERA5 for different regions because its performance depends on local orography and large-scale circulation. It is concluded that ERA5 is suitable to describe the wind resource of sites influenced by global patterns. Still, caution must be taken for sites near the ocean or on a complex orography unless bias correction is made.

Chapter 5

Wind power temporal and spatial variability

Wind power is characterized by significant variability. A greater share of this variable renewable energy on the electric matrix means less overall predictability in how much electricity can be generated by the system. When the wind power generation decreases, other power plants must be scheduled to compensate for the gap between generation and demand. The challenge to accurately predict and schedule appropriate generation increases; hence, more flexibility will be needed to balance the system.

One of the mechanisms to increase flexibility is expanding the generation area (Table 1.1). The wind variability can be reduced by interconnecting the wind power generation of different places [23]. Assessing the spatial correlation of wind resources is an important and relevant topic. If two sites with low correlation are joined, the wind power generation would have fewer gaps because when one of the sites is not generating, the other is generating. Knowing the wind characteristics could improve the wind reliability by planning the harvesting of the wind [24].

This chapter focuses on characterizing wind resource variability and understanding its temporal and spatial features. The methodology is presented in Section 5.1. In section 5.2 the wind variability is analyzed monthly and hourly, and also nationally with country maps and regionally with radar charts of the capacity factor. In section 5.3 the characteristics of the wind resource are presented. The following section, 5.4, provides measures of the interconnection potential (wind complementarity), estimating the Pearson correlation coefficient between the capacity factor time series per site and region (Subsection 5.4.1), and measuring the generation hours increment by joining two regions (Subsection 5.4.2).

5.1 Chapter methodology

This section explains the methodology followed to measure and describe the wind power variability and complementarity. The analysis was carried out on a local and regional scale. There were made-up time series of each region's highest hourly wind speed for the regional analyses. The process to create them is the following:

1. The wind speed time series of a site was fixed (base).
2. Every hour of the base was compared with the wind speed of the other sites.
3. If an hour had a higher wind speed than the base, it took its place.

5.1.1 Temporal and spatial variability

In Section 5.2, the regional wind power variability was analyzed monthly and hourly. The maps in Figure 5.2 and Figure 5.1 show for the whole Mexican domain the mean capacity factor of 1979-2019 for each month and pairs of hours. The maps were created by taking the mean wind speed of the 41 years by month and hour and then evaluating them on the polynomial that fits the Vestas V90 wind turbine's power curve. To reduce the number of maps presented in Figure 5.1, the 24 hours of a day were divided into 12 periods, showing the mean capacity factor of two hours.

In Subsection 5.2.1, the regional wind variability was analyzed using the mean CF's of the 41 years by month and hour. The regional time series were used, and radar charts embodied the change.

5.1.2 Regional wind resource description

The different place's wind resources were analyzed (Section 5.3) to help understand the spatial correlation and wind behavior per region. The analyzed wind speed and capacity factor data are from 2017, 2018, and 2019, which correspond to the demand data's available years. Two graphic resources were used: the hourly profiles and the heatmaps with the Pearson correlation coefficient of the wind speed and capacity factor time series of the sites in the same region.

5.1.3 Wind complementarity

In Section 5.4, two methods are proposed to measure the interrelation of the regional wind resources: counting the increase in generation hours and estimating the Pearson's

Correlation Coefficient, both methods between two regions. The results are presented through heatmaps.

The increase in generating hours was measured using the index with a CF below 0.2. The process followed is the next one:

1. A base region was selected. Its indexes with a CF below 0.2 were identified and saved on a list.
2. The joined region is selected. Its indexes with a CF below 0.2 were added to the previous list.
3. It was counted the number of times the indexes appeared on the list. A one was added to a new list when the index was repeated. Meaning that if it appears two times, in both regions, there is no generation at that hour, but if it only appears one time, there is generation in one region.
4. The number of ones representing the hours with no generation was counted and subtracted from 8760 to have the total number of generating hours.

Complementary plots

In this chapter, in Subsection 5.2.1, Temporal variability of regional wind power, and Section 5.3, Regional wind resource characteristics, there are only presented the plots that exemplify a case or that have a behavior that challenges to follow its description just with the text. Nevertheless, the plots of all the regions for this subsection and section are presented at the end of this document in the Appendix A.

5.2 Temporal variability of wind resources in Mexico

The diurnal variation patterns of the CFs at the height of 100 m for 1979-2019 are shown in Figure 5.1. Diurnal patterns that match all regions are detected. The capacity factors increase from 14:00, being higher between 18:00 and 01:00, and lower between 8:00 and 11:00. The time at which the capacity factor is the highest and the lowest is diverse across the regions; this will be further discussed in the following subsection.

There are regions with low capacity factors during all hours of the day. These regions are located in the Sierra Madre Occidental, Sierra Madre Oriental, Trans-volcanic Belt, and Sierra Madre del Sur. Contrary to the monthly scale, the hourly scale shows hours in which the CF increases, that is, between 14:00-19:00; this can be seen in the band of the Sierra Madre Oriental as it is less wide.

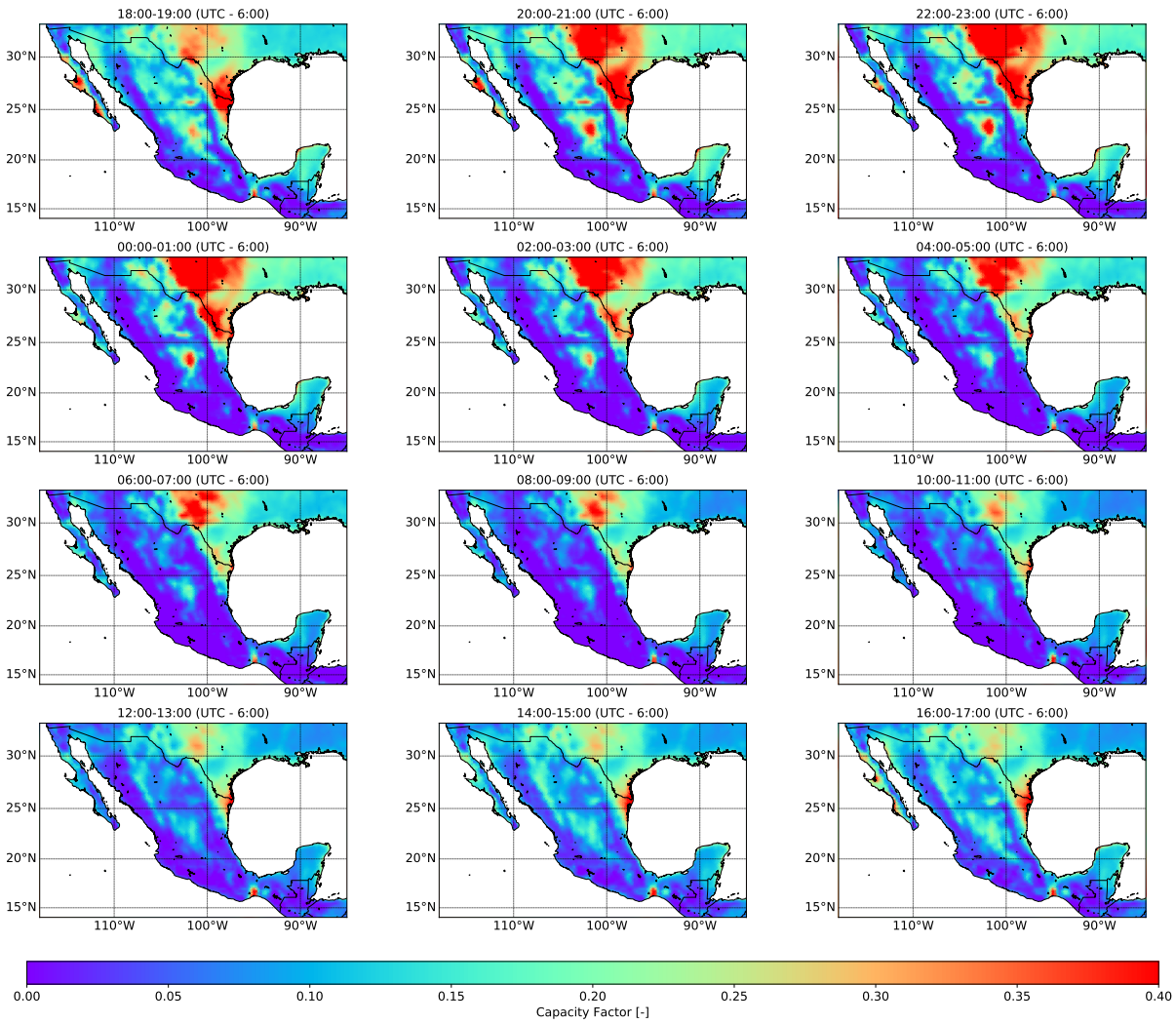

Figure 5.1: Mean capacity factor by hour of 1979-2019. The hour is presented in UTC-6. Diurnal patterns are appreciated. The CF increases at 14:00 and starts to decrease at 02:00. The red zones represent high CF values 0.30-0.40 (BCS, NES, OCC, and ORI2 regions). The purplish blue zones represent low CF values 0.00-0.10 (regions located in the Sierra Madre Occidental, Sierra Madre Oriental, Eje Neovolcánico, and Sierra Madre del Sur)

In the middle of the Sierra Madre Oriental and Occidental, the region that limits San Luis Potosí and Zacatecas shows a good wind resource. Unfortunately, there are no sites available to analyze it in more detail for this area. Zacatecas sites (ZC01 and ZC02) are located below this area and are affected by the Sierra Madre Occidental. This area reports higher values in the late evening 20:00-01:00, so it has the potential to complement during this time the NOR, OCC, and CEN regions.

The heat exchange due to the earth's warming by the sun explains part of the diurnal patterns. The earth's surface is heated by the sun, the temperature of the air close to the ground starts to increase; thus, the warm air starts to rise from the ground, and the cold

air starts to sink, forming the mixed layer [23]. In regions like BCA and BCS, the diurnal patterns are affected by breeze due to the land-ocean interaction [73].

Figure 5.2 shows the monthly variation patterns of the mean CFs at the height of 100 m for 1979-2019. For most of the regions in Mexico, the greatest CFs appears during spring. For example, in March, April, and May, the West Coast of Baja California Sur and the Yucatan Peninsular are colored with red and light blue, respectively, while in the other months, their color changes tending to lower CF values. Additionally, the lowest CF tends to occur during August and September. The Tehuantepec Isthmus is an exception; this region has higher capacity factors during winter and lowers during summer; however, its values are significant.

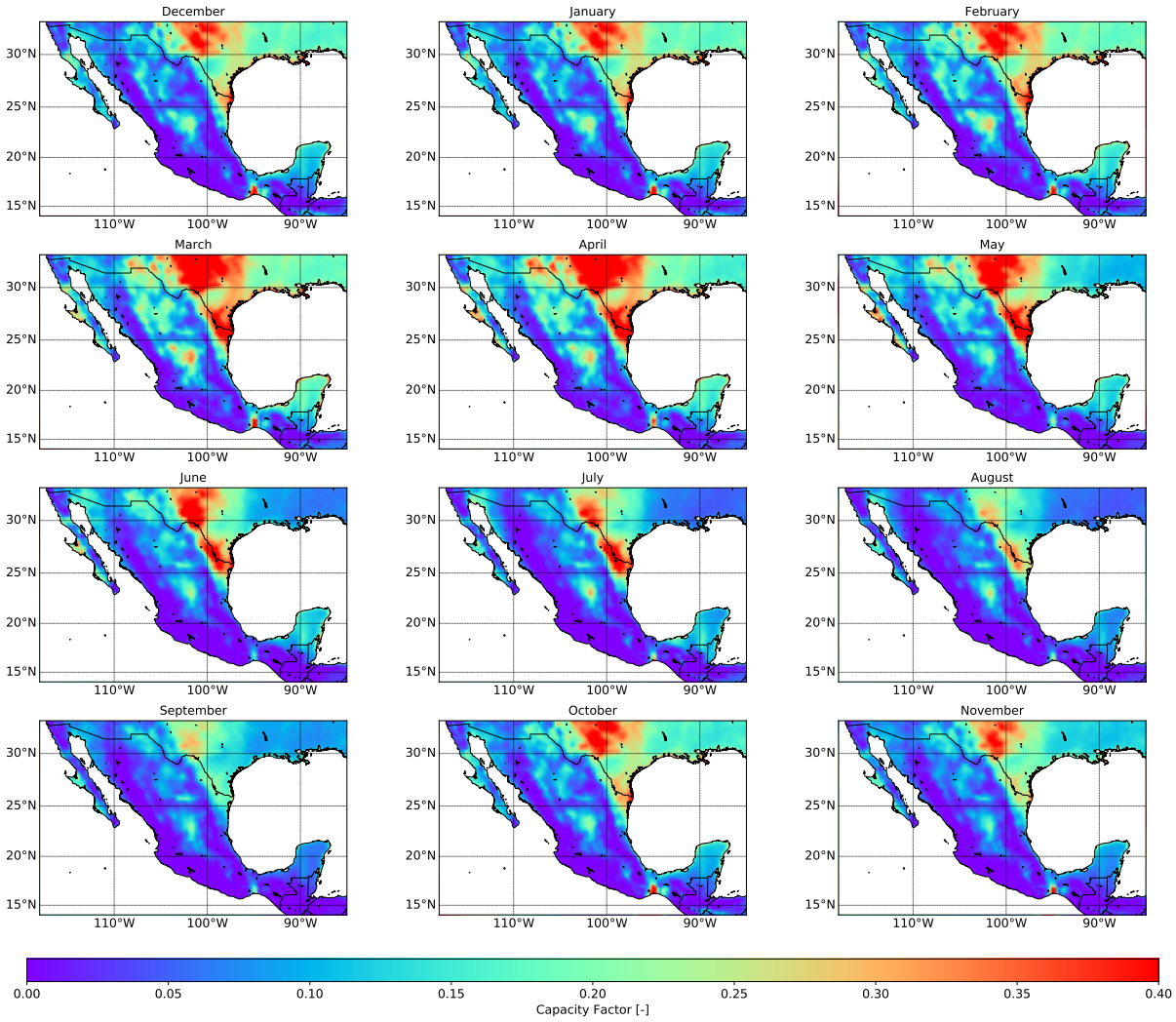

Figure 5.2: Mean capacity factors by month of 1979-2019. High CFs are presented with red and low CFs with purple. CFs are higher in most parts of the country during spring and lower during summer. The ORI2 and NES region have a good wind resource; they report high CF values in most months except May-September, and September-November, respectively.

Again as it was observed in Figure 5.1 the regions located in the Sierra Madre Occidental, Sierra Madre Oriental, Trans-volcanic Belt, and the Sierra Madre del Sur have low capacity factors throughout the year. It is land with many mountains, very rough, where wind speeds are affected by obstacles; thus, low wind speeds are reported.

5.2.1 Temporal variability of regional wind power

In this section, the regional time series are studied. Radar charts with the hourly and monthly mean CF of 1979-2019 are presented in Figure 5.3 and 5.4, respectively.

In the hourly analysis, four patterns were detected for the highest CF. Most of the cases occur in the daytime; just three regions report higher CF during the nighttime. In NTE (Figure 5.3a) and OCC, the highest CF are at 00:00-01:00 and 22:00-21:00, respectively. In three regions, BCA (Figure 5.3b), CEN, and ORI2 (Figure 5.3c), the maximum generation hours are reported in the early afternoon (14:00-15:00); BCA has another period after midnight (01:00-02:00). In BCS, NOR, and ORI, are reported in the late afternoon (16:00-17:00). In NES and PEN, in the evening, 17:00-18:00 and 18:00-19:00, respectively. Therefore, if the regions are joined together, the grid could approximately work with the generation hours peaks from 14:00 to 1:00. Also, the radar chart of ORI2 has an exciting shape since it is circular, meaning that the CF is constant during the year, the values are around 0.7, and when the highest CF is reported, the value is 0.8.

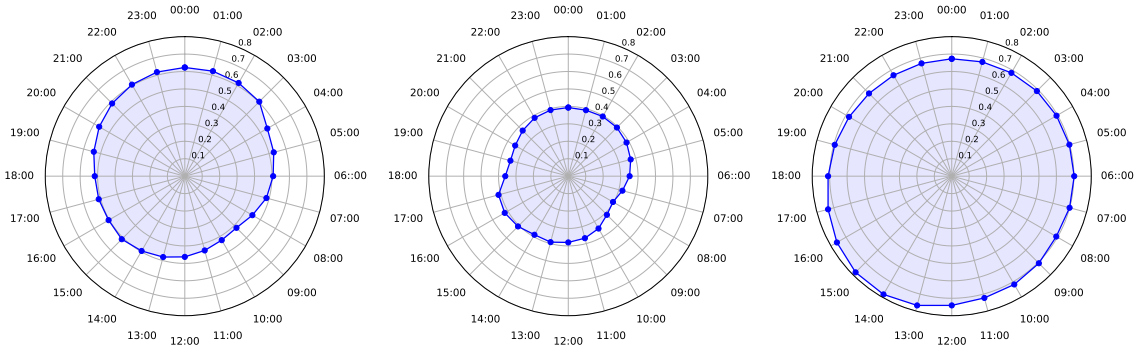

(a) NTE (b) BCA (c) ORI2

Figure 5.3: Regional mean Capacity Factor by hour for 1979-2019 (BCA, NTE, and ORI2). The hour is presented in UTC-6. In BCA (b) and ORI2 (c), the highest CFs are in the daytime at 14:00-15:00 (also after midnight in BCA due to sea breeze); in NTE (a), the highest CFs occur at night (00:00-01:00). In BCA (b) and NTE (a), the lowest CFs occur before noon at 06:00-07:00 and 09:00-10:00, respectively; in ORI2 (c), the lowest CFs occur at 22:00-23:00. However, the CF behavior of this region does not change too much throughout the day.

Concerning the lowest CFs, four patterns were detected. In five regions, the lowest CFs occur between 08:00-10:00: BCS, NOR, NTE (Figure 5.3a), OCC, and ORI. In the early morning in three regions, BCA (06:00-07:00, Figure 5.3b), NES, and CEN (08:00-09:00). In ORI2 (Figure 5.3c) at 22:00-23:00, and PEN at 11:00-12:00. ORI2 has a high CF before noon when nine regions do not, so that this region could help others during their low-generation period.

Four cases were found for the highest CF by month (Figure 5.4). In seven regions, the CF is higher in spring: BCA (Figure 5.4a), BCS (December too), NTE, NES, OCC, CEN, and PEN. In the NOR region (Figure 5.4b) during winter. The ORI region (Figure 5.4c) is a mix, with the highest CF during winter and spring. Lastly, in the ORI2 region (Figure 5.4d), during November, December and January.

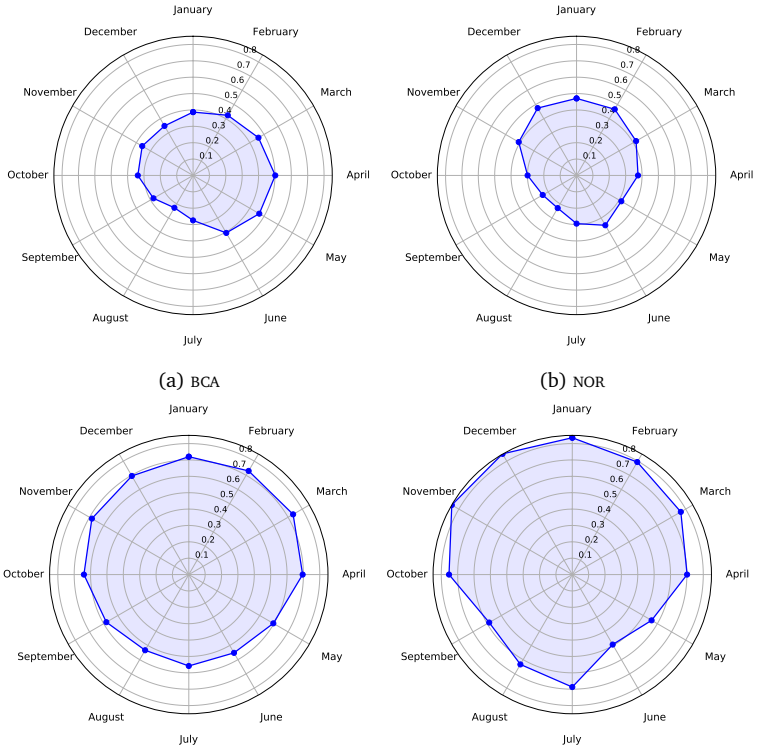

(a) BCA (b) NOR

(c) ORI (d) ORI2

Figure 5.4: Regional mean Capacity Factor (CF) by month of 1979-2019 (BCA, NOR, ORI and ORI2). The four cases and the three cases of the highest (max) and lowest (min) CF are presented: BCA (a) max is in spring, and min during January, August and September; NOR (b) during winter (max), and August and September (min); ORI (c) during winter and spring (max), and during summer (min); ORI2 (d) in November, December and January (max), and in May and June (min).

About the lowest CF by month, three patterns were found (Figure 5.4). Six regions have their lowest CF during August and September: BCA (January too), BCS (January too), NOR, NTE (January too), NES (October too), and PEN. During summer in the OCC,

CEN, and ORI region. Lastly, in ORI2 during May and June.

Aspects related to complementarity are seen. These aspects will extensively be discussed in Section 5.4, but mentioning a case during summer, when the capacity factors are low in the Tehuantepec Isthmus, they are around 0.4 in the NES region; therefore, these are areas with the possibility of complementing each other. Also, as the CFs of the Tehuantepec Isthmus are remarkable during the year, this region could help with electricity generation, at various times of the year, to the other regions; for example, in November, it is colored red while most of the map is blue (Figure 5.2).

The regional diurnal patterns could be different from what is seen on the country maps because now the time series of discrete points are compared, and the local topography could affect them.

In Figure 5.5 the highest and lowest CFs for the 41 years studied are presented. The highest CFs have been reported in the past century. The year in which the most number of regional maximums CFs were reported was 1998, with three regions, BCS, NOR, and ORI (• points). In the current century, the capacity factors reported corresponded to the lower values of the whole period, which is the case of ORI2 (2019), CEN (2018), OCC (2018), PEN (2016), and BCA (2001). The lowest CFs of ORI and ORI2 are higher than the highest capacity factors of the other regions. The CF's magnitude relates to what was presented in Figure 4.11; for example, the CF for the CEN region is around 0.15.

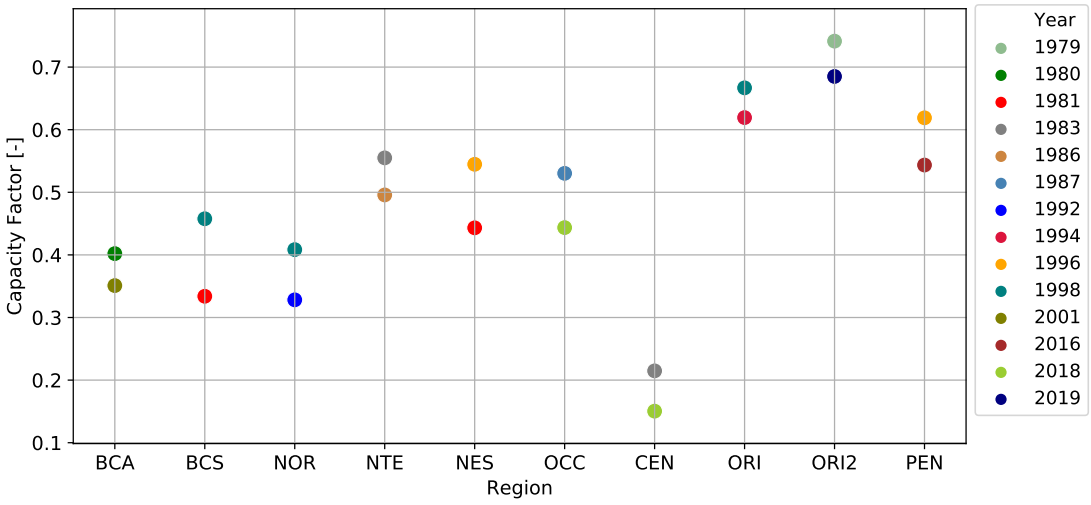

Figure 5.5: Value and year of the highest and lowest CF by region of 1979-2019. The y-axis gives the value of the CF, and the color of the point gives the year. For example, in BCA, the maximum CF was 0.4 in 1980.

5.3 Regional wind resource characteristics

This section describes the behavior and relation of the wind speed (5.3.1) and capacity factor (5.3.2) of the regions with more than one site. By analyzing the hourly profiles and heatmaps, specific characteristics were appreciated. These remain the same for the three years (2017, 2018, and 2019). The peak's characteristics are discussed in the next chapter.

5.3.1 Wind speed

Regarding the wind speed, the patterns found are:

- **BCS** (Figure A.3). This region has three sites: BCS1, BCS2, and BCS3. The annual hourly profiles are similar between the sites. There is a cluster on the heatmap between BCS2 and BCS1, with a Pearson coefficient around 0.70. These sites are near each other. In winter and fall, the hourly profiles of BCS2 and BCS3 are similar. In summer and spring, the hourly profiles of the three sites have similar behavior. The site with the lowest wind speeds is BCS2.

- **NTE** (Figure A.5). This region has five sites: CH01, CH02, CH03, CH04, and CH05. All sites' annual and seasonal, hourly profiles have similar behavior, except in summer, CH05 and CH01, and in spring, CH03. In summer, CH05 and CH01 are similar but different from the others. In spring, while the other sites go up rapidly around 09:00, CH03 goes up until 16:00. There are two clusters on the heatmap, one formed by CH02, CH03, and CH04, and the other with CH05 and CH01. The Pearson's of these two clusters are in the range 0.80-1.00. The correlation between these two clusters is between 0.50-0.60. The site with the highest wind speed is CH02.

- **NES** (Figure A.7). This region has three sites: TM01, TM02, and TM03. The annual and seasonal hourly profiles of the three sites have similar behavior. There is a cluster on the heatmap between TM02 and TM03. The Pearson's between them is 1.00, with the other site, TM01 the Pearson is 0.86 ± 0.01, this site is the one with the lowest wind speed for this region.

- **OCC** (Figure A.9). This region has three sites: ZC01, ZC02, and JAL1. The annual and seasonal hourly profiles of the three sites have similar behavior. There is a cluster on the heatmap between the sites located in Zacatecas. The Pearson values

are 0.97 ± 0.01 between the Zacatecas sites, and these with JAL1 have a Pearson of 0.73 ± 0.03. ZC02 has higher wind speeds, and ZC01 has lower wind speeds.

- **ORI** (Figure 5.6). This region has six sites: GR01, HG01, PB01, PB02, VZ01, VZ02. All sites' annual and seasonal hourly profiles have similar behavior, except PB02 for all seasons and GR01 in summer and fall. In all the sites, the wind speed increases from 10:00 am. However, in PB02, the peak is displaced in summer and spring by 2 hours, and during winter and fall it does not have a horizontal C-shape, unlike it has a more linear behavior. In summer, GR01 has similar behavior to PB02; it does not have a horizontal C-shape like the other its shape is like an M; in fall, the peak does not drop so drastic as in summer, it looks softened. Three clusters in the heatmap can be observed. One is PB01-VZ01, with Pearson's values of 0.82 and 0.83. Another is PB01-HG01, with Pearson's values of 0.64 and 0.66. As PB01 is similar to VZ01, the other cluster is VZ01-HG01 with Pearson's values of 0.56 ± 0.01. The other correlations are weak, with values around 0.2. The site with the lowest wind speed is GR01.

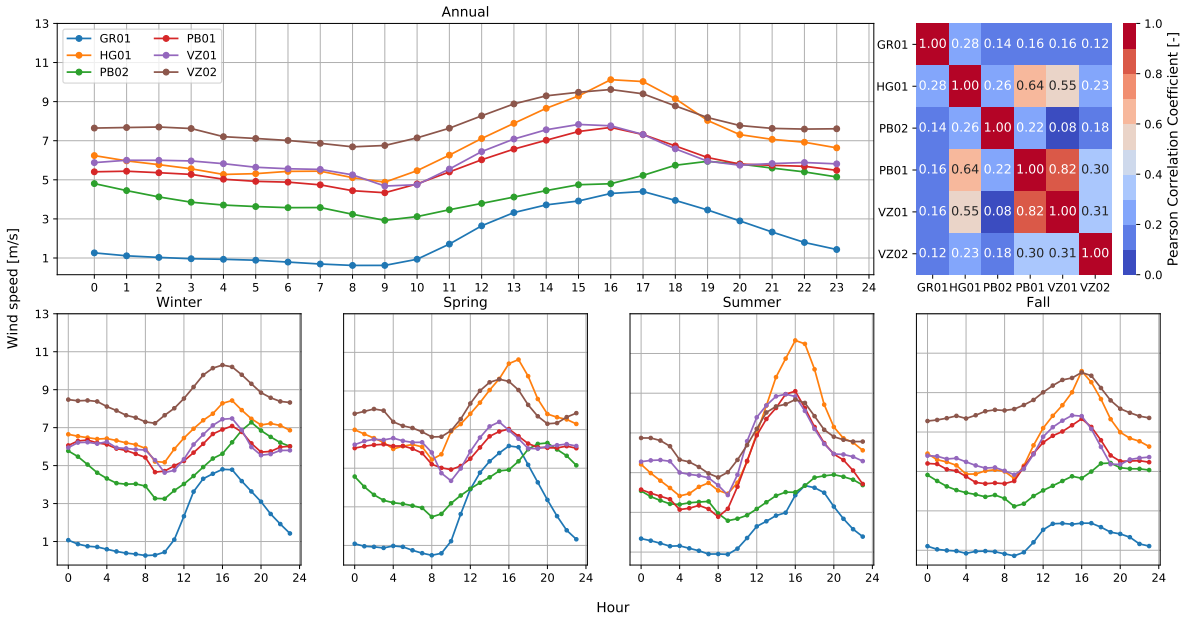

Figure 5.6: Annual and seasonal wind speed hourly profiles of ORI sites. Four of the six sites of this region have similar behavior in the hourly profiles; however, PB02 is different for all the year and GR01 for summer and fall. The heatmap presents one cluster representing the correlation between PB01 and VZ01. Between the other sites, the correlation is weak.

- **ORI2** (Figure A.13). This region has five sites: OA01, OA03, OA04, LV01, and CI01. The annual and seasonal hourly profiles of the first four sites in Oaxaca have similar

behavior. Although visually, the hourly profile of CI01 is not similar to the others, it has a strong correlation with them, with Pearson's values of 0.83 ± 0.03. The other sites form a cluster with Pearson's values of 0.99. CI01 is the site with the lowest wind speed.

- **PEN**. This region has two sites: YC01 and YC02. The annual and seasonal hourly profiles of the three sites have similar behavior. The Pearson between the two sites is 0.95 ± 0.01. YC01 has higher wind speeds than YC02.

5.3.2 Capacity Factor

The capacity factor behavior is similar to the wind speed behavior described before for all regions, except in the NTE and ORI region:

- **NTE** (Figure 5.7). Just during fall, the hourly profiles of all sites have similar behavior. CH05 and CH01 look similar to them but different from the rest in winter and summer. In spring, before 09:00, the behavior of the five sites is similar, but after this hour, three behaviors are noticed: CH05 and CH01, CH02 and CH04, and CH03 is another, its CF starts to rise until 16:00, while in the other sites is after 09:00.

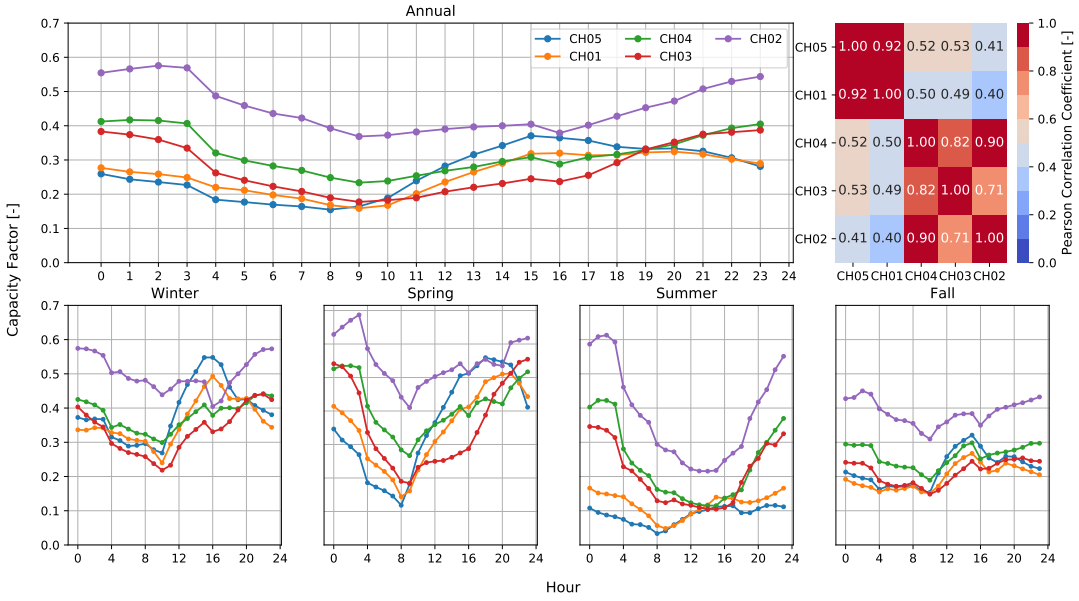

Figure 5.7: Annual and seasonal capacity factor hourly profiles of NTE sites. In fall, the behavior of all the sites is alike. In summer and winter, two patterns are detected, one between CH05 and CH01 and the other between CH04, CH03 and, CH02. What happens in summer and winter happens in spring except for CH03, which is different from all the others after 9 o'clock.

- **ORI** (Figure A.12). The only thing different from what was mentioned in the previous subsection regarding this region is GR01 in the fall. For this season, the hourly profile of this site has a little bump, but it is almost a horizontal line x ≈ 0.03 because of the power curve filter.

The clusters described on the heatmaps remain the same, however, the values decreased. As the power curve works as a filter, there is a big change in the low values when comparing the wind speeds that used to be around the same value. Now one have a value and the following one could be zero, so the standard deviation increases, thus the Pearson correlation coefficient $\left(r = \frac{cov_{xy}}{\sigma x \sigma y}\right)$ decreases. An example is in the NTE region using the wind speeds time series, the Pearson's value between CH01-CH02 is 0.55, but using the CF time series, the value change to 0.40.

5.4 Potential of wind power interconnection

In this section, the results of the two methods proposed: correlation between sites and regions (Subsection 5.4.1) and the number of generating hours (Subsection 5.4.2), to measure the complementary of the wind power are presented.

5.4.1 Spatial correlation of wind power

Figure 5.8 presents the correlation heatmap between the CFs of all sites for 2019. The sites are grouped by region. Three types of clusters can be observed. Sites that have a strong positive correlation (r > 0.7), sites that have a negative correlation (r < 0), and sites with a weak correlation (0 < r > 0.3).

The sites with a strong positive correlation are located in the same region. Some of them are near each other, so their behavior is similar (as presented in the previous section). This type of cluster is presented in purple and blue. The highest correlation of the sites in the same region is 0.99 between OA04 and OA01; these sites are just 177.5 m apart. The highest correlation of the sites not in the same region is 0.59 between JAL1 and EM01.

Sites with negative correlations show an excellent opportunity to complement the electricity generation between them. This type of cluster is presented in dark orange. The lowest correlation of the sites in the same region is 0.08 between PB02-GR01. There is a large number of cells colored pale yellow and pale orange. Although its correlation is not negative, they represent an opportunity for complementarity because the values are low.

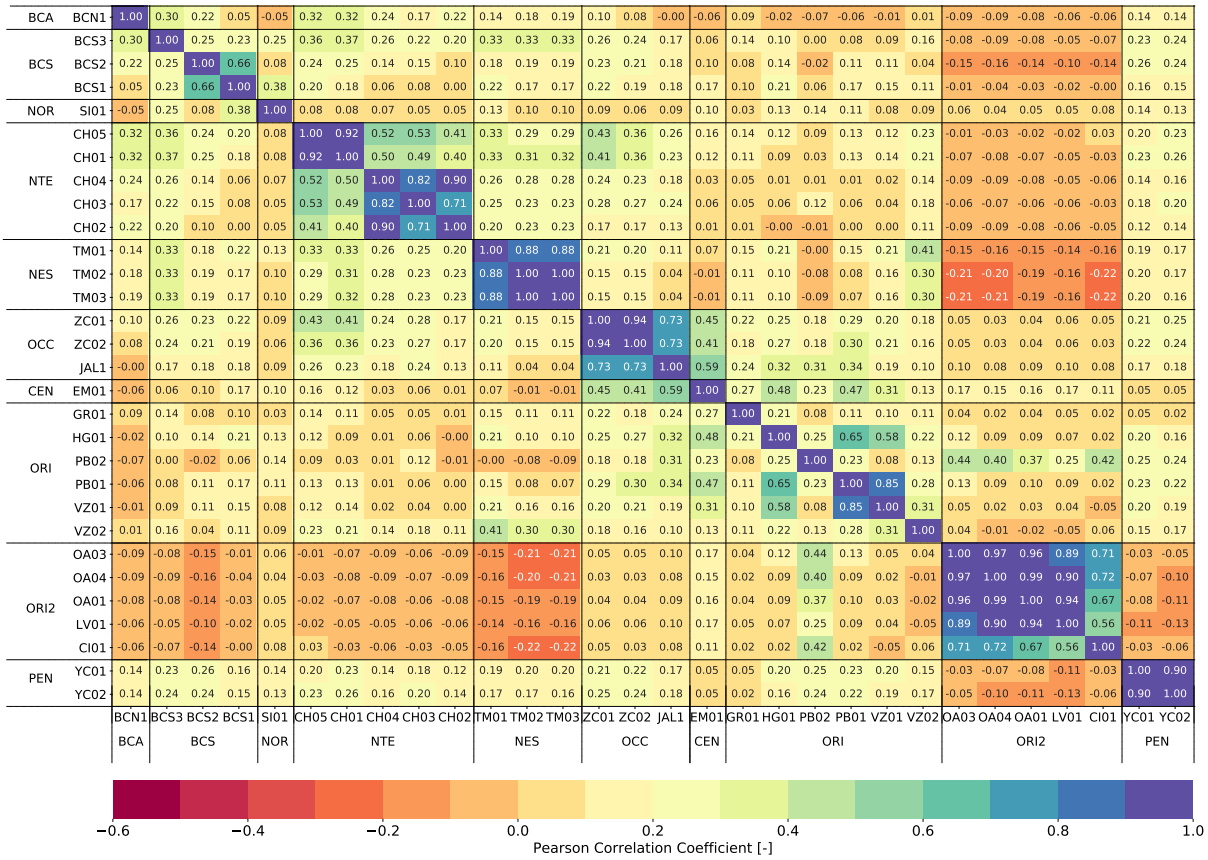

Figure 5.8: Correlation coefficient for sites pairs estimated using capacity factor data of 2019. Cells colored with purple and blue represent a high correlation. Cells colored with dark orange and red represent a low correlation. Having low correlation values is an opportunity to complement.

Many cells represent a low correlation between sites that are not in the same region, for example:

- BCS1 - CH02 (0.00). Which could be a factor that motivates the interconnection of the BCA and BCS regions with the Interconnected National System.)
- PB02 - CH01 (0.03)/CH04 (0.01)/CH02 (-0.01).
- YC02 - OA01 (-0.11)/LV01 (-0.13)

Between the regions, the complementarity is mainly noticed as a combination with the ORI2 region. For 5 of 9 regions, the ORI2 column/row shows a negative correlation (dark orange) for mostly all the combining sites, except ORI2-NOR, ORI2-OCC, ORI2-CEN, and ORI2-ORI.

The different Pearson's values show that the wind resource across Mexico is diverse. Some reasons that explain this are the extent of the territory by having different macro-scales and local conditions affecting [65].

Figure 5.9 presents the correlation heatmap between the regional CFs. In this plot, a few cells with values above 0.4 are shown. The negative correlation between ORI2-BCA, ORI2-BCS, ORI2-NTE, ORI2-NES, and ORI2-PEN remains higher with the NES region with a value of -0.17. Other negative correlations include BCA: BCA-NOR and BCA-CEN; the BCA region is far from CEN but close to NOR; they adjoin with Baja California and Sonora, so the potential to complement each other is considerable.

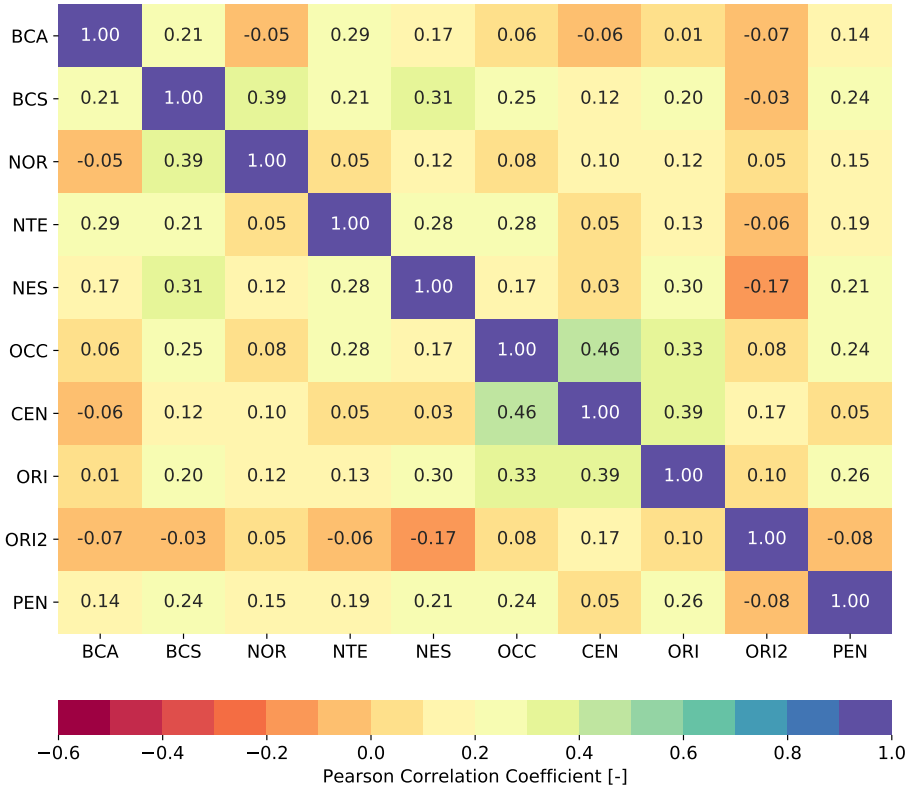

Figure 5.9: Correlation coefficient for regions pairs estimated using capacity factor data of 2019. A large number of cells are colored pale yellow or pale orange representing a weak correlation. Combinations with ORI2 and BCA region are colored dark orange representing a negative correlation.

The clusters representing strong positive correlation disappears as now they are integrated into the regional time series. Ten cells represent a moderate correlation, colored in light green and green, with values in the range [0.3-0.4]. The location of these sites could affect and describe their correlation as most of them are in the Trans-volcanic Belt.

As mentioned before, the pale yellow and pale orange cells also represent the potential to decrease wind variability, and the need to invest in grid connection is remarkable.

Pearson's values between the regional CFs time series change throughout the seasons (Figure 5.10). The negative correlations with the ORI2 region and the moderate correlation between OCC and CEN region increase in winter. In summer, unseen (in the other

seasons and annually) negative correlations arise in the NOR, NTE, NES, and OCC region; also, during this season, the potential to complement ORI2 and PEN is the most distinguished of all the seasons and regions. In fall and spring, there are fewer negative correlations. During spring, the values are higher, resulting in a pale yellow map, although negative correlations are still appreciated in combinations with BCA, CEN, ORI2, and PEN. In fall, the value between BCA and ORI2 stands out as the second-highest of all the values reported in all the regions and seasons.

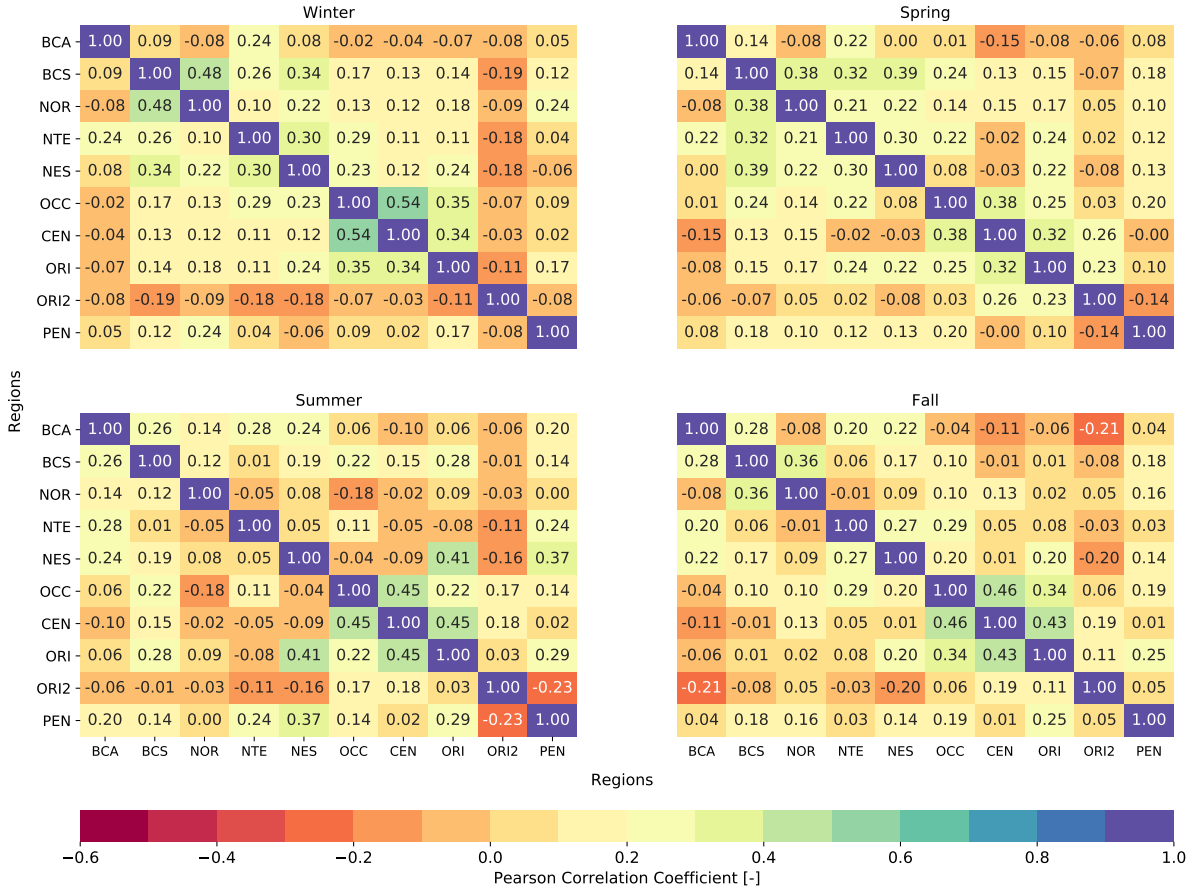

Figure 5.10: Correlation coefficient for regions pairs by season estimated using capacity factor data of 2019. In winter, the negative correlations with ORI2 increase. Summer is the season with higher negative correlations among other regions that are not ORI2. In spring and fall, there are fewer negative correlations.

5.4.2 Number of generating hours

The number of generating hours by region and combining two regions is presented in Figure 5.11. The number of hours corresponds to those with a CF above 0.2 [1].

[1]The capacity factor of wind energy according to [74] ranges between 20% and 43%, so the lower value of the range was taken.

The number of generating hours is proportional to the wind resource. The regions characterized with a high resource have generating hours above 7000; these regions are NES, ORI, ORI2, and PEN. In the CEN region, for 2019, 68% of the wind speeds are below 5 m/s; therefore, the annual CF is low, and the number of generating hours too, 2366. In the other regions, the resource is moderate, below 7000 but above 5200 hours. The ORI region has more generating hours than the other regions because its sites have low correlations (Subsection 5.3.1), so they complement. In ORI2, although its generating hours are 740 less than ORI, it has a higher CF because it has a more extensive generation.

Whichever the combination is, the number of hours increases. The diagonal of the heatmap represents the generation hours of each region. The color change on the cells above, beside, or below the diagonal represents a more significant number of hours. The combination of any region with the CEN region is the one that gives the smallest increase in hours. In six of the ten regions, the combination that gives the maximum increment in hours is with the ORI region, except for NES, ORI, ORI2, and PEN. For these four is ORI2 except in ORI2, which is with PEN.

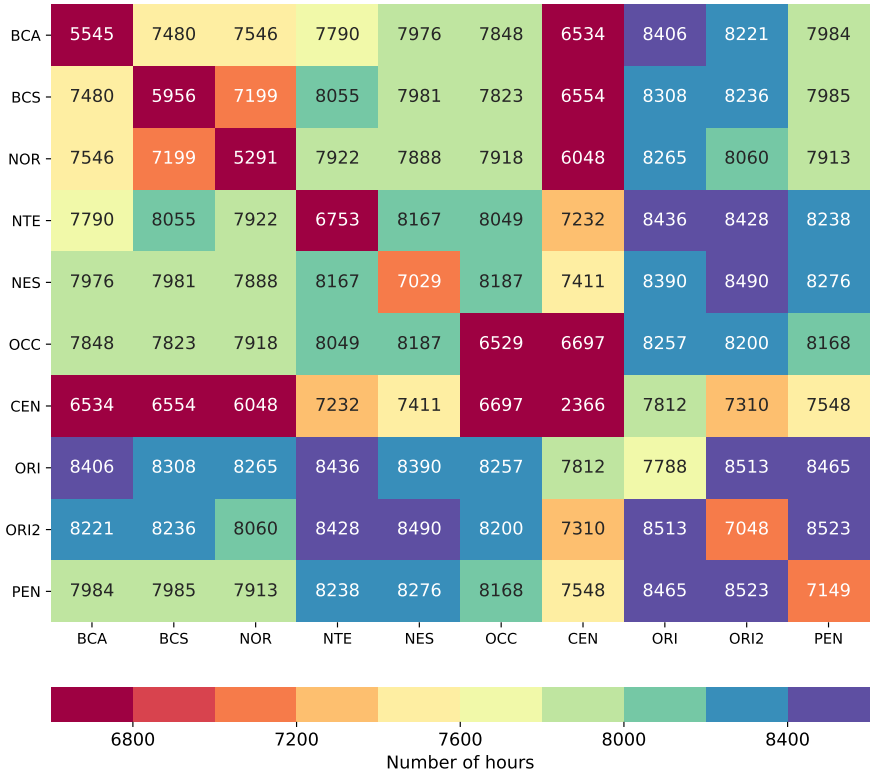

Figure 5.11: Number of generating hours by region and combining two regions using capacity factor data of 2019. The counted hours have a CF above 0.2. The number of hours is proportional to the resource. Any combination increases the value obtained with one region.

The percentage of increment also depends on the wind resource. Regions with a high wind resource also report a high number of generating hours, and they will not need a massive quantity from the others to reach 8760. The increment percentage for BCA, BCS, and NOR is 36.10% ± 3.83%, in CEN is 72.99%, in ORI 11.09%, and for the rest of the regions is 21.21% ± 2.91 %.

With non of the combinations, there is wind generation in all the hours of the year.

5.5 Chapter summary

This chapter describes the wind resource characteristics of the study sites, identifies temporal and spatial patterns, measures the interconnection potential, and gives a proposal of complementarity cases between regions. The results from Chapter 4 were helpful in the development of this chapter, as it was concluded that ERA5 data is reliable if a post-processing method like bias correction is applied. The time series wind speeds of the study sites for the same year were obtained from ERA5, applying to them the bias correction found before, and then, the analysis was performed.

It is remarkable how the wind variability could decrease by combining the wind energy generation of different sites located across Mexico and how the potential of complementarity between regions is significant. It is also notable the importance of investing in electrical infrastructure to interconnect sites and regions.

Chapter 6

Demand and wind power correspondence

The use of wind power to support electricity demand is a profitable option. By using wind power instead of non-renewable sources, several advantages arise, for example: reducing fossil fuel combustion decreases GHG emissions that cause climate change; also, implementing wind power diversifies the electrical matrix, which strengthens the country's energy security by reducing the dependency on imported fuels [8].

The variability of wind resources poses a challenge to the management of electrical grids; in order to reduce that risk, new strategies are fundamental [75]. If the resource behavior is well understood, different approaches could be followed for the best harnessing of the wind, for example, interconnecting to have a constant generation (Chapter 5). Then it could be related to the electricity demand to define its best integration into electric systems to contribute to electricity supply.

In this chapter, the potential of wind power to meet electricity demand in Mexico is investigated. The electricity demand variable is added in the analysis to describe the wind generation and electricity demand compatibility in terms of behavior and magnitude of the demand satisfied. First, the methodology is presented in Section 6.1. Following this, the results of comparative analyses performed between the electricity demand and the wind power generation curve, weekly and daily, are presented for 2019 in Section 6.2. Next, in Section 6.3, data of the wind electricity generation and the electricity demand for three years 2017-2019 is compared using the Pearson correlation coefficient. Then, in Section 6.4, it is studied the simultaneous occurrence of wind generation and electricity demand events classified in 9 categories (low, medium, and high) for 2019. Lastly, in Section 6.5, it is estimated, under certain circumstances and considering the temporal variability of the wind resource, the installed capacity needed to accomplish two-thirds of the clean electricity generation target of Mexico for 2024.

6.1 Chapter methodology

This section explains the methodology followed to describe wind power and electricity demand behavior jointly, measure its correspondence, and estimate the magnitude of the wind power installed capacity required to contribute with a defined percentage of the demand.

6.1.1 Wind power generation and electricity demand curves

In the first section, 6.2, the hourly and weekly profiles of the CF and electricity demand are studied. The data used are the regional time series for 2019 of both variables. The profiles were divided by season. The electricity demand was normalized by the maximum value reported per region. The seasons' patterns were analyzed for each variable, and the common patterns were discussed.

6.1.2 Wind-Demand analysis

In Section 6.3, the correlation between electricity demand and CF was estimated using the Pearson Correlation Coefficient. The regional CFs time series (Subsection 5.1) and the regional electricity demand time series for 2017-2019 were used. The data (wind-demand) from the same region was correlated per month. The hourly and daily averages of the variables were used since different patterns are appreciated. In addition to the monthly regional analysis, an annual inter-regional analysis was carried out, correlating the regional CF with the electricity demand of the region and with the rest of the other regions (Figure 6.1). The results obtained are presented through heatmaps.

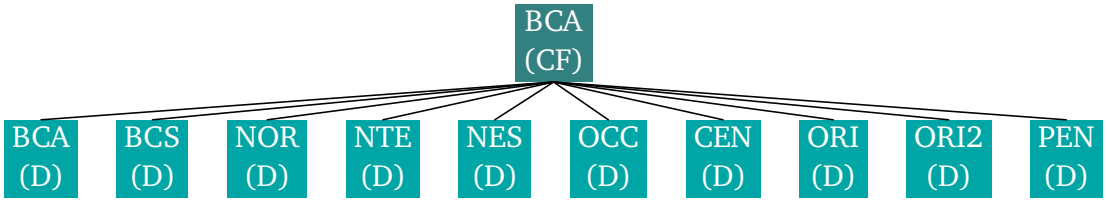

Figure 6.1: Inter-regional (wind-demand) correlation for BCA."CF" refers to the Capacity Factor and "D" to the electricity demand. The CF time series is correlated with each of the regional electricity demand time series.

In Section 6.4 it is studied the simultaneous occurrence of demand and wind power events. The data used are hourly regional time series of electricity demand and CF for 2019. Each hour has been categorized as low, medium, or high, based on:

– The terciles of the regional electricity demand.

– The value of the CF.

The electricity demand classification using the terciles is based on [34]. The CF proposed classification is: 0.00-0.20, low; 0.20-0.40, medium; and 0.40-1.00, high. The terciles were not used for the CF classification because the data distribution could misplace the ranges, as regions with low wind resources will report as high wind the low CFs, and regions with high resources will report as low wind the moderate CFs.

Depending on the value of each variable, the hours were grouped in 9 categories:

– Low Wind - Low Demand
– Low Wind - Medium Demanda
– Low Wind - High Demand
– Medium Wind - Low Demand
– Medium Wind - Medium Demand
– Medium Wind - High Demand
– High Wind - Low Demand
– High Wind - Medium Demand
– High Wind - High Demand

The number of times the nine combinations of the categories happen per month is presented as percentage frequency using bar charts for each region.

6.1.3 Meeting renewable energy target for 2024

In Section 6.5, it is estimated the installed capacity required to meet two-thirds of the renewable energy target of Mexico for 2024 while having a constant generation. It is considered that the sites and regions are interconnected; energy losses are not considered; and in all the sites, the technology used is the wind turbine Vestas V90-2MW. The methodology of this section splits into the following steps:

1. The electricity demand was forecasted for 2024 by region applying the growth-rate-based method (Subsection 2.3). The base year was considered 2019, so this year's time series electricity demand was used.
2. The magnitude of the demand to be supplied was estimated, considering the current wind power installed capacity and the target to be achieved.
3. The Annual Energy Production (AEP, Ec. 2.2) by region and site was estimated.
4. The regions and sites that combined have the highest constant generation were selected.
5. The installed capacity required, assuming 2 MW wind turbines, to supply the electricity demand estimated in 2 was calculated using the AEP of the sites selected in 4.

6.2 Demand and capacity factor profiles

Through the analyses of the hourly and weekly profiles, several patterns emerge. First, the description of the electricity demand and CF by day of the week (Subsection 6.2.1) is presented, then by the hour of the day (Subsection 6.2.2).

6.2.1 Weekly profiles

For all the regions, the day on which the demand is the lowest is Sunday. The day with the highest demand varies along the regions and the seasons. In Table 6.1 it is presented the day with the highest demand by region. For example, in summer and fall, in the CEN region is Tuesday, but in winter and spring is Thursday; for the PEN region, Wednesday is the day with the highest demand in summer and fall, but in spring is Tuesday and in winter is Thursday. Spring shows an interesting pattern since the days reported are only Tuesday and Thursday. Also, in winter, except for NTE, the days are Thursday and Friday.

Region	Summer	Spring	Fall	Winter
BCA	Thursday	Thursday	Tuesday	Thursday
BCS	Thursday	Thursday	Thursday	Friday
NOR	Wednesday	Thursday	Wednesday	Friday
NTE	Tuesday	Thursday	Friday	Monday
NES	Friday	Tuesday	Tuesday	Friday
OCC	Tuesday	Thursday	Wednesday	Thursday
CEN	Tuesday	Thursday	Tuesday	Thursday
ORI/ORI2	Tuesday	Thursday	Thursday	Friday
PEN	Wednesday	Tuesday	Wednesday	Thursday

Table 6.1: Day with the highest electricity demand by season for 2019.

The season with the highest demand for all the days is summer, except in the NOR and PEN regions. In the NOR region is fall from Saturday to Wednesday, and summer on Thursday and Friday; in PEN is summer for all the days except Saturday, which is spring. The lowest demand is winter for BCA, BCS, NOR, NTE, NES, OCC, ORI, and PEN, and fall for the CEN region.

Regarding the CFs, there are no weekly patterns that remain the same for all the regions. However, the seasons where the CFs are high and low could be identified. The CFs have a greater value for winter and spring and a lower value for summer and fall except in NES (just spring and fall, respectively), and in ORI and ORI2, Saturday has a peak in fall.

Therefore, the contribution to the electricity demand will be the highest during winter and the lowest during summer. Also, it will contribute more on Sundays as it is the day with the lower demand. On the other days, the contribution will depend on the season. In Figure 6.2 the weekly profile of BCA is presented, where what was commented before is appreciated.

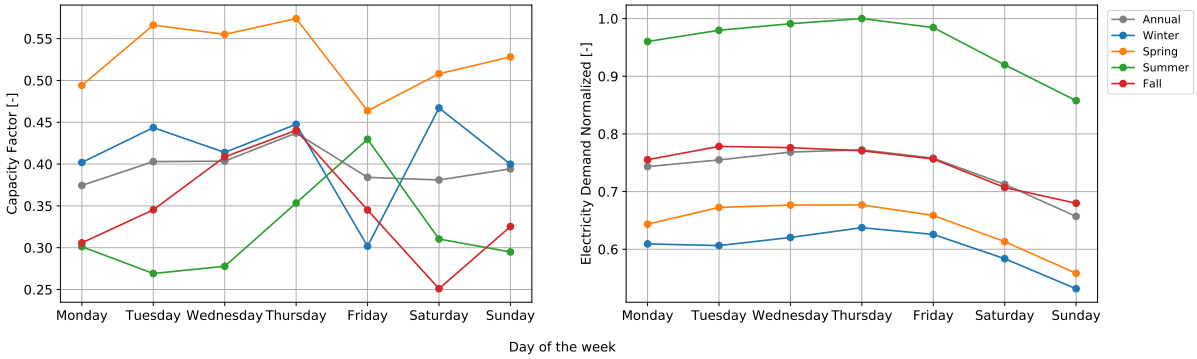

Figure 6.2: Weekly Capacity Factor and Electricity Demand profile by season for BCA 2019. On Sundays, the demand is the lowest. The CF does not have weekly patterns. During spring, the CF reports higher values and the demand during summer.

6.2.2 Hourly profiles

The hourly profiles show the potential of wind power to complement electricity demand on a daily scale. Generally, the demand curves have an S shape, with a constant growth where it reaches a plateau, and in some cases, there is a double peak (BCA, BCS, OCC, ORI, and ORI2 (Figure 6.3a)); this does not apply to the NTE region where the curve has a C shape (Figure 6.3b). Regarding the CF's, for most regions, the peak is pronounced and corresponds to the peak hours of the demand in the evening (Figure 6.3a); this does not apply for BCA because this region does not have one peak, it has varied peaks (Figure 6.3c); also, in the NTE the behavior between the demand and the power generation is inverse, and in PEN, when the demand is growing up the CF goes down, but then the values increase rapidly (Figure 6.3d).

The patterns remain in all the seasons for all the regions; it only changes the magnitude. The demand is higher during summer, except in NOR, which is fall. The CF's are higher during spring and winter, but in NES and NOR, there are a couple of hours (15:00 and 18:00, 14:00 and 15:00, respectively) where it is higher during summer, which is a good thing to complement the high demand of this season in all the country.

As the behavior is not the same between regions, the diverse distribution of peaks could be harnessed (as mentioned in Chapter 5) for complementary.

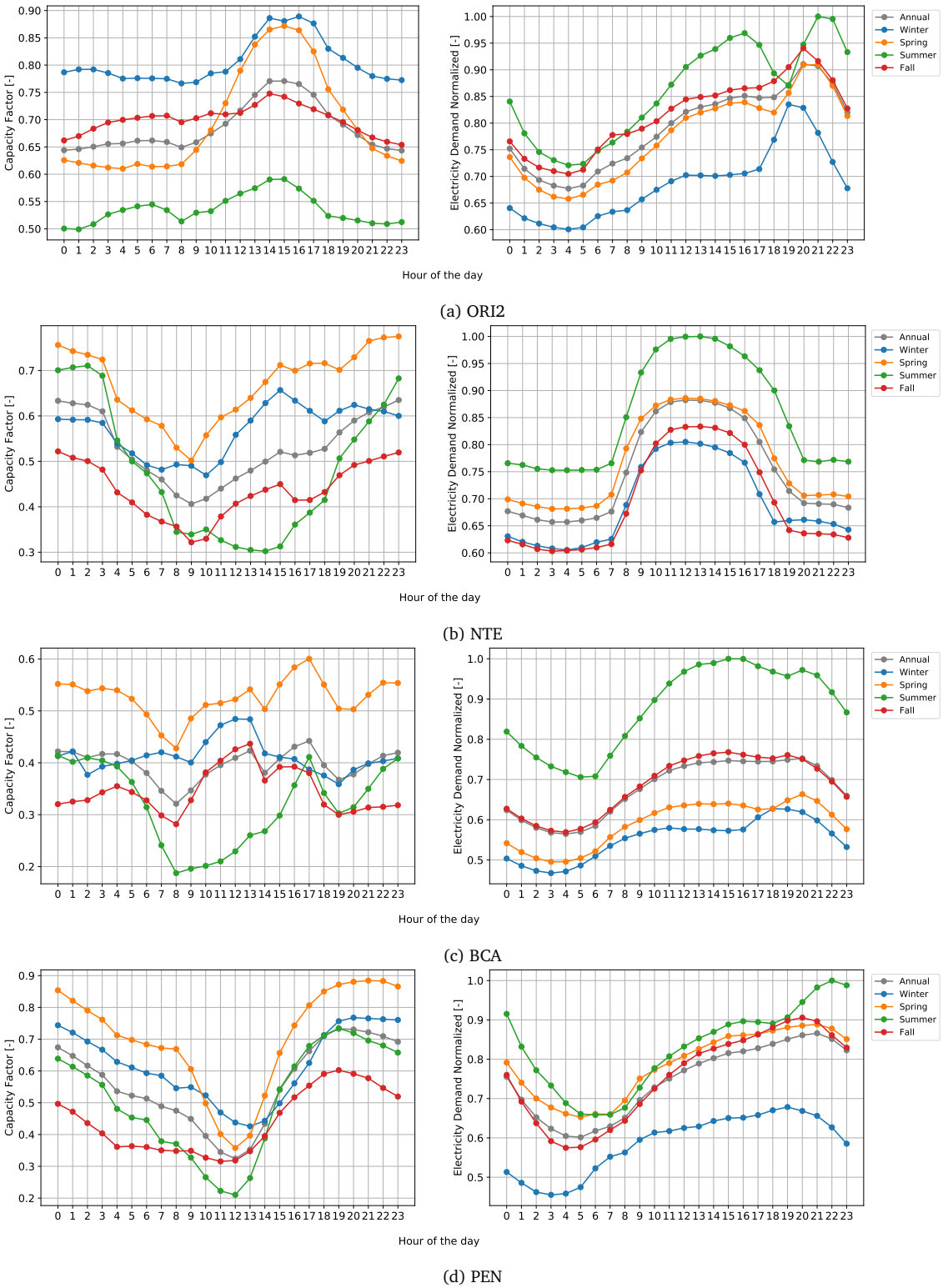

(a) ORI2

(b) NTE

(c) BCA

(d) PEN

Figure 6.3: Hourly Capacity Factor and Electricity Demand profile by season for ORI1 (a), NTE (b), BCA (c) and PEN (d) 2019.

6.3 Wind power and electricity demand correlation

The correlation between the CF and the electricity demand is presented in the following figures, using hourly time series (Figure 6.4) and daily time series (Figure 6.5). Both time scales were used because they show different patterns.

The Pearson values correspond to weak and moderate negative and positive correlations. With the hourly data, the values range between -0.29 to 0.44, and with the daily data between -0.51 and 0.57.

In Figure 6.4 most of the cells are green (57/120), representing a correlation between 0.1-0.3. There are no red cells. ORI2 is the region where the wind power has a better correlation with the demand, while NTE is the region where the wind power has the worst correlation with the demand; this behavior is explained by the demand curve, which shape is inverse to the CF curve (Figure 6.3b).

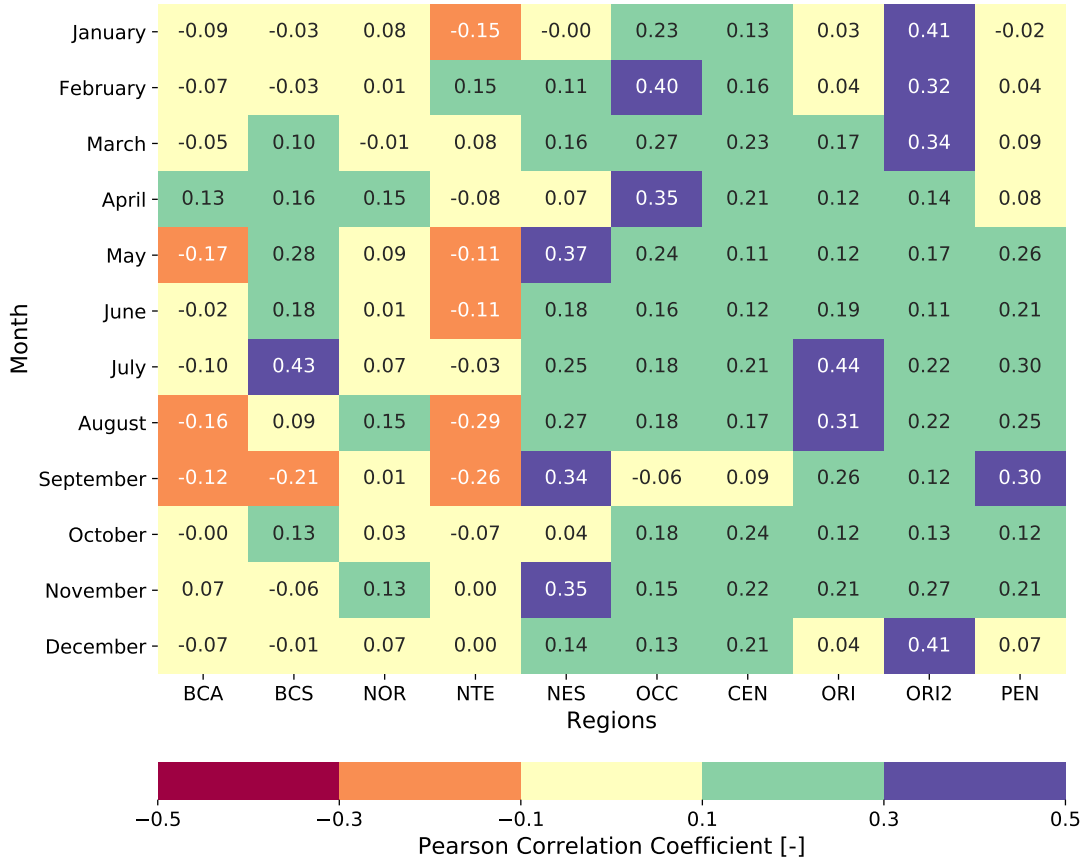

Figure 6.4: Pearson Correlation Coefficient between regional electricity demand and capacity factor per region by month using hourly data of 2017-2019. The orange cells represent a weak negative correlation, and the blue cells have a moderate positive correlation.

In the southeastern regions of Mexico, seasonal patterns are observed. In ORI and PEN, the correlation is lower during winter and higher during summer and fall; in ORI2, it is higher during winter and lower during summer and fall. The correlation is higher in the CEN region during winter, which is beneficial because the demand is the maximum.

As the electricity demand is high, any wind power contribution is profitable. If big wind farms are considered, the behavior induces storage mechanisms. The cells do not have a blue color during winter and spring, except for ORI2 and OCC; however, it is known that the resource is high. Therefore, it could be stored to be used when required or at the best time for its use.

In Figure 6.5, the Pearson values change drastically compared to the ones obtained using hourly time series. Before, most of the cells were green, but they changed to yellow, orange, and purple. ORI2 continues being the region with the best correlation, and now the region with the worst is BCS, having two red cells.

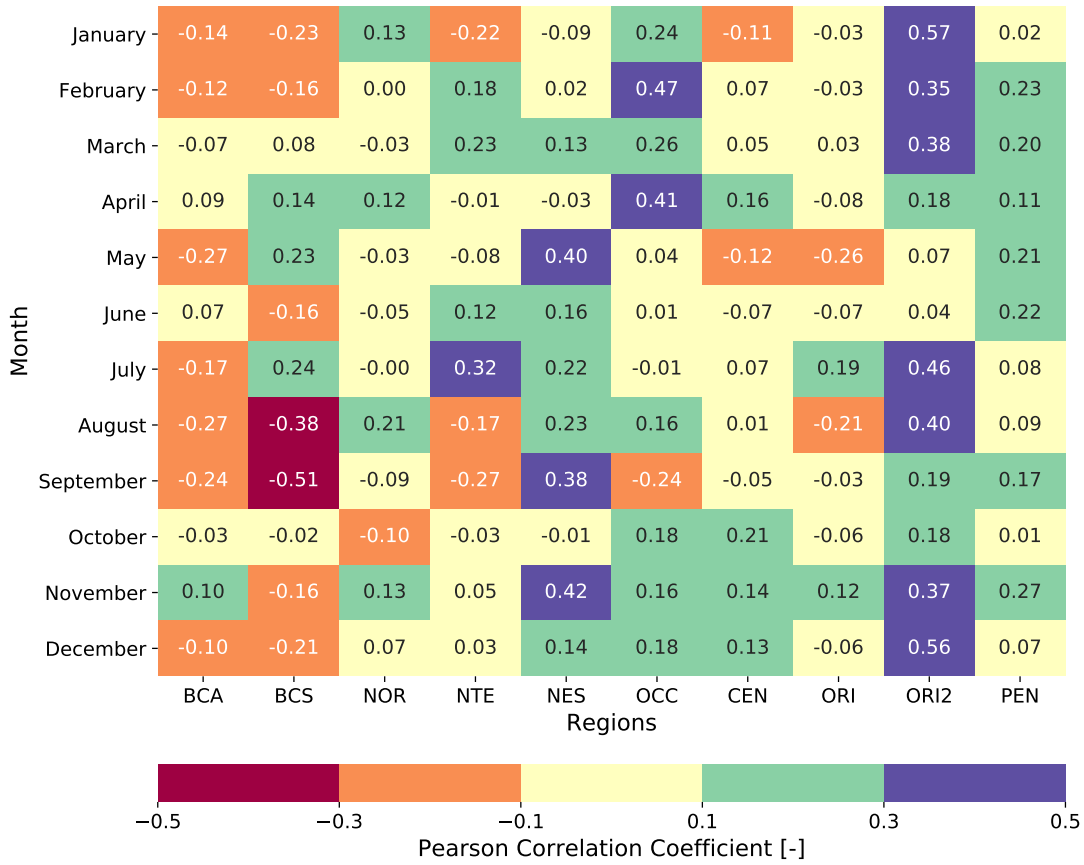

Figure 6.5: Pearson Correlation Coefficient between regional electricity demand and capacity factor per region by month using daily data of 2017-2019. The red cells represent a moderate negative correlation, and the blue cells a moderate positive correlation.

This behavior is related to the hourly and weekly profiles of Section 6.2. As mentioned before, the weekly CFs do not follow any pattern, by contrast with the demand, which is lower on Sundays; this affects the Pearson results. On the other hand, the hourly data show a better correlation because some hours correspond between the CFs and the demand.

The objective outlined in Chapter 5 is to have a constant generation, but what happens when the wind resource of one region is used to complement the demand of others is presented in Figure 6.6. The values range from -0.30-0.16. The correlation is weak and moderate negative except for NES, CEN, and ORI2. The row of ORI and ORI2 has the same values because it is the same demand. Annually CEN region could support the demand of other regions. The results strengthen the idea of storage energy or pursuing the objective of having a constant generation.

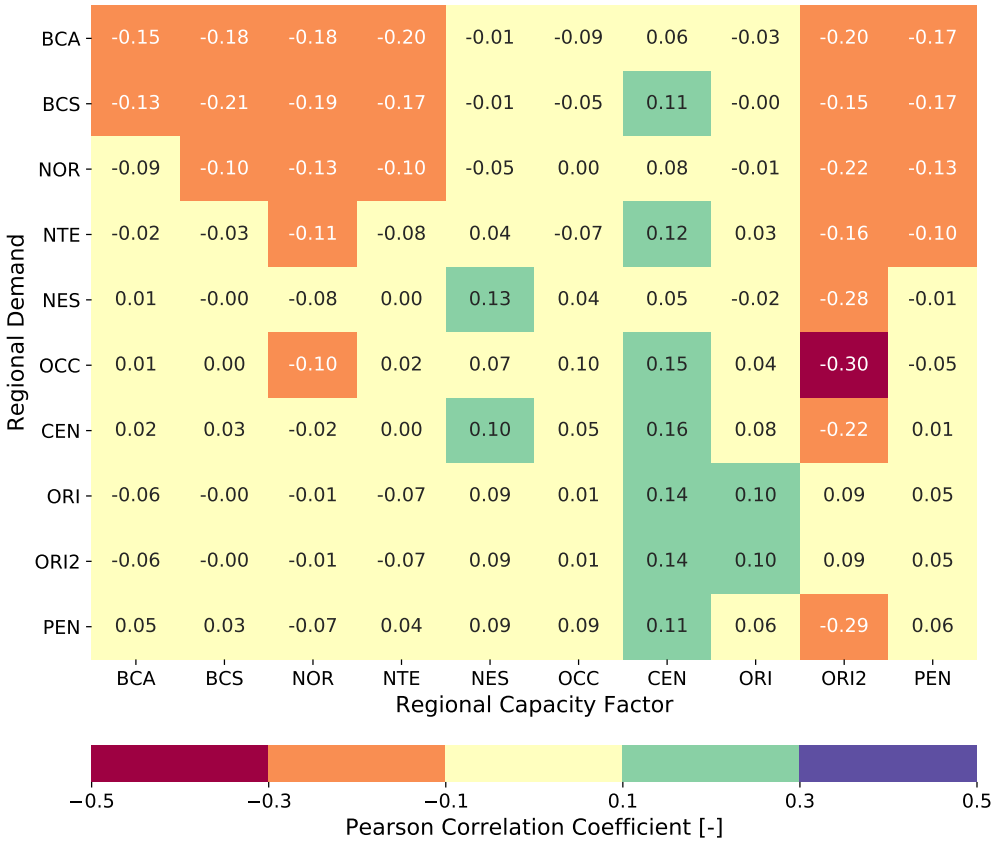

Figure 6.6: Annual Pearson Correlation Coefficient between regional demand and capacity factor using hourly data of 2017-2019. Rows are Demand vs CF, and columns CF vs Demand.

If there is a constant generation, other methods will be needed before measuring the correlation, such as optimization models. First, wind farms will have to be designed; then, depending on the contribution, the best arrangements will be selected to have a

constant generation. Although the generation will be constant, the values will not be because of the resource, high or low; consequently, the correlation could be measured using the Pearson Correlation Coefficient.

6.4 Demand and wind power simultaneous occurrence

Wind energy and demand events (low, medium, and high) occurrence results for 2019 are presented in Figure 6.7. Reiterating that the electricity demand events are defined using the terciles and the CF value categorizes the wind power events (below 0.20, between 0.20-0.40, above 0.40).

In general, the distribution of the modes corresponds to the previous discussion related to the occurrence of the high and low electricity demand and wind power generation (Subsection 5.2.1 and Section 6.2):

- The modes associated with **high electricity demand** (darker colors) predominantly happen in spring and summer, between April and September. For example, 98.92% of the events are in the high demand category for August in the BCA region.
- The modes associated with **high wind power generation** (brown bars) mainly occur in spring and winter, between November and May. For example, 55.51% of the BCS region events are in the high wind category for February.
- The modes associated with **low electricity demand** (lighter colors) principally occur in winter and spring, between November and March. For example, 81.72% of events are in the low demand category for January in the NOR region. Wind power contributes more to the demand when it is high and the demand is low. This situation is represented with light brown bars.
- The modes associated with **low wind power generation** (green bars) broadly occur in summer and fall, between June and November. For example, 41.11% of the events in the NTE region are in the low wind category for September.

Having dark brown bars representing high wind and high demand in summer is advantageous. Two relevant aspects are stressed: 1) if the merit order is followed to supply the electricity demand, the wind power energy will be more convenient to be used, because it has a lower price; 2) during this season, the wind resource is generally low if predictive maintenance is scheduled for these months because the losses of stopping the wind turbine will be lighter, knowing that there are hours with high demand and high wind could be helpful to determine the best days to do the maintenance.

Figure 6.7a, 6.7b, and 6.7c present the results for BCA, BCS, and NOR region. These regions are located in the northwest of the country. They have similarities in the first months: January, February, and March, where only six categories exist, events with high demand are not reported.

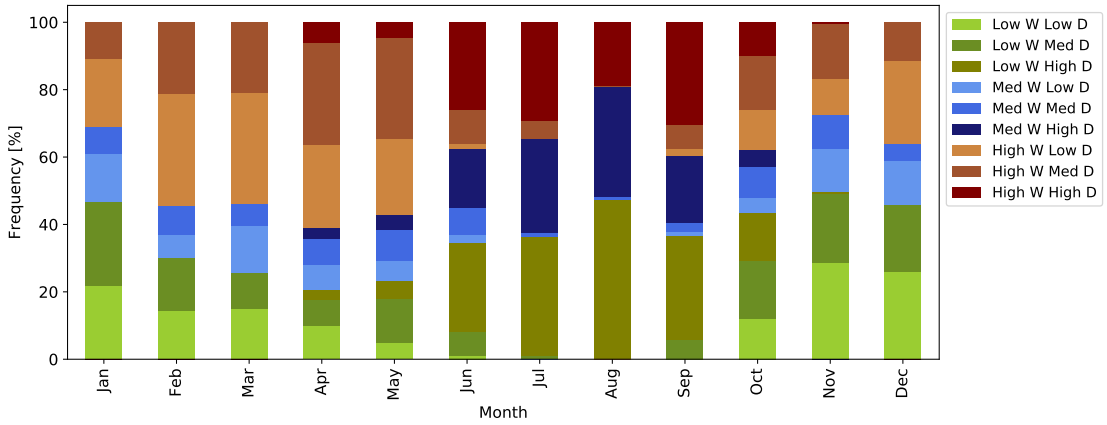

(a) BCA

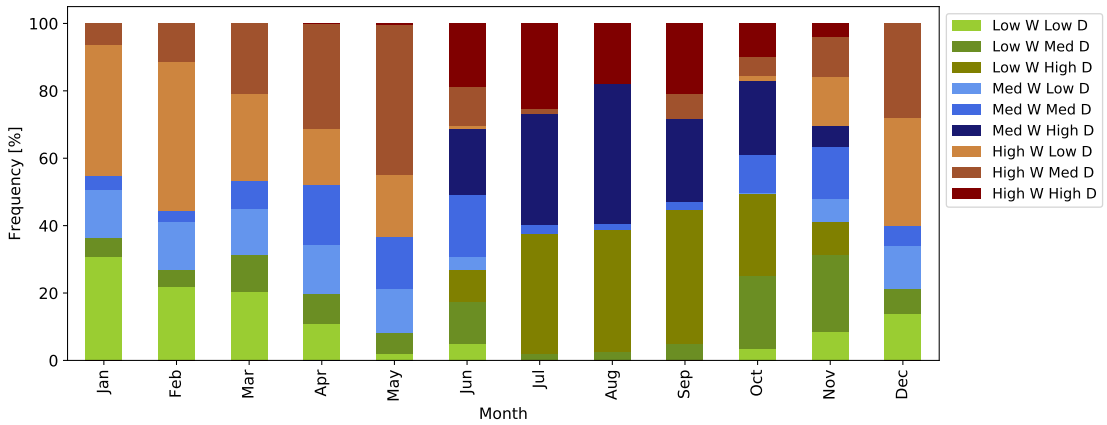

(b) BCS

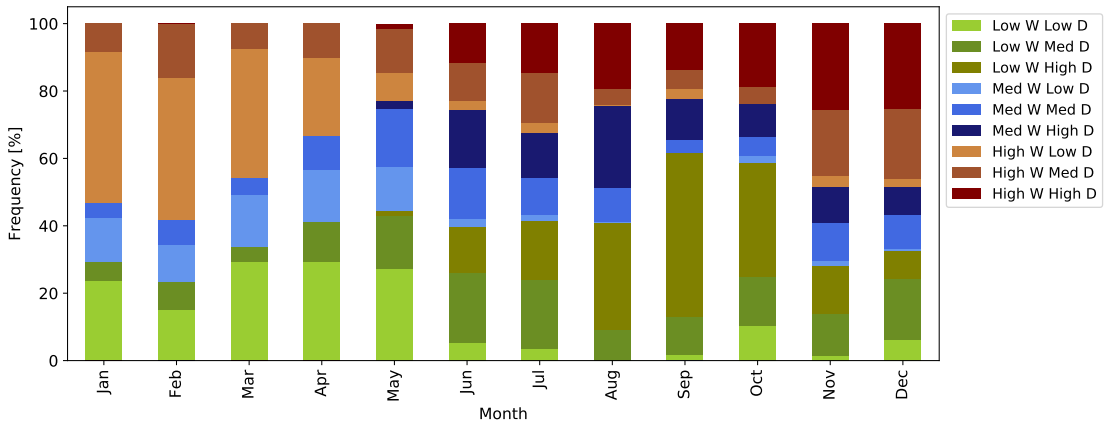

(c) NOR

Figure 6.7d, 6.7e, and 6.7f present the results for NTE, NES, and OCC region. These regions are located in the north and west of the country. A relevant aspect regarding the NTE regions is that the nine events are reported in all the months. In the NES and OCC region, high-demand events are not reported for January and February and December and January, respectively.

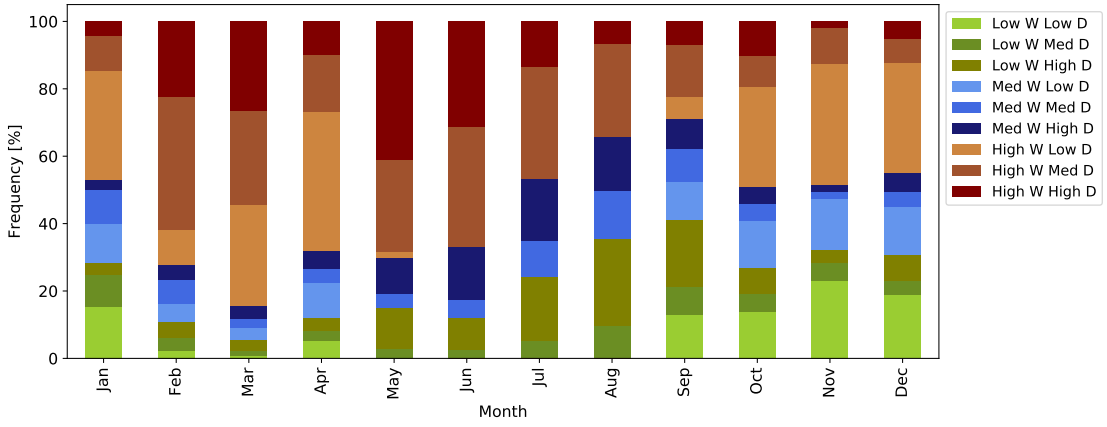

(d) NTE

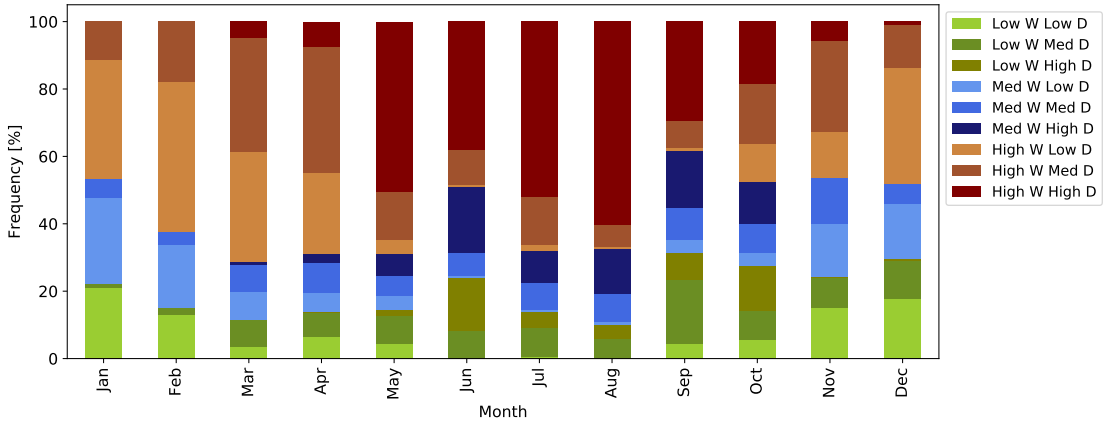

(e) NES

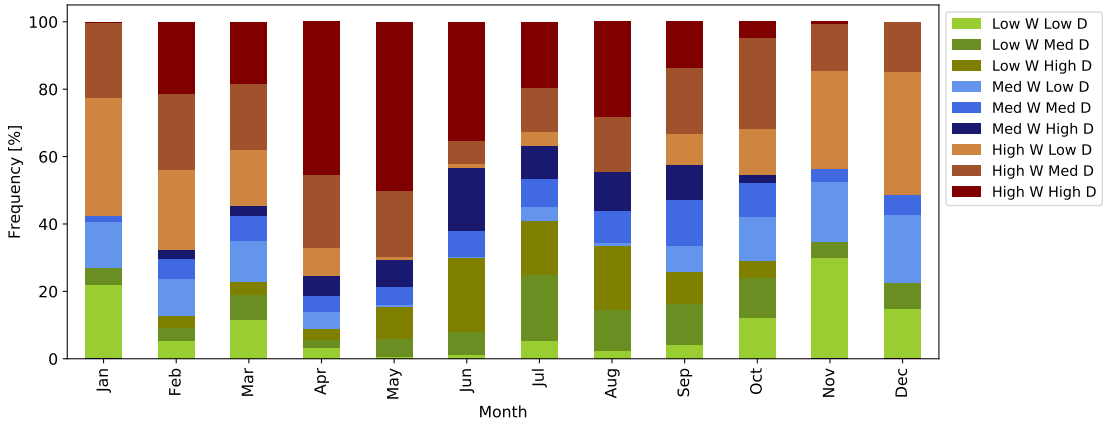

(f) OCC

Figure 6.7g, 6.7h, and 6.7i present the results for CEN, ORI, and ORI2 region. These regions are located in the center and southeast of the country. As expected, the CEN region has many events with low wind, above 50% in all months. In contrast, the ORI and ORI2 regions have many high wind events, also above 50% in all the months.

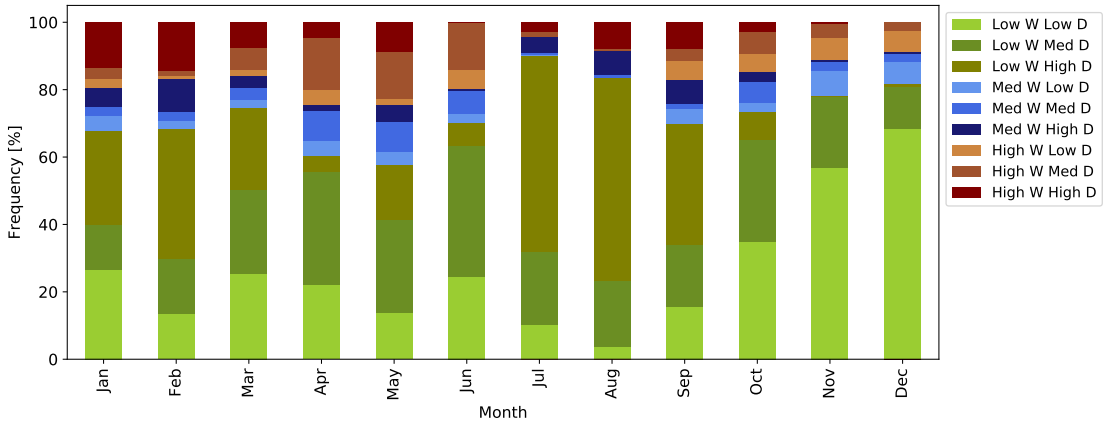

(g) CEN

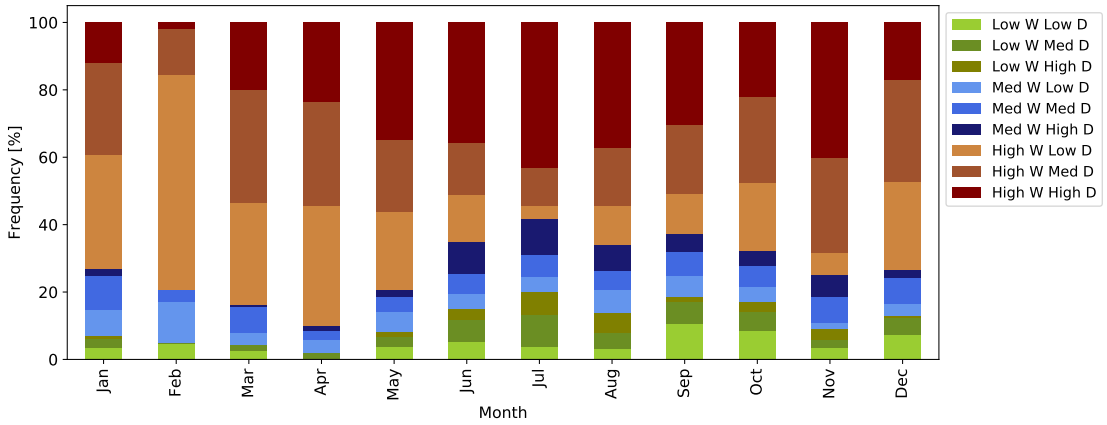

(h) ORI

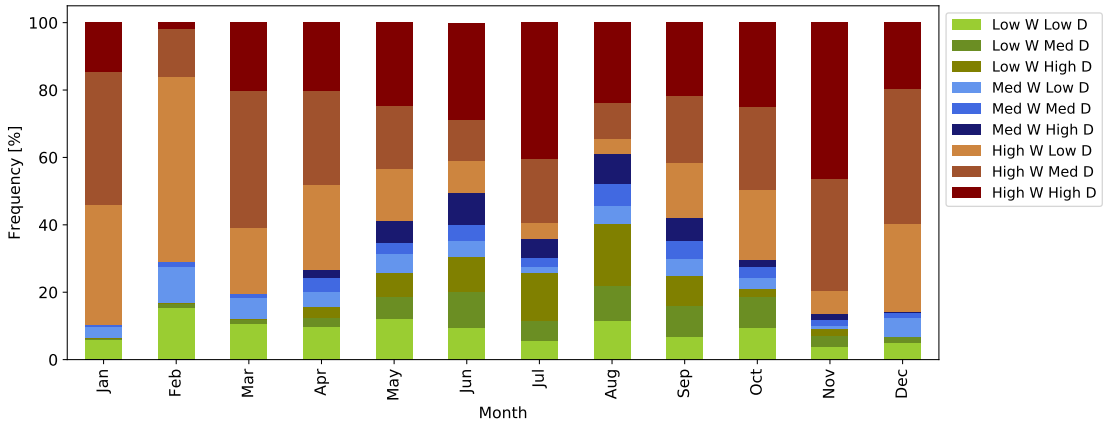

(i) ORI2

Figure 6.7j present the results for the PEN region. This region is located in the south-east of the country. The nine events are reported in all months except January, which presents an interesting behavior only showing four events, one of them, "high wind and low demand," with a large number of events (71.37%).

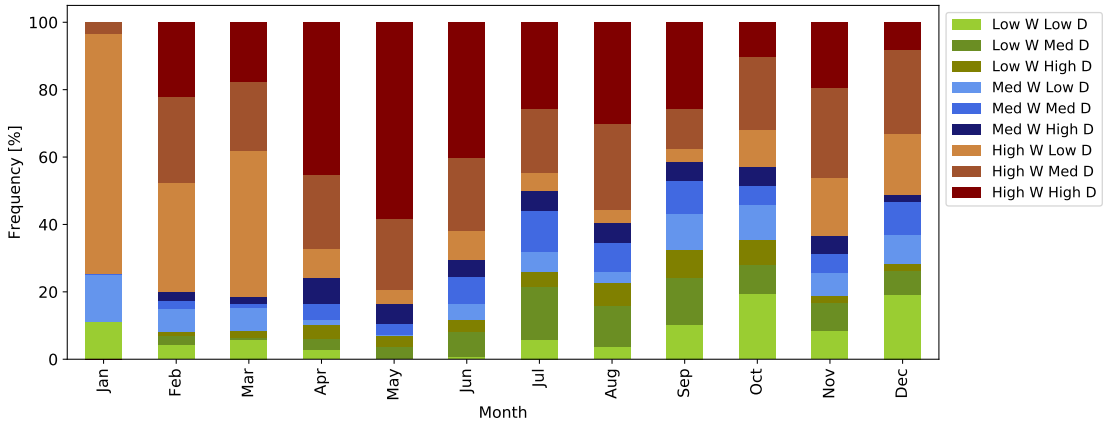

(j) PEN

Figure 6.7: Frequency of wind and demand events simultaneous occurrence for 2019. "W" means wind power generation, and "D" means electricity demand.

In order to illustrate better Figure 6.7, in Figure 6.8 are presented the results for the PEN region using a scatter plot. The lines represent the limits of the categories, and the point's color intensity represents the number of events. For example, in January in Figure 6.7j, there is a large number of events with high wind and low demand, and it is presented in Figure 6.8 with dark blue on the corresponding section. Another example is in December, where the cloud of points is mainly located below the high demand limit line (Figure 6.8), and it is seen in Figure 6.7j with thin bars of dark colors, which represent high demand.

Additionally to what has been discussed, an international complementarity can be studied. Mexico has interconnection points with the United States of America (California and Texas), Belice, and Guatemala [54]. The energy exchange could be planned, considering the resource of the border regions, in the south: ORI2 and PEN, and in the north: BCA, NOR, NTE, and NES, and the demand curves. If the installed capacity allows it, the wind power could contribute to supply the demand in the other countries; this has been raised in Europe [25].

6.5 Meeting electricity goal with constant wind power

This section presents the installed capacity required to achieve two-thirds of Mexico's clean energy generation target for 2024 [76] considering a constant generation.

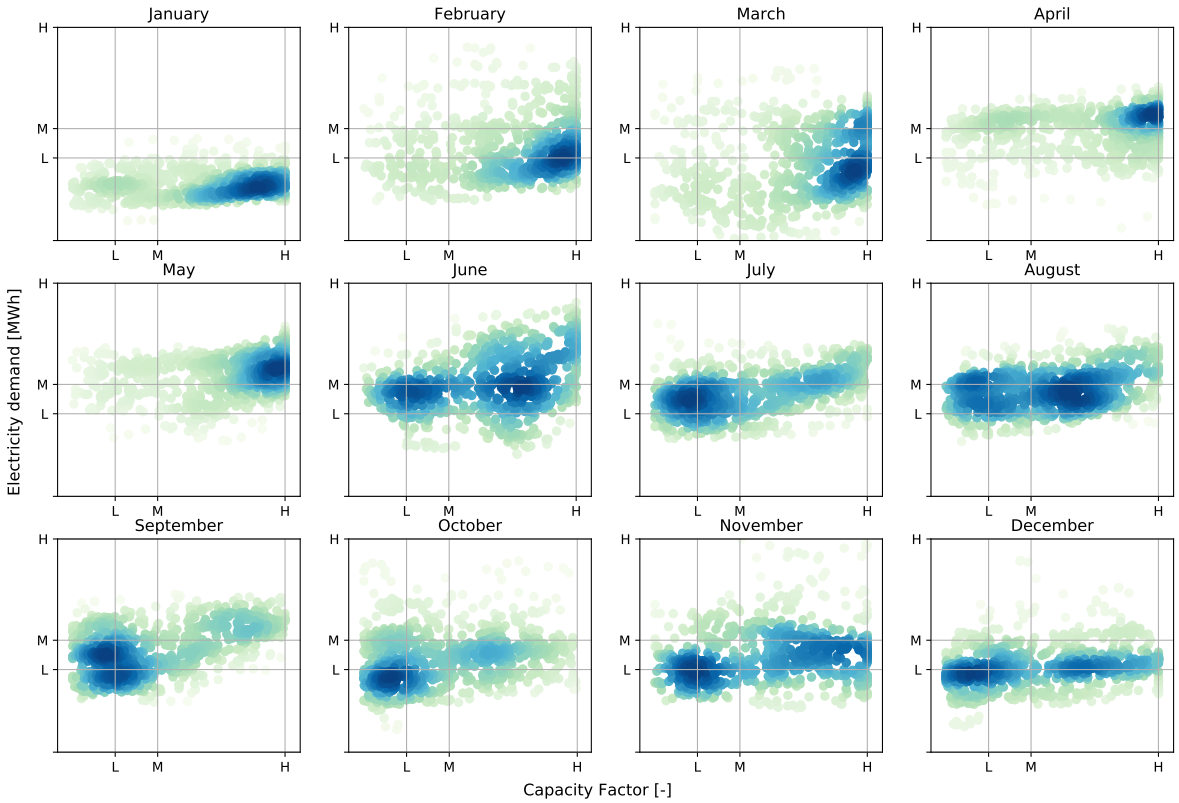

Figure 6.8: Scatter plot of the CF and electricity demand events by month. The lines represent the category limit, and the color of the points the number of events, darker blue: many events, light green: few events.

6.5.1 Annual Energy Production

Using the Vestas V90-2MW wind turbine power curve, and without the consideration of losses, the Annual Energy Production (AEP) estimated by region for 2019 is presented in Table 6.2.

Region	EAP [GWh]
BCA	6.95
BCS	6.79
NOR	6.53
NTE	9.27
NES	8.87
OCC	8.41
CEN	2.87
ORI	11.34
ORI2	12.00
PEN	9.83

Table 6.2: Annual Energy Production by region for 2019

The results of Table 6.2 reflect what was commented in Chapter 5. The regions with a high generation, ORI and ORI2, stand out, with ORI2 having the most special value since their CF are the highest (Figure 5.3c). CEN is the region with the lowest generation due to its low wind speed values. There are regions with medium (BCA, BCS, NOR) and medium-high (NOR, NTE, NES, OCC, PEN) generation, which are the same commented on in the generation hours heatmap (Figure 5.11).

The results are only for one wind turbine. However, it should be remembered that the highest CFs per hour are used; even so, the values are high since the wind resource across Mexico is meaningful.

The valuable wind resource of Mexico is supported by estimating the EAP by site. In Table 6.3, the results of the ten sites with the highest production are presented.

Site	EAP [GWh]	Region
LV01	11.25	ORI2
OA01	10.66	ORI2
OA03	10.15	ORI2
YC01	9.79	PEN
OA04	9.46	ORI2
VZ02	8.41	ORI
TM02	8.23	NES
CH02	7.95	NTE
TM03	7.89	NES
ZC02	7.23	OCC

Table 6.3: Annual Energy Production by site for 2019

As noticed, the sites have a high EAP; some report a value as high as the region; for example, LV01 has a value of 11.25 GWh, 0.75 GWh less than the region value. Even though the value is high and an option could be to use just one site because of its significant value, what is mainly pursued when different sites combine is increasing the number of generating hours. Another example is TM02, which has a value of 8.23 GWh and the NES region of 8.87; however, the number of generating hours only for this site is 6558, combining it with the other region sites: TM01 and TM03, the number increase to 7029.

The AEP presented in Table 6.3 illustrate the diverse wind resource in Mexico. The ten sites belong to six of the ten regions. Four sites belong to ORI2, which is known as a region with an excellent resource. However, the rest are all around Mexico, showing the enormous potential to develop wind energy in different locations of Mexico.

The sites with the highest production are used since it is desired to have the highest constant generation. Furthermore, other scenarios can be created considering the proximity of the regions/sites, the network infrastructure, the node congestion, among other aspects.

6.5.2 Electricity demand forecasting

The electricity demand for 2019 and its projection for 2024 by region is presented in Figure 6.9. The national electricity demand for 2019 is 317.22 TWh and for 2024 is 369.97 TWh. In 2018, the electricity consumption per capita reported by the International Energy Agency (IEA) for Mexico was 2.3 MWh/capita; countries with the same value are Panama, Mongolia, and Arabia [77].

The magnitude of the demand has been of secondary importance until this section. In Section 6.2 and 6.3, the critical parameter was the electricity demand behavior to study the complementarity between wind and demand; and in Section 6.4 the terciles were used, not the values. However, now the demand value is essential to determine the wind power installed capacity required to meet a percentage of it.

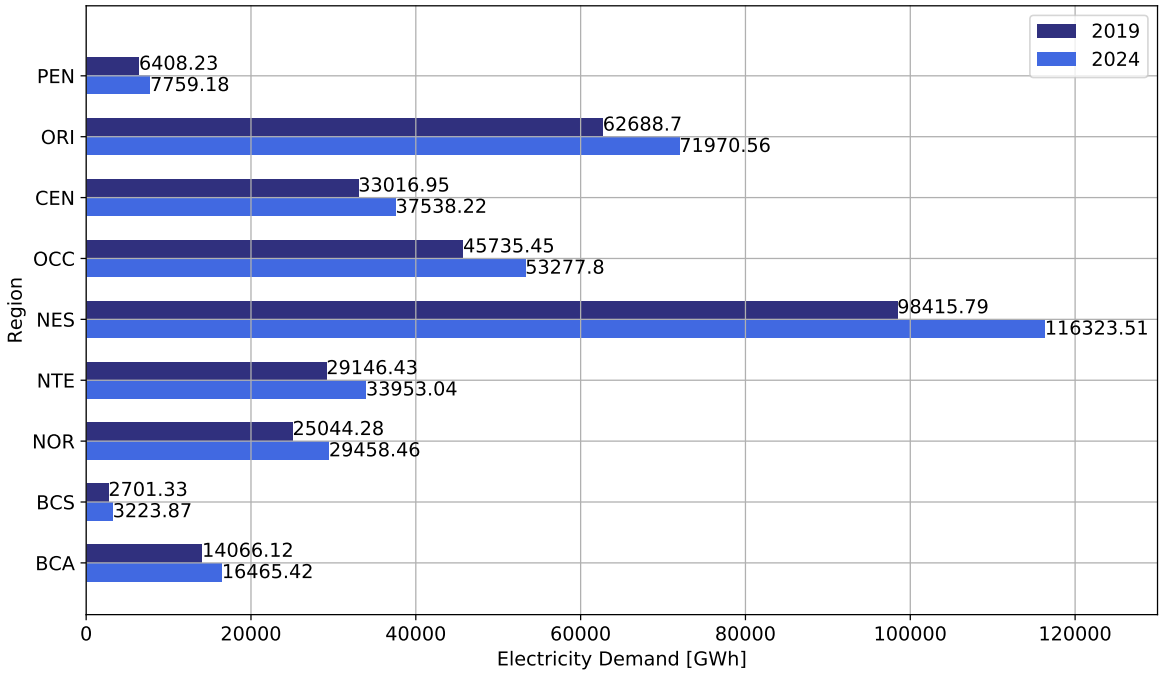

Figure 6.9: Electricity demand forecasting for 2024 by region. The projection is made using the growth-rate based method. The dark blue bars represent the demand for 2019, and the blue bars the demand for 2024.

The electricity demand varies within the country. The region with the highest demand is NES, and with the lowest is BCS. The value is influenced by the number of states in the region, the population, the principal activities (for example, tourism or industry), among other aspects.

6.5.3 Towards renewable energy 2024 target achievement

Mexico in the General Law of Climate Change establishes that: "The Energy Secretariat in coordination with the Federal Electricity Commission and the Regulatory Commission Energy will promote that the electricity generation [1] from clean energy sources reaches at least 35% by 2024 [76]".

In different countries, wind power has contributed with two-thirds of the target [8]; in Mexico, two-thirds would be the 23.33%. In 2019 the installed capacity contributed 6.20% to the electricity generation [3]. Assuming the demand value for 2024, that would represent 5.30 %; then, 18.03% would be required to achieve two-thirds of the goal for 2024. Only assuming one-third (11.67%), the missing percentage is 6.37%. The percentages commented along with their corresponding values are presented in Table 6.4.

2019		
Electricity demand [TWh]	Wind power generation [TWh]	Wind power contribution [%]
317.22	19.61	6.20
2024		
Electricity demand [TWh]	Wind power generation [TWh]	Wind power contribution [%]
369.97	66.71	18.03
369.97	23.57	6.37

Table 6.4: Wind power generation required to achieve the electricity demand proposed target for 2024.

Regional scale

The maximum constant generation is obtained by combining NTE, ORI, ORI2, and PEN on a regional scale. Summed up their AEP, the value per wind turbine is:

$$10.61 \ \frac{GWh}{Wind\ turbine} \ [2]$$

[1] In the following estimations, demand was taken as the goal value, not generation.
[2] It may differ from the sum of the values shown in Table 6.2 because of the decimals.

The number of wind turbines and installed capacity needed to accomplish **18.03%** (two-thirds) and **6.37%** (one-third) of electricity demand are presented in Table 6.5. It is considered a technology of 2 MW, and that all turbines have the same generation.

Wind power contribution [%]	Wind turbines	Installed capacity [MW]
18.03	6,287	12,574
6.37	2,221	4,442

Table 6.5: Installed capacity and wind turbines required to achieve the electricity demand proposed target for 2024 on a regional scale

Local scale

The maximum constant generation is obtained on a local scale by combining LV01, YC01, TM02, VZ02, and CH02. Summed up their AEP, the value per wind turbine is:

$$9.13 \ \frac{GWh}{Wind\ turbine}$$ [3]

The number of wind turbines and installed capacity needed to accomplish **18.03%** (two-thirds) and **6.37%** (one-third) of electricity demand are presented in Table 6.6. It is considered a technology of 2 MW, and that all turbines have the same generation.

Wind power contribution [%]	Wind turbines	Installed capacity [MW]
18.03	7,309	14,618
6.37	2,583	5,166

Table 6.6: Installed capacity and wind turbines required to achieve the electricity demand proposed target for 2024 on a local scale

The estimated regional installed capacity is lower than the local installed capacity. Interconnecting regions seems like a profitable option because it increases the number of generating hours and decreases the number of wind turbines. It would be interesting to compare costs to interconnect the sites and to install more wind turbines.

Regarding the values, the estimated wind power generation for 2024, considering one-third of the goal, is similar to the value reported on the evolution of wind power generation for that year, presented in the Prospective of Renewable Energies 2017-2031 [78] (Figure 6.10). If the goal is to achieve two-thirds of the target, efforts should be increased.

[3] It may differ from the sum of the values shown in Table 6.3 because of the decimals.

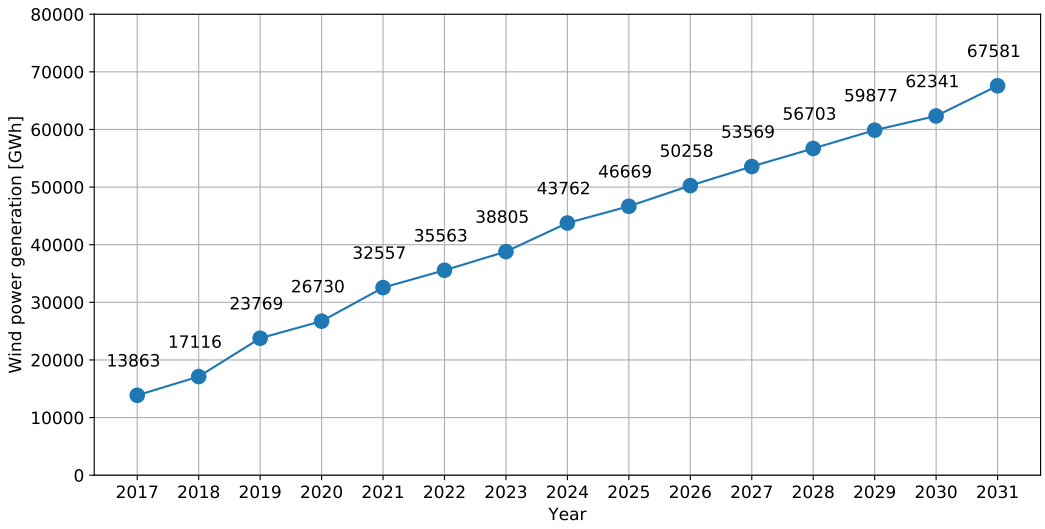

Figure 6.10: Evolution of wind power generation 2017-2031. Data obtained from [78]

6.6 Chapter summary

This chapter describes wind power and electricity demand behavior jointly, measures its correspondence, and estimates the magnitude of the wind power installed capacity required to contribute to a defined demand percentage.

Regarding the dynamics of generation and demand, the contribution of wind will be the highest during Sunday and winter and, in the majority of the regions, the peaks of wind generation correspond to the peaks of electricity demand. The difference between the demand and generation curves could decrease by interconnecting regions; although every contribution is valuable, the correlation values were weak, so the scope is to focus on constant generating; the maximum constant AEP is obtained with four regions or five sites. Comparing the wind evolution planned on the Prospective of Renewable Energies 2017-2031 with Mexico's 2024 clean energy goal, using the study sites, it was seen that Mexico should increase the planned installed capacity of wind energy if 2/3 of the 35% want to be met with it.

Here are demonstrated the principles for planning wind power development based on wind speed behaviors, relating it with the regional resource and the demand. It is highlighted the need and advantages of investing in electrical infrastructure to interconnect; also, on energy storage systems if it is not possible to have constant generation, and on "smart grid" technologies to apply other techniques to increase the grid flexibility, for example, adjust electricity generation curves to demand load curves, and then the data obtained from these type of technologies could be used to forecast or manage the electrical system.

Chapter 7

Conclusions

This work has addressed the importance of describing wind speed dynamics to use the results for increasing the flexibility of the grid by wisely expanding the generation area, contributing to the grid's reliability. The regional and local wind complementarity and the duality of wind generation and electricity demand have been studied. The results are divided into three stages: the performance of ERA5 reanalysis data to represent wind resources in Mexico (Chapter 4), the wind power temporal and spatial variability (Chapter 5) and the demand and wind power correspondence (Chapter 6). Below are commented the general conclusions from this work, and the recommendations and future work (Section 7.1).

The first stage could be considered part of the methodology to obtain reliable data for the next stages. The main conclusion is that ERA5 appropriately reproduces the dynamics but its performance reproducing the magnitude of the values depends on the region and post-processing, like bias correction. The bias correction has a more significant impact on the data distribution than on the Person Correlation Coefficient. Before bias correction, underestimation occurred in all the sites and overestimation in five sites; also, because of the difference of the values, the data distribution on scatter plots was not similar to the observations, and the linear regression line was far from the identity line. After the bias correction, the dynamics remain conserved, and the values are better aligned to the observations. Additionally, the Pearson Correlation Coefficient improves as the average time increases as local effects are minimized. Another striking result is that if annual values want to be estimated, ERA5 data bias-corrected is recommended because results are practically the same as the observations.

Focusing on the performance of ERA5 for the study sites, the r values results go between 0.35-0.89. The weakest correlations happen for the sites located in the Baja California Peninsula and the Trans-volcanic Belt (central region) because of the rapid tran-

sition between land and sea and the complex orography. Due to large-scale circulation, the strongest correlations occur for the sites located in Tamaulipas, Oaxaca, and Chiapas.

The second stage highlights the wind resource diversity in Mexico as an advantage to complement between regions, decreasing the variability of the resource. Common patterns were found, such as greatest CFs during spring, lowest during August and September, an increment of the CF between 18:00-01:00, and a reduction between 8:00-11:00. Even though shared characteristics appear, the correlation measuring complementarity potential had coefficients between - 0.22 and 1.00. The correlation values decreased as the distance increased on the sites from the same region, but between regions, there was no pattern, which is a positive thing because different possibilities of interconnection exist; also, the correlation heatmap is colored pale yellow, which is another representation of the potential to interconnect. There is an outstanding region, ORI2, which could complement many regions throughout the year. Contrary to ORI2, regions with low resources during all year are located in the Sierra Madre Occidental, Sierra Madre Oriental, Eje Neovolcánico, and Sierra Madre del Sur.

While interconnecting regions, the focus is to decrease the variability; having fewer gaps is a measure against it, which could be translated into the number of generating hours (hours with a CF above 0.2). This number is proportional to the wind resource; the regions characterized with a high resource have generating hours above 7000, like NES with 7029 hours; CEN, which has a mean wind speed of 4 m/s, has 2366 hours. Combining regions, whichever is the combination, the number of hours increases; the percentage of increment also depends on the wind resource; regions with many hours on their own will not need a massive quantity from the others.

In the third stage, it is shown the importance of harvesting wind focusing on the electricity demand. Before analyzing both variables jointly, they were studied separately, from it, it was found that for all the regions, the day on which the demand is the lowest is Sunday, the season with the highest demand for all the days is summer, except in the NOR (fall and summer) and PEN (summer and spring) regions, and the season with the lowest demand is winter for BCA, BCS, NOR, NTE, NES, OCC, ORI, and PEN, and fall for the CEN region. Therefore, the contribution to the electricity demand will be the highest during Sundays of winter and the lowest during summer.

About the correspondence between electricity generation and demand, three aspects are underlined. The first is that the demand curves are similar to the generation curve for six regions (BCA, BCS, OCC, ORI, and ORI2) where the peaks correspond. The second aspect is that the correlation between generation and demand has weak and moderate negative and positive values, between the own demand and the demand of other regions.

Using the correlation method shows that the dynamics are not equal; however, from what was seen before, the dynamics are similar just in a few hours when the peak occurs, even though the generation will be happening and any contribution is valuable. About this, ORI2 is the region where wind power has a better correlation with the demand, and CEN is the region that has a better correlation with the demand of other regions. The last aspect is related to the characterization of generation and demand in modes, there are regions characterized by high wind in many hours during all months, principally the ones located in the south and southeast of Mexico (ORI, ORI2, and PEN), and the others have not regular behavior, demonstrating that the wind is diverse across Mexico but also in every site.

Regarding the constant generation, sites and regions were combined on the second stage, and the hours increased but not up to 8760. Four regions will be needed to have the maximum constant generation: NTE, ORI, ORI2, and PEN, or five sites LV01, YC01, TM02, VZ02, and CH02. Using the time series studied in this project, the number of wind turbines with a rated power of 2MW needed to meet the goal for both scenarios, regional and local, is 6287 and 7309, respectively. As the regional time series are formed with the highest CF of the sites of the same region, the number of wind turbines is less, so interconnecting regions seems like a profitable option; this action could reduce the stress on the electrical network with new transmission and distribution lines.

Overall, this thesis has highlighted the potential of the wind resource in Mexico to complement wind generation between regions to decrease the variability and increase the flexibility of the grid. Furthermore, this work has described wind resources across Mexico and the demand of the nine control regions of the SEN, allowing the understanding of consumption and generation patterns to plan its development and management. Therefore, it is hoped that this work will be helpful to motivate the investment in electrical infrastructure and renewable energies towards a low-carbon country.

7.1 Recommendations and future work

Based on the analysis made and while the project was developing, some ideas came up to continue with wind complementarity analysis or new research. The recommendations and future work are listed below[1]:

- **Seasonal correlation**: Pearson's values between the regional CFs time series change throughout the years, so it is essential to use one year of measurement and, if possible, more than one. Also, the seasonal correlation was analyzed regionally, but it

[1] In no particular order

would be interesting to analyze it between sites of the same region; this can zoom in on the dynamics and explain in more detail why the correlation between sites of the same region is strong when they are grouped on regional time series but later the generation hours have a significant increment.

- **Scheduled maintenance:** When the wind patterns were described in Chapter 5 it was mentioned that the maintenance could be scheduled when the wind speeds are low, which happen mainly during August and September. However, if it is going to be a quick check during this time or at another time of the year, it could be considered the hours of the events mentioned in Chapter 6 Section 6.4 to determine the best hours.
- **Increase events resolutions:** The events presented in Chapter 6 Section 6.4 indicate the number of hours by month, it would be interesting to know the patterns by week, and also to see at what time of the day they happen.
- **Wind turbine selection:** Throughout the project, a single turbine was used, the Vestas V90, however, it would be an excellent tactic to select the wind turbine depending on the resource of the site. If the site has high wind resource using a wind turbine with a higher nominal power, the resource would be better utilized, obtaining more energy and at the same time reducing the number of wind turbines needed to meet Mexico's target of clean energy.
- **Power curve:** The method to recreate the power curve can be adjusted to the site considering the air density. The air density influences the turbine's performance; the lower the density, the less energy is produced. If specific power curves are created for each site, energy production results could be obtained according to the situation of the place. To obtain the air density, if there are no measurements, the variables of temperature, pressure, and relative humidity can be obtained from reanalysis data such as ERA5 and then use formulas with which the air density is estimated from these meteorological variables, one formula that could be used is the revised CIPM-2007 [79].
- **Virtual Power Plants:** The work developed could be linked and improved with the concept of virtual power plants. Including concepts of power electronics, the wind generation of different sites could be studied again as an aggregated and coordinated system.
- **Meteorology knowledge:** The results of ERA5 performance could be supported with meteorological knowledge about the interactions of the atmosphere.

- **International complementarity:** As mentioned in Chapter 5 Mexico exchanges energy with the United States, Belice, and Guatemala, so the complementarity of the demand could be expanded, including their consumption and generation time series.
- **Significance testing:** the Pearson Correlation coefficient sometimes is estimated when there are not many data points, like when using daily average per month. Doing this testing will be valuable to highlight the most critical datasets and decide their grouping.
- **Interpolate results:** The results obtained provide much information regarding ERA5 performance in Mexico, Mexican wind complementarity, and correspondence of wind generation and demand for Mexico. It is recommended that the results obtained are used for nearby sites with similar conditions of orography and wind circulation, this regarding ERA5 performance and wind patterns results. The results obtained with the regional time series should not be considered typical of the region because they are constructed with the time series o discrete points; if it is considered a more extensive area, the results might be different.

The ideas mentioned above are shared to expand and improve the research of the topic developed on this work and is not limited to include more.

References

[1] Yergin, D. (2021). The New Map. Energy, Climate, and the Clash of Nations. *The Journal of World Energy Law Business*, *14*(2), 129–132. https://doi.org/10.1093/jwelb/jwab010

[2] Secretaría de Energía. (2019). Balance nacional de energía 2018. https://www.gob.mx/cms/uploads/attachment/file/528054/Balance_Nacional_de_Energ_a_2018.pdf

[3] Iniciativa Climática de México. (2021). Observatorio de la Transición Energética en México. https://obtrenmx.org/

[4] Diario Oficial de la Federación de México. (2015). Ley de transición energética. http://dof.gob.mx/nota_detalle.php?codigo=5421295&fecha=24/12/2015

[5] Sherwood, S. (2013). Where Do Winds Come From? Nature Education Knowledge, 4(2), p. 5.

[6] Huth, J. E. (2013). *The lost art of finding our way*. Harvard University Press. https://doi.org/doi:10.4159/harvard.9780674074811

[7] International Renewable Energy Agency. (2020). *Renewable Energy Statistics 2020*. https://www.irena.org/-/media/Files/IRENA/Agency/Publication/2020/Jul/IRENA_Renewable_Energy_Statistics_2020.pdf

[8] Asociación Mexicana de Energía Eólica. (2019). El potencial eólico mexicano: Oportunidades y retos en el nuevo sector eléctrico. https://amdee.org/Publicaciones/AMDEE-PwC-El-potencial-eolico-mexicano.pdf

[9] Goodrich. (2020). Energy Business Opportunities : Mexico 2024 Energy Business Opportunities : Mexico 2024, p. 33. https://www.goodrichriquelme.com/pdf/energyopportunitiesmexico1Q2020.pdf

[10] Cochran, J., Miller, M., Zinaman, O., Milligan, M., Arent, D., Palmintier, B., O'Malley, M., Mueller, S., Lannoye, E., Tuohy, A. et al. (2014). *Flexibility in 21st century power systems* (tech. rep.). National Renewable Energy Lab.(NREL), Golden, CO (United States). https://www.nrel.gov/docs/fy14osti/61721.pdf

[11] Zhang, J., Draxl, C., Hopson, T., Monache, L. D., Vanvyve, E., & Hodge, B.-M. (2015). Comparison of numerical weather prediction based deterministic and probabilistic wind resource assessment methods. *Applied Energy*, *156*, 528–541. https://doi.org/https://doi.org/10.1016/j.apenergy.2015.07.059

[12] Veronesi, F., Grassi, S., & Raubal, M. (2016). Statistical learning approach for wind resource assessment. *Renewable and Sustainable Energy Reviews*, *56*, 836–850. https://doi.org/https://doi.org/10.1016/j.rser.2015.11.099

[13] Manwell, J. F., McGowan, J. G., & Rogers, A. L. (2010). *Wind energy explained: Theory, design and application*. John Wiley & Sons. https://doi.org/10.1002/9781119994367

[14] Bucci, G., Ciancetta, F., Fiorucci, E., Gallo, D., Landi, C., & Luiso, M. A low-cost ultrasonic wind speed and direction measurement system. In: *2013 ieee international instrumentation and measurement technology conference (i2mtc)*. 2013, 505–510. https://doi.org/10.1109/I2MTC.2013.6555469.

[15] Durán, L., Martínez, R, & Zubiaur, R. (2020). Uso de la técnica lidar para la obtención de perfiles verticales de viento. *Acta de las Jornadas Científicas de la Asociación Meteorológica Española*, (31). https://repositorio.aemet.es/bitstream/20.500.11765/5620/1/7B_Duran.pdf

[16] Bauer, P., Thorpe, A., & Brunet, G. (2015). The quiet revolution of numerical weather prediction. *Nature*, *525*(7567), 47–55. https://doi.org/10.1038/nature14956

[17] Michalakes, J, Dudhia, J, Gill, D, Henderson, T, Klemp, J, Skamarock, W, & Wang, W. The weather research and forecast model: Software architecture and performance. In: *Use of high performance computing in meteorology*. World Scientific, 2005, pp. 156–168. https://doi.org/10.1142/9789812701831_0012

[18] Cannon, D. J., Brayshaw, D. J., Methven, J., Coker, P. J., & Lenaghan, D. (2015b). Using reanalysis data to quantify extreme wind power generation statistics: A 33 year case study in great britain. *Renewable Energy*, *75*, 767–778. https://doi.org/10.1016/j.renene.2014.10.024

[19] Hersbach, H., Bell, B., Berrisford, P., Hirahara, S., Horányi, A., Muñoz-Sabater, J., Nicolas, J., Peubey, C., Radu, R., Schepers, D. et al. (2020). The era5 global reanalysis. *Quarterly Journal of the Royal Meteorological Society*, *146*(730), 1999–2049. https://doi.org/10.1002/qj.3803

[20] deCastro, M., Costoya, X., Salvador, S., Carvalho, D., Gómez-Gesteira, M., Sanz-Larruga, F. J., & Gimeno, L. (2019). An overview of offshore wind energy resources in europe under present and future climate. *Annals of the New York Academy of Sciences*, *1436*(1), 70–97. https://doi.org/10.1111/nyas.13924

[21] Sedgwick, P. (2012). Pearson's correlation coefficient. *Bmj*, *345*. https://doi.org/10.1136/bmj.e4483

[22] Yu, R., Li, J., & Chen, H. (2009). Diurnal variation of surface wind over central eastern china. *Climate dynamics*, *33*(7-8), 1089. https://doi.org/10.1007/s00382-008-0478-3

[23] Ren, G., Wan, J., Liu, J., & Yu, D. (2020). Assessing temporal variability of wind resources in china and the spatial correlation of wind power in the selected regions. *Journal of Renewable and Sustainable Energy*, *12*(1), 013302. https://doi.org/10.1063/1.5129290

[24] Fant, C., Gunturu, B., & Schlosser, A. (2016). Characterizing wind power resource reliability in southern africa. *Applied energy*, *161*, 565–573. https://doi.org/10.1016/j.apenergy.2015.08.069

[25] Malvaldi, A, Weiss, S, Infield, D, Browell, J, Leahy, P, & Foley, A. M. (2017). A spatial and temporal correlation analysis of aggregate wind power in an ideally interconnected europe. *Wind Energy*, *20*(8), 1315–1329. https://doi.org/10.1002/we.2095

[26] McVicar, T. R., Van Niel, T. G., Li, L. T., Roderick, M. L., Rayner, D. P., Ricciardulli, L., & Donohue, R. J. (2008). Wind speed climatology and trends for australia, 1975–2006: Capturing the stilling phenomenon and comparison with near-surface reanalysis output. *Geophysical Research Letters*, *35*(20). https://doi.org/10.1029/2008GL035627

[27] Castro, R., & Crispim, J. (2018). Variability and correlation of renewable energy sources in the portuguese electrical system. *Energy for Sustainable Development*, *42*, 64–76. https://doi.org/10.1016/j.esd.2017.10.005

[28] Widén, J., Carpman, N., Castellucci, V., Lingfors, D., Olauson, J., Remouit, F., Bergkvist, M., Grabbe, M., & Waters, R. (2015). Variability assessment and forecasting of renewables: A review for solar, wind, wave and tidal resources. *Renewable and Sustainable Energy Reviews*, *44*, 356–375. https://doi.org/10.1016/j.rser.2014.12.019

[29] Liu, L., Wang, Z., Wang, Y., Wang, J., Chang, R., He, G., Tang, W., Gao, Z., Li, J., Liu, C. et al. (2020). Optimizing wind/solar combinations at finer scales to mitigate renewable energy variability in china. *Renewable and Sustainable Energy Reviews*, *132*, 110151. https://doi.org/10.1016/j.rser.2020.110151

[30] Rosa, C. d. O. C. S., da Silva Christo, E., Costa, K. A., & dos Santos, L. (2020). Assessing complementarity and optimising the combination of intermittent renew-

able energy sources using ground measurements. *Journal of Cleaner Production*, *258*, 120946. https://doi.org/10.1016/j.jclepro.2020.120946

[31] Pupo-Roncallo, O., Campillo, J., Ingham, D., Hughes, K., & Pourkashanian, M. (2019). Large scale integration of renewable energy sources (res) in the future colombian energy system. *Energy*, *186*, 115805. https://doi.org/10.1016/j.energy.2019.07.135

[32] Kies, A., Schyska, B., Viet, D. T., von Bremen, L., Heinemann, D., & Schramm, S. (2017). Large-scale integration of renewable power sources into the vietnamese power system. *Energy Procedia*, *125*, 207–213. https://doi.org/10.1016/j.egypro.2017.08.188

[33] Vidal-Amaro, J., Østergaard, P. A., & Sheinbaum-Pardo, C. (2015). Analysis of large-scale integration of renewable energy sources in the mexican electricity system. *Trans. Ecol. Environ*, *195*, 449–461. https://doi.org/10.2495/ESUS150381

[34] Drew, D. R., Coker, P. J., Bloomfield, H. C., Brayshaw, D. J., Barlow, J. F., & Richards, A. (2019). Sunny windy sundays. *Renewable Energy*, *138*, 870–875. https://doi.org/10.1016/j.renene.2019.02.029

[35] Bell, W. P., Wild, P., Foster, J., & Hewson, M. (2015). Wind speed and electricity demand correlation analysis in the australian national electricity market: Determining wind turbine generators' ability to meet electricity demand without energy storage. *Economic Analysis and Policy*, *48*, 182–191. https://doi.org/10.1016/j.eap.2015.11.009

[36] Yáñez, J. P., Kunith, A., Chávez-Arroyo, R., Romo-Perea, A., & Probst, O. (2014). Assessment of the capacity credit of wind power in mexico. *Renewable energy*, *72*, 62–78. https://doi.org/10.1016/j.renene.2014.06.038

[37] Hernández-Escobedo, Q, Manzano-Agugliaro, F, & Zapata-Sierra, A. (2010). The wind power of mexico. *Renewable and Sustainable Energy Reviews*, *14*(9), 2830–2840. https://doi.org/10.1016/j.rser.2010.07.019

[38] Perea-Moreno, A.-J., Alcalá, G., & Hernandez-Escobedo, Q. (2020). Seasonal wind energy characterization in the gulf of mexico. *Energies*, *13*(1), 93. https://doi.org/10.3390/en13010093

[39] Cancino-Solórzano, Y., & Xiberta-Bernat, J. (2009). Statistical analysis of wind power in the region of veracruz (mexico). *Renewable Energy*, *34*(6), 1628–1634. https://doi.org/10.1016/j.renene.2008.11.018

[40] Hernandez-Escobedo, Q., Garrido, J., Rueda-Martinez, F., Alcalá, G., & Perea-Moreno, A.-J. (2019). Wind power cogeneration to reduce peak electricity demand in mex-

ican states along the gulf of mexico. *Energies*, *12*(12), 2330. https://doi.org/10.3390/en12122330

[41] Konstantinidis, E., & Botsaris, P. Wind turbines: Current status, obstacles, trends and technologies. In: *Iop conference series: Materials science and engineering*. *161*. (1). IOP Publishing. 2016, 012079. https://iopscience.iop.org/article/10.1088/1757-899X/161/1/012079/pdf

[42] Bhattacharyya, S. C. (2011). *Energy economics: Concepts, issues, markets and governance*. Springer Science & Business Media. https://doi.org/10.1007/978-0-85729-268-1

[43] Hernández G. (2020). Análisis de modelos globales y mesoescala en la evaluación del recurso eólico (Master's thesis. Universidad Nacional Autónoma de México). http://132.248.9.195/ptd2019/diciembre/0798867/Index.html

[44] Racero C. (2012). Viabilidad de un Parque Eólico con Sistema de Almacenamiento de Energía Mediante el uso de Modelos de Predicción. (Bachelor's thesis. Universidad de Sevilla). http://bibing.us.es/proyectos/abreproy/5116/fichero/Cap\%C3\%ADtulo+2.pdf

[45] Rabbani, R, & Zeeshan, M. (2020). Exploring the suitability of merra-2 reanalysis data for wind energy estimation, analysis of wind characteristics and energy potential assessment for selected sites in pakistan. *Renewable Energy*, *154*, 1240–1251. https://doi.org/10.1016/j.renene.2020.03.100

[46] Kirkland, E. J. (1998). *Advanced computing in electron microscopy*. Springer. https://doi.org/10.1007/978-3-030-33260-0_1

[47] Soriano, E., Mediero, L., & Garijo, C. (2019). Selection of bias correction methods to assess the impact of climate change on flood frequency curves. *Water*, *11*(11), 2266. https://doi.org/10.3390/w11112266

[48] Cannon, A. J., Sobie, S. R., & Murdock, T. Q. (2015a). Bias correction of gcm precipitation by quantile mapping: How well do methods preserve changes in quantiles and extremes? *Journal of Climate*, *28*(17), 6938–6959. https://doi.org/10.1175/JCLI-D-14-00754.1

[49] Trinh-Tuan, L., Matsumoto, J., Tangang, F. T., Juneng, L., Cruz, F., Narisma, G., Santisirisomboon, J., Phan-Van, T., Gunawan, D., Aldrian, E. et al. (2019). Application of quantile mapping bias correction for mid-future precipitation projections over vietnam. *SOLA*. https://doi.org/10.2151/sola.2019-001

[50] Department of Statistics and Data Science. (1998). *Linear Regression*. Yale University. http://www.stat.yale.edu/Courses/1997-98/101/linreg.htm

[51] Mukaka, M. (2012). Statistics corner: A guide to appropriate use of correlation in medical research. *Malawi Medical Journal*, *24*(3), 69–71. https://pubmed.ncbi.nlm.nih.gov/23638278/

[52] Meteorological Versus Astronomical Seasons. (2016). National Oceanic and Atmospheric Administration's National Centers for Environmental Information. https://www.ncei.noaa.gov/news/meteorological-versus-astronomical-seasonse

[53] Halffter, G., & Morrone, J. J. (2017). An analytical review of halffter's mexican transition zone, and its relevance for evolutionary biogeography, ecology and biogeographical regionalization. *Zootaxa*, *4226*(1), 1–46. https://doi.org/10.11646/zootaxa.4226.1.1

[54] Centro Nacional de Control de la Energía. (2021a). Demanda del sistema eléctrico nacional. https://www.cenace.gob.mx/Paginas/Publicas/Info/DemandaRegional.aspx

[55] Coburn, J. J. (2019). Assessing wind data from reanalyses for the upper midwest. *Journal of Applied Meteorology and Climatology*, *58*(3), 429–446. https://doi.org/10.1175/JAMC-D-18-0164.1

[56] European Center For Medium Range Weather Forecast. (2021). Copernicus Climate Data Store. https://cds.climate.copernicus.eu/#!/home

[57] National Institute of Electricity and Clean Energy. (2020). Mexican wind atlas. http://aems.ineel.mx/

[58] Electrical Research Institute. (2013). Action plan to eliminate barriers to the development of wind power generation in mexico. https://erc.undp.org/evaluation/evaluations/detail/2981#

[59] Hahmann, A. (2016). El Atlas Eólico Mexicano (AEM): Descripción del proyecto y resultados preliminares. http://ejkrause.com.mx/mwpcamps/bitacorapdf/24-AndreaHahmann.pdf

[60] Borja, M. (2003). Proyecto Eólico. Boletín IIE, octubre-diciembre del 2003. https://www.ineel.mx/boletin042003/tend.pdf

[61] Instituto de Investigaciones Eléctricas. (2005). Plan de acción para eliminar barreras para el desarrollo de la generación eoloeléctrica en México. http://www.nacionmulticultural.unam.mx/mezinal/docs/178.pdf

[62] Centro Nacional de Control de la Energía. (2021b). Estimación de la Demanda Real. https://www.cenace.gob.mx/Paginas/SIM/Reportes/EstimacionDemandaReal.aspx

[63] Secretaría de Energía. (2015). Manual de Medición para Liquidaciones, p. 19.

[64] Gelaro, R., McCarty, W., Suárez, M. J., Todling, R., Molod, A., Takacs, L., Randles, C. A., Darmenov, A., Bosilovich, M. G., Reichle, R. et al. (2017). The modern-era retrospective analysis for research and applications, version 2 (merra-2). *Journal of climate*, *30*(14), 5419–5454. https://doi.org/10.1175/JCLI-D-16-0758.1

[65] Morales-Ruvalcaba, C. F., Rodriguez-Hernandez, O., Martinez-Alvarado, O., Drew, D. R., & Ramos, E. (2020). Estimating wind speed and capacity factors in mexico using reanalysis data. *Energy for Sustainable Development*, *58*, 158–166. https://doi.org/10.1016/j.esd.2020.08.006

[66] Secretaría de Energía. (2019). Prospectiva del Sector Eléctrico 2018-2032, p. 63. https://base.energia.gob.mx/Prospectivas18-32/PSE_18_32_F.pdf

[67] Vestas. (2012). 2-MW-Product-Brochure. https://people.unica.it/danielecocco/files/2012/04/2-MW-Product-Brochure.pdf

[68] Kaiser-Weiss, A., Kaspar, F, Heene, V, Borsche, M, Tan, D., Poli, P, Obregon, A, & Gregow, H. (2015). Comparison of regional and global reanalysis near-surface winds with station observations over germany. *Advances in Science and Research*, *12*(1), 187–198. https://doi.org/10.5194/asr-12-187-2015

[69] Staffell, I., & Pfenninger, S. (2016). Using bias-corrected reanalysis to simulate current and future wind power output. *Energy*, *114*, 1224–1239. https://doi.org/10.1016/j.energy.2016.08.068

[70] Korotyshkin, D., Merzlyakov, E., Sherstyukov, O., & Valiullin, F. (2019). Mesosphere/lower thermosphere wind regime parameters using a newly installed skiymet meteor radar at kazan (56° n, 49° e). *Advances in Space Research*, *63*(7), 2132–2143. https://doi.org/10.1016/j.asr.2018.12.032

[71] European Centre for Medium-Range Weather Forecasts. (2020). Era5. https://www.ecmwf.int/en/forecasts/datasets/reanalysis-datasets/era5

[72] Gupta P. & Follette-Cook M. (2020). Merra-2 reanalysis. https://arset.gsfc.nasa.gov/sites/default/files/airquality/workshops/SCAQMD/D3P2_MERRA2.pdf

[73] Turrent, C., & Zaitsev, O. (2014). Seasonal cycle of the near-surface diurnal wind field over the bay of la paz, mexico. *Boundary-layer meteorology*, *151*(2), 353–371. https://doi.org/10.1007/s10546-014-9908-4

[74] Secretaría de Energía. (2017). Reporte de Inteligencia Tecnológica. Energía eólica en tierra. https://www.gob.mx/cms/uploads/attachment/file/280276/IT_E_lica_12DIC17.pdf

[75] Torres, P., Ekonomou, L, & Karampelas, P. The correlation between renewable generation and electricity demand: A case study of portugal. In: *Electricity distribution*. Springer. 2016, 119–151. https://doi.org/10.1007/978-3-662-49434-9_5

[76] DOF, México. (2012). Ley general de cambio climático. *Published June*, *6*, 2012. http://www.diputados.gob.mx/LeyesBiblio/pdf/LGCC_061120.pdf

[77] International Energy Agency. (2019). Atlas of Energy. Electricity Consumption per Capita (MWh/capita). http://energyatlas.iea.org/#!/tellmap/-1118783123/1

[78] Secretaría de Energía. (2017). Prospectiva de Energías Renovables 2017-2031. https://www.gob.mx/cms/uploads/attachment/file/284342/Prospectiva_de_Energ_as_Renovables_2017.pdf

[79] Picard, A., Davis, R., Gläser, M, & Fujii, K. (2008). Revised formula for the density of moist air (cipm-2007). *Metrologia*, *45*(2), 149. https://iopscience.iop.org/article/10.1088/0026-1394/45/2/004/meta

Appendix A

Complementary plots of Chapter 5

In this appendix are presented the plots used as a tool to describe the temporal variability (Subsection 5.2.1) and wind resource characteristics (Section 5.3) by region, not shown in Chapter 5.

A.1 Temporal Variability of regional wind power

The hourly and monthly radar charts of the CF by region are presented in Figure A.1 and A.2, respectively.

A.2 Regional wind resource characteristics

The hourly profiles and heatmaps for each region with more than one site are presented below using wind speed and capacity factor time series.

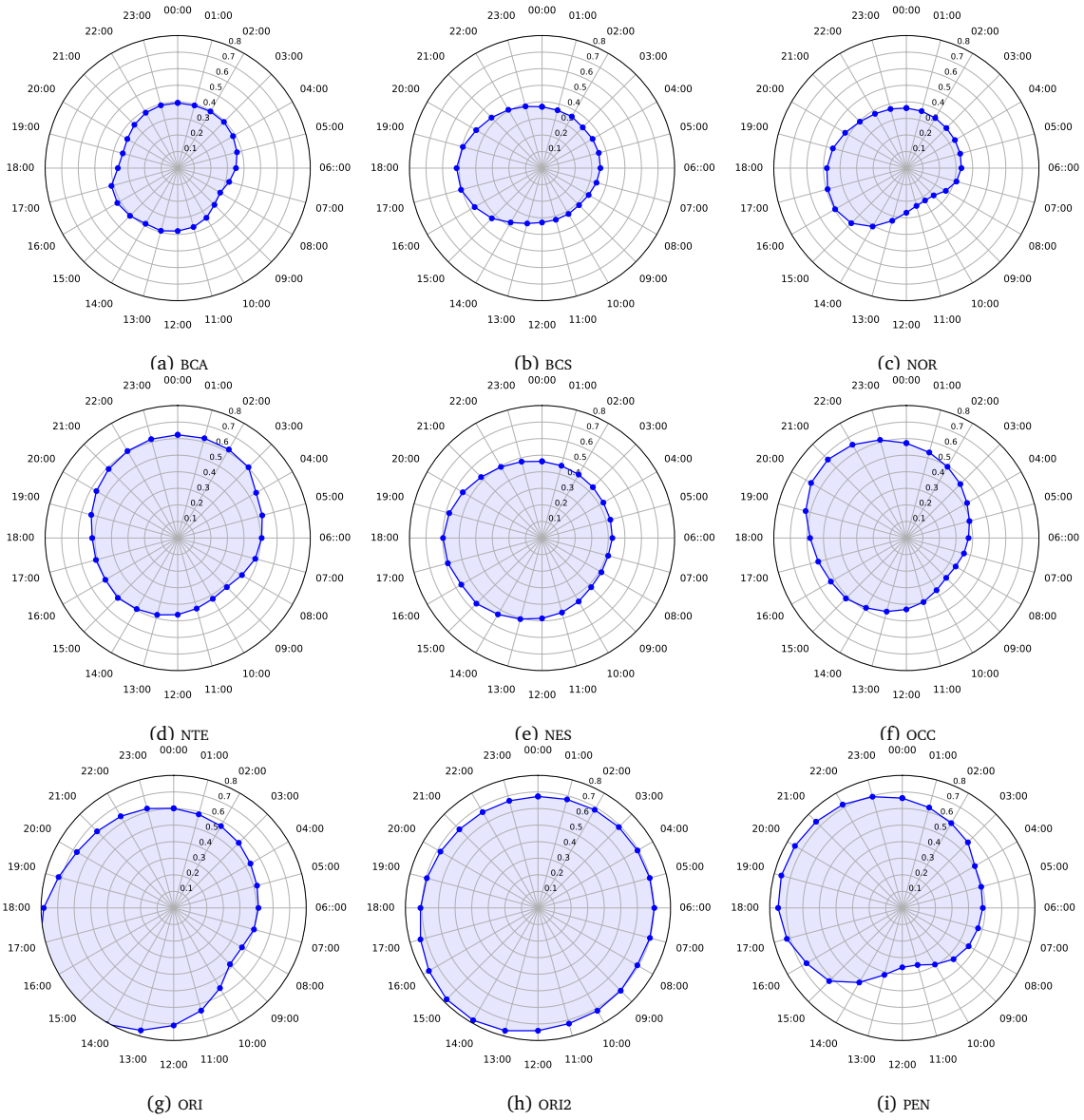

(a) BCA (b) BCS (c) NOR

(d) NTE (e) NES (f) OCC

(g) ORI (h) ORI2 (i) PEN

Figure A.1: Regional mean Capacity Factor by hour of 1979-2019.

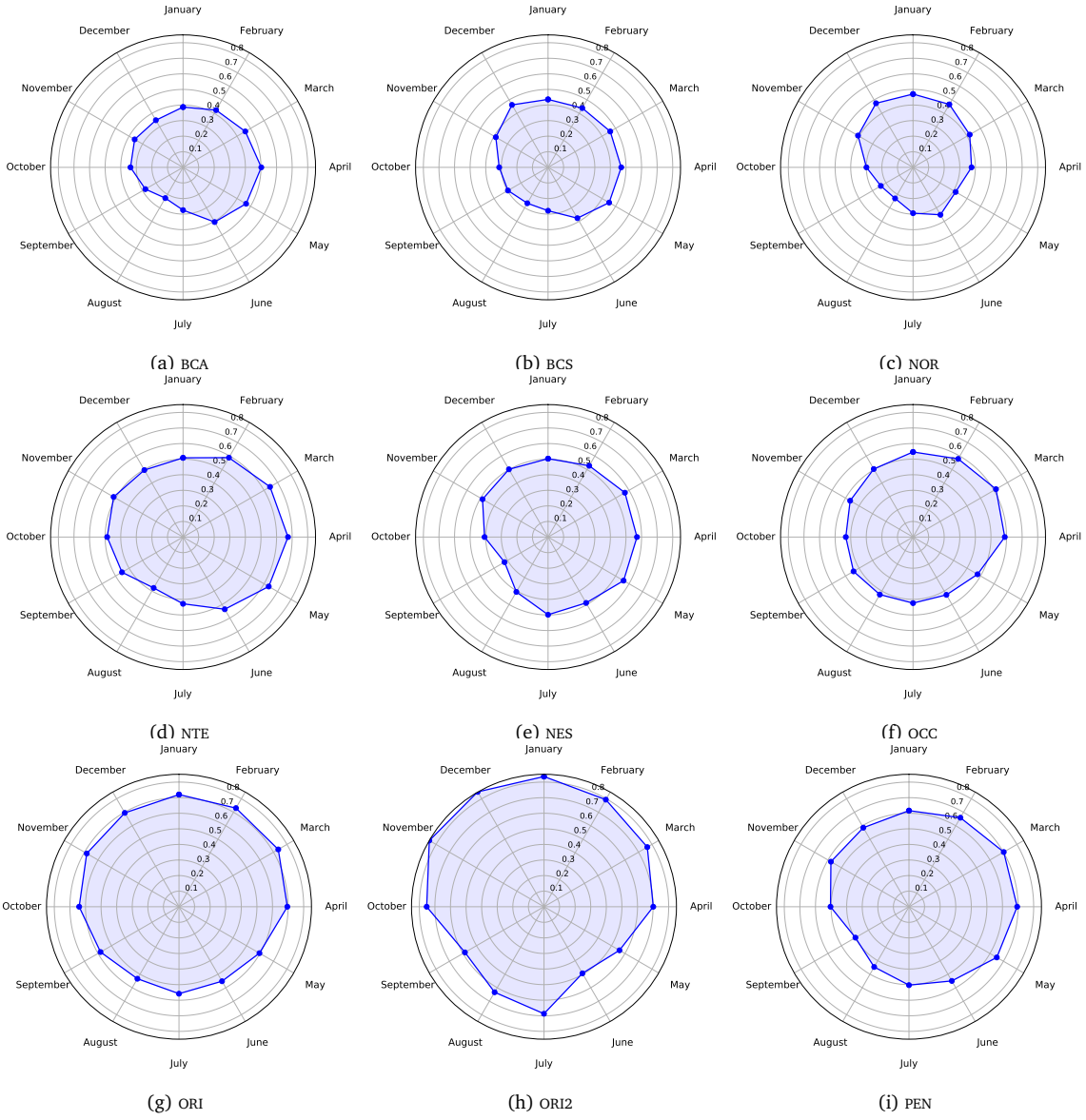

(a) BCA (b) BCS (c) NOR

(d) NTE (e) NES (f) OCC

(g) ORI (h) ORI2 (i) PEN

Figure A.2: Regional mean Capacity Factor by month of 1979-2019.

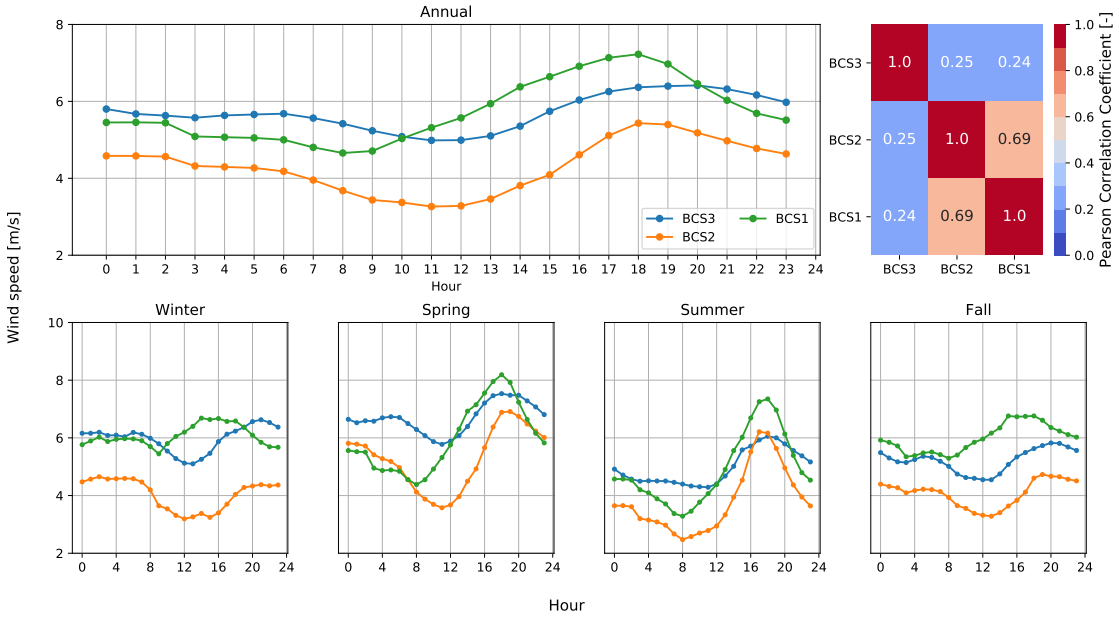

Figure A.3: Annual and seasonal wind speed hourly profiles of BCS sites.

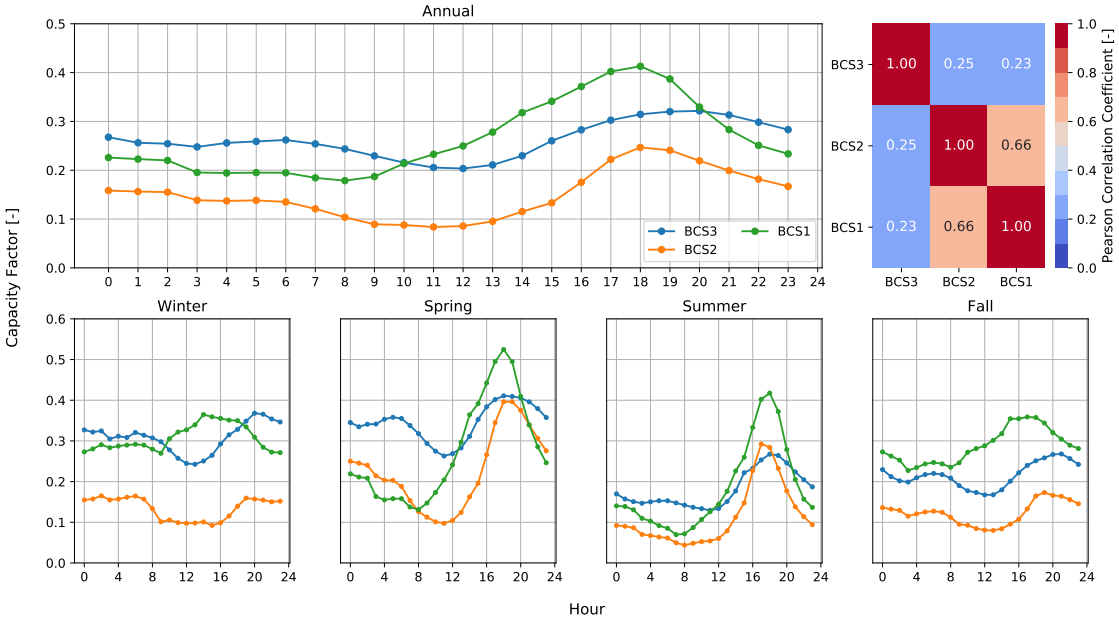

Figure A.4: Annual and seasonal capacity factor hourly profiles of BCS sites.

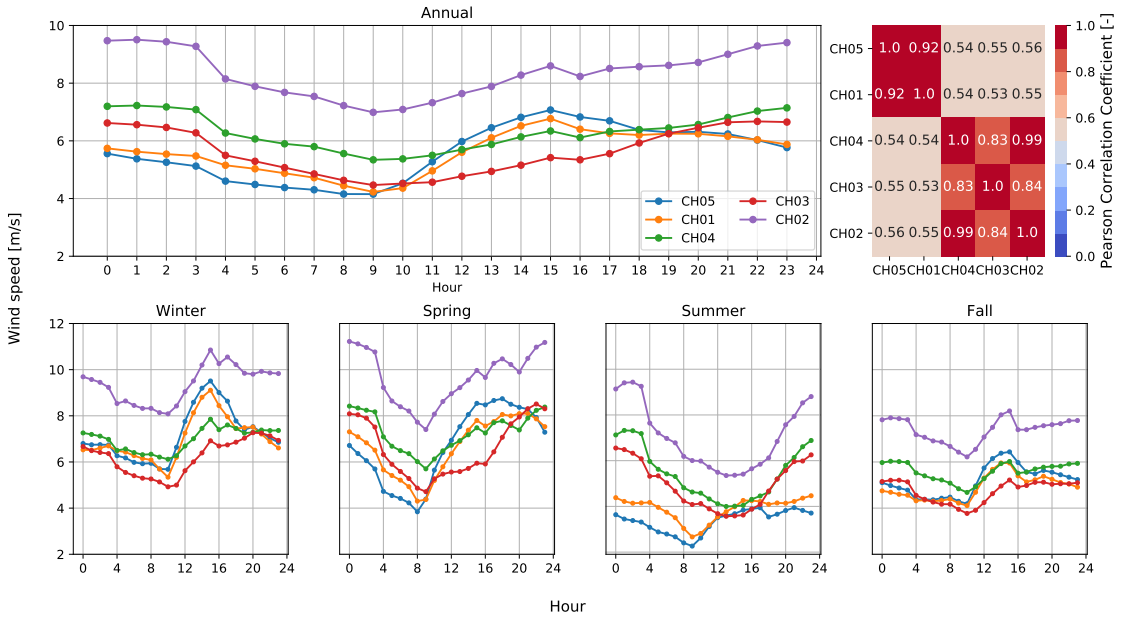

Figure A.5: Annual and seasonal wind speed hourly profiles of NTE sites.

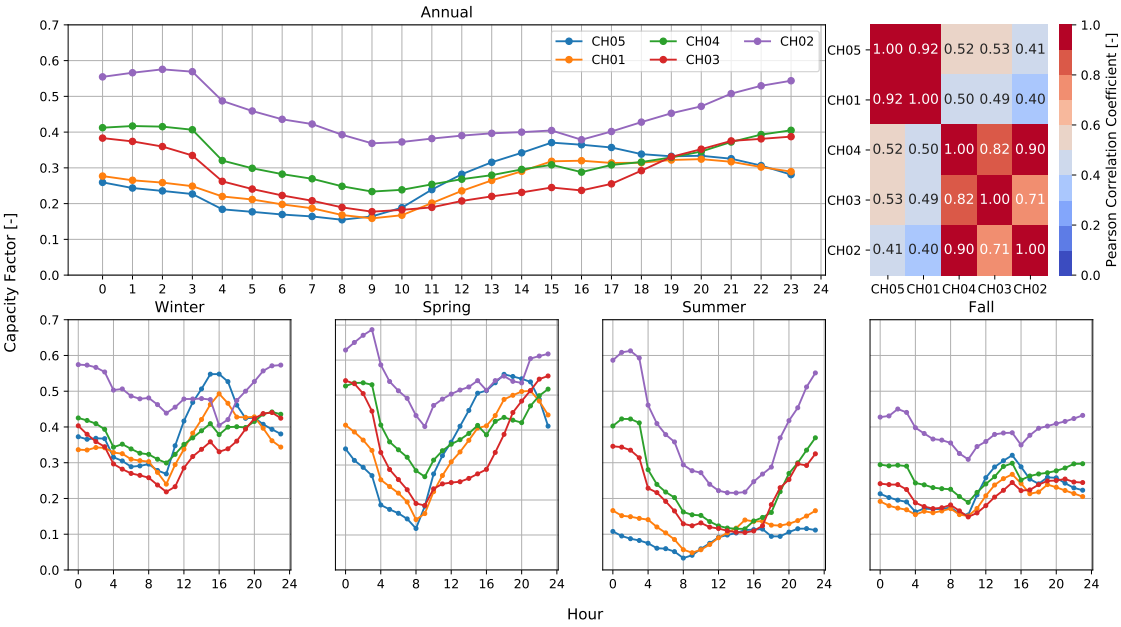

Figure A.6: Annual and seasonal capacity factor hourly profiles of NTE sites.

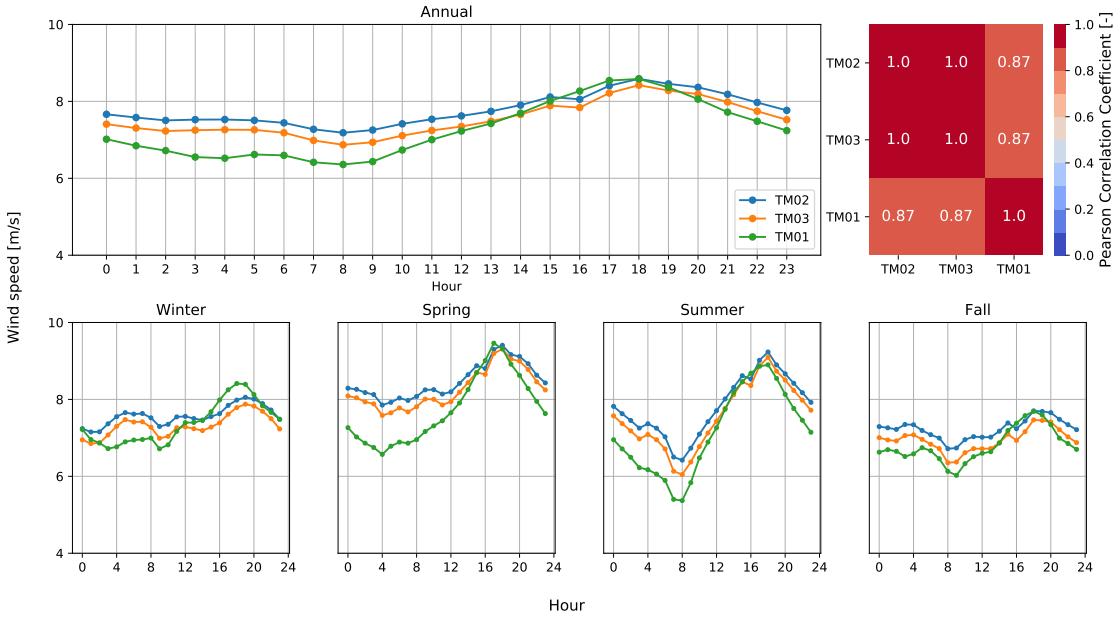

Figure A.7: Annual and seasonal wind speed hourly profiles of NES sites.

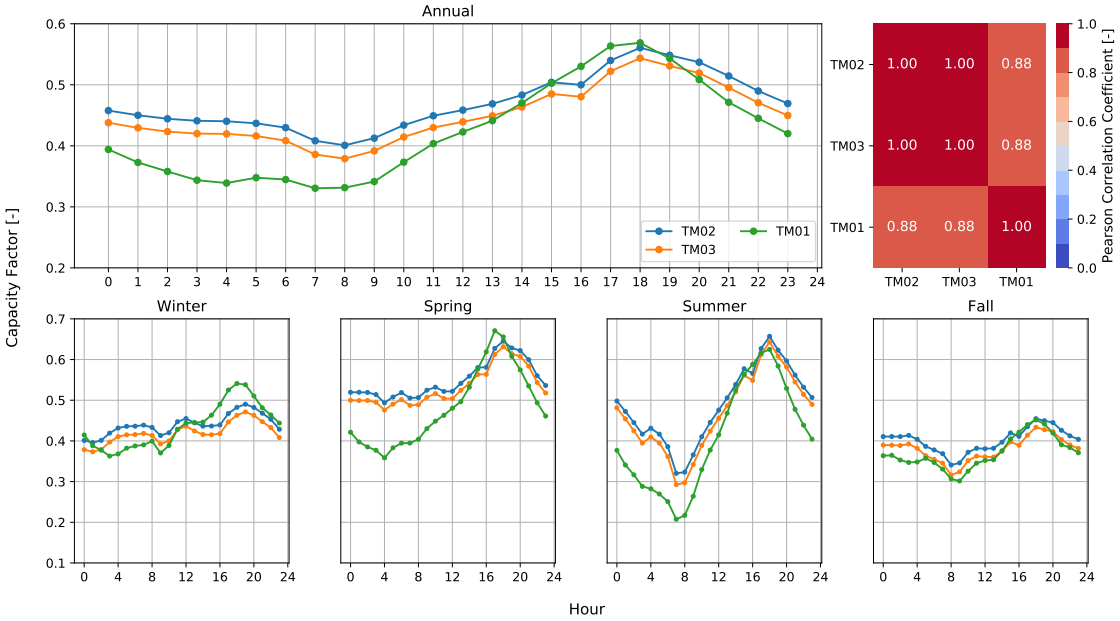

Figure A.8: Annual and seasonal capacity factor hourly profiles of NTE sites.

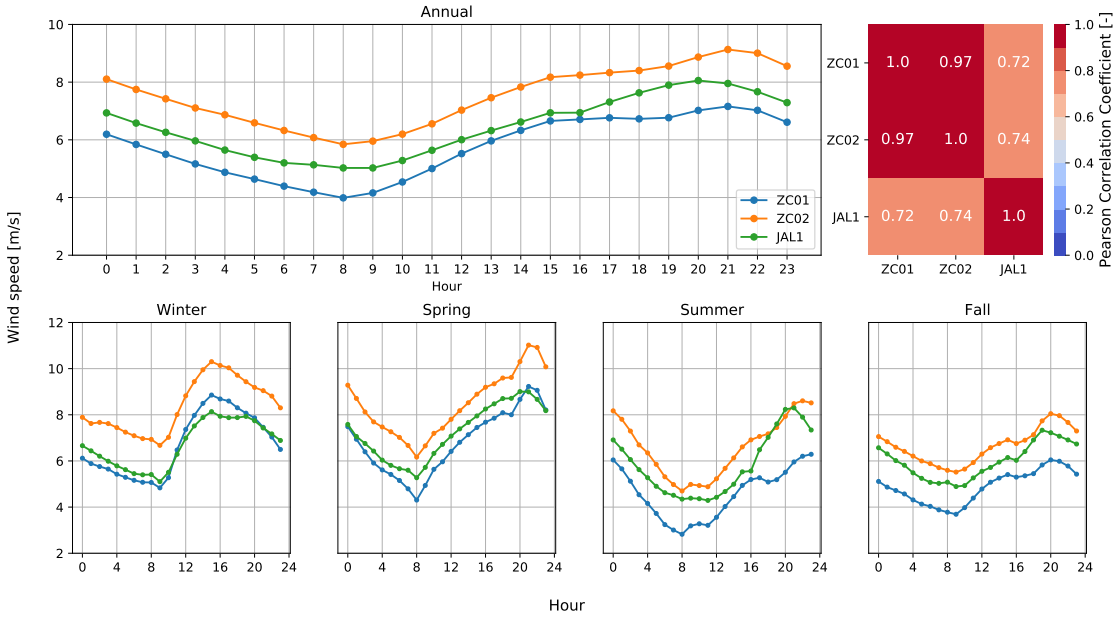

Figure A.9: Annual and seasonal wind speed hourly profiles of OCC sites.

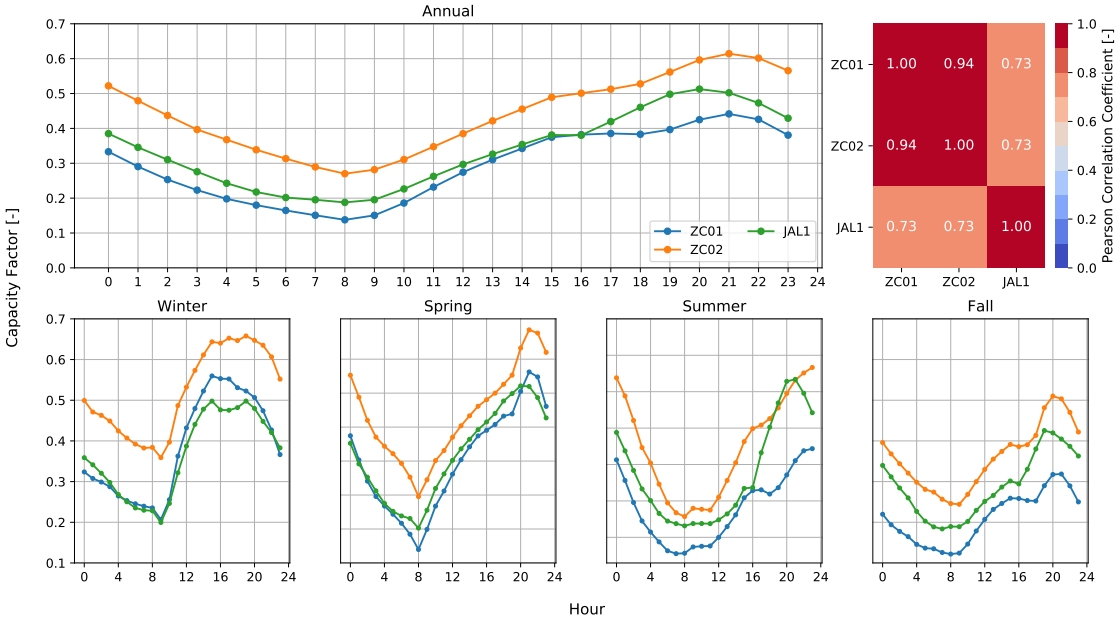

Figure A.10: Annual and seasonal capacity factor hourly profiles of OCC sites.

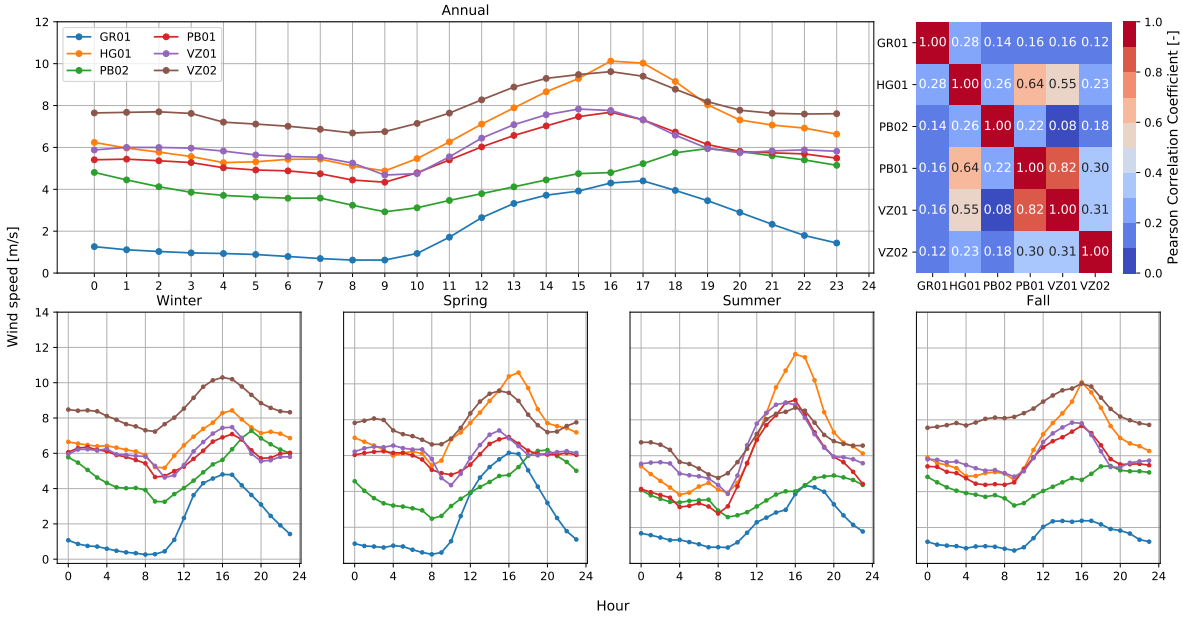

Figure A.11: Annual and seasonal wind speed hourly profiles of ORI sites.

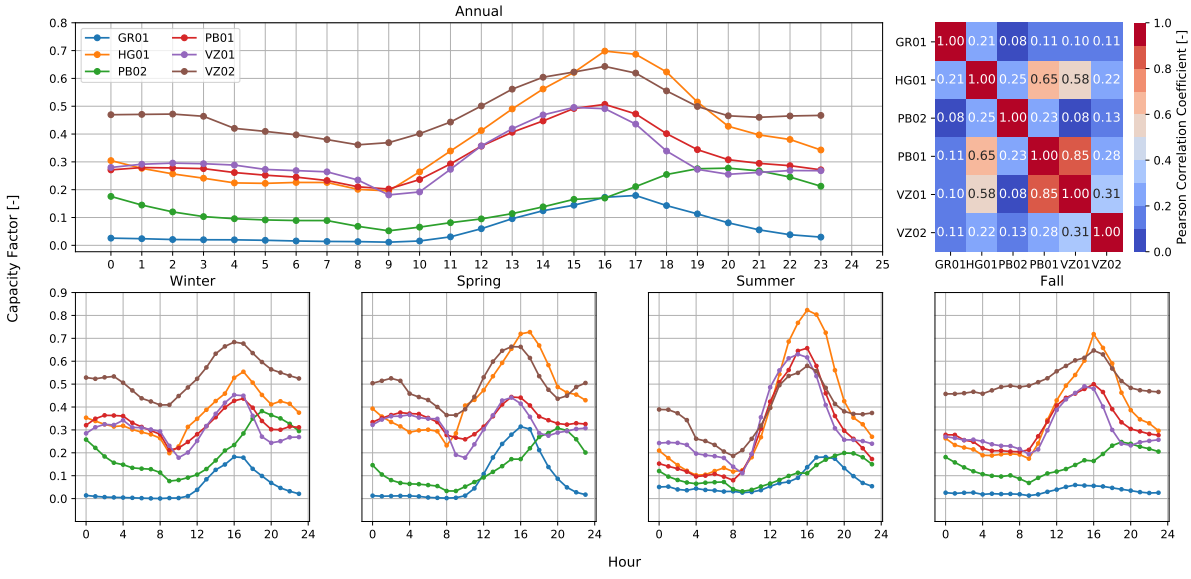

Figure A.12: Annual and seasonal capacity factor hourly profiles of ORI sites.

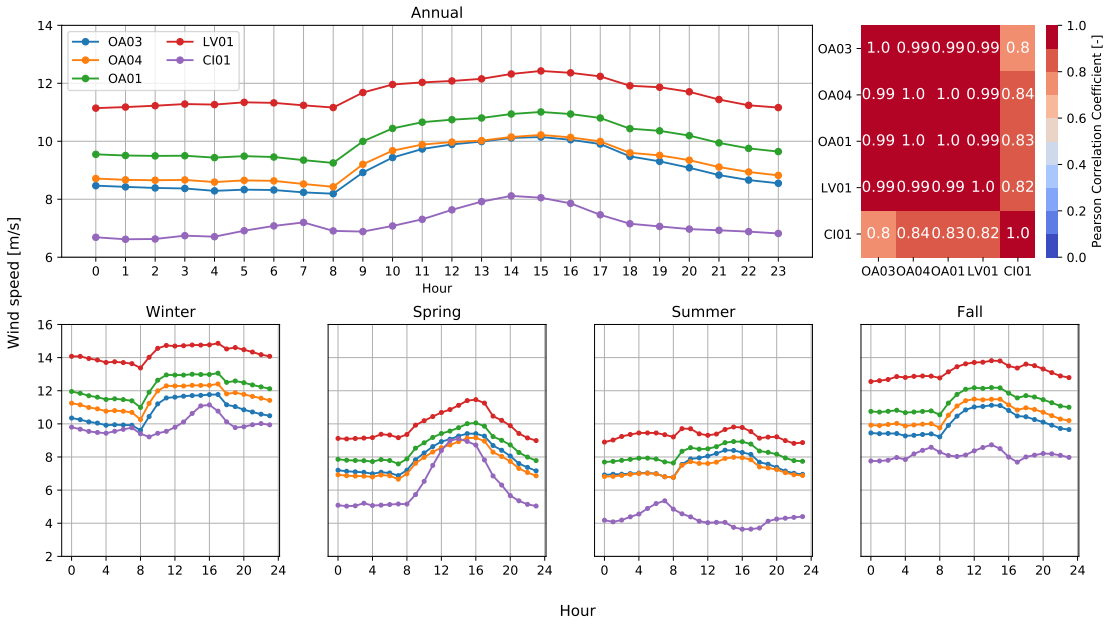

Figure A.13: Annual and seasonal wind speed hourly profiles of ORI2 sites.

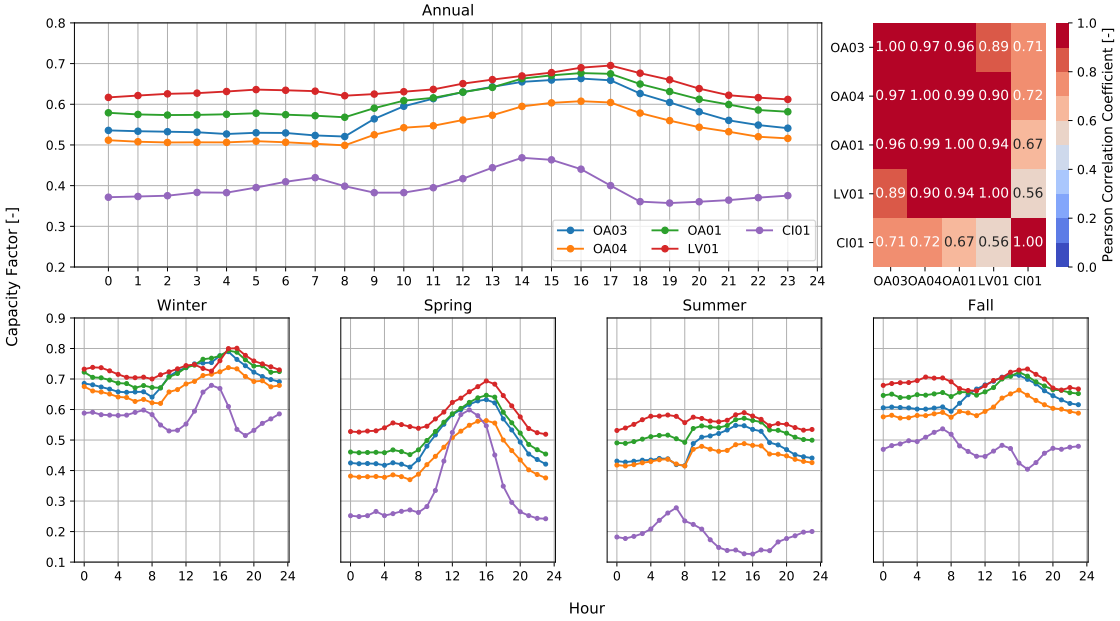

Figure A.14: Annual and seasonal capacity factor hourly profiles of ORI2 sites.